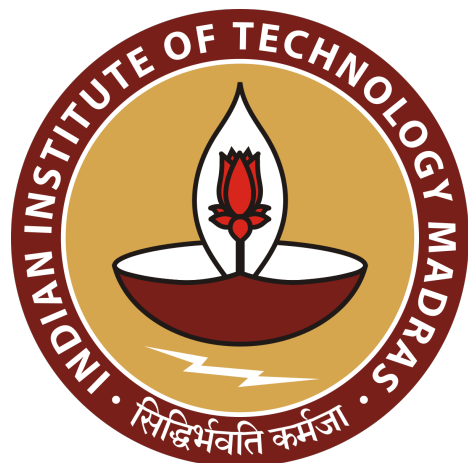


AS5213 : Design of MAV/UAV

---

## UAV for afforestation/reforestation

---



Department of Aerospace Engineering

Indian Institute of Technology, Madras

# Contents

	Page
<b>1 <u>Introduction</u></b>	<b>10</b>
1.1 Existing solutions . . . . .	11
1.2 Proposal . . . . .	11
1.2.1 The Mission Statement . . . . .	12
1.2.2 Brief Overview of Desired Capabilities of the UAV . . . . .	12
1.2.3 Features and Functions . . . . .	13
1.2.4 Mission Profile . . . . .	13
1.2.5 Desired Requirements and Mission Specifications . . . . .	14
1.3 Comparison with Similar Aircraft and Literature Survey . . . . .	16
<b>2 First Weight Estimation</b>	<b>21</b>
2.1 Payload Weight Estimation . . . . .	22
2.1.1 Choice of Power Plant . . . . .	22
2.2 Battery Weight Estimation . . . . .	23
2.2.1 Power required-Cruise . . . . .	24
2.2.2 Power required-Take off and Landing . . . . .	25
2.2.3 Power required-Climb/Descent . . . . .	25
2.2.4 Power Required-Loiter . . . . .	26
2.2.5 Power required-Seed Dispersal . . . . .	26
2.2.6 Total Battery weight . . . . .	26
2.3 Empty Weight Estimation . . . . .	27
2.4 Maximum Takeoff Weight Estimation . . . . .	28
<b>3 Power Plant Specifications</b>	<b>32</b>
3.1 Calculating $C_{D_0}$ . . . . .	32
3.1.1 $S_{wet}$ for wing . . . . .	33
3.1.2 Swet for fuselage . . . . .	34
3.1.3 Swet for horizontal/Vertical Tail . . . . .	34
3.1.4 Previous aircraft data . . . . .	35
3.2 P/W Calculation for each segment . . . . .	37
3.2.1 Cruise . . . . .	38

3.2.2	Loiter . . . . .	38
3.2.3	Take off and Landing . . . . .	38
3.2.4	Climb . . . . .	39
3.2.5	Descent . . . . .	39
3.3	Total Power . . . . .	39
3.4	Selection of Configuration and Motor . . . . .	40
3.4.1	Configuration of the UAV . . . . .	40
3.4.2	Motor Selection . . . . .	42
3.4.3	LiPo Battery calculations: . . . . .	44
<b>4</b>	<b>Wing Loading</b>	<b>48</b>
4.1	Constraint Based on Stall Velocity ( $V_{stall}$ ) . . . . .	48
4.1.1	Calculating $V_{stall}$ . . . . .	48
4.1.2	Determining the Take off distance and roughness value . . . . .	49
4.2	Wing Loading for Take off . . . . .	50
4.3	Wing loading for Stall speed . . . . .	51
4.4	Wing loading for Maximum speed . . . . .	51
4.5	Wing loading for Cruise . . . . .	52
4.6	Wing loading for Climb . . . . .	52
4.7	Wing loading for Maximum Ceiling . . . . .	53
4.8	Wing loading for Sustained turn . . . . .	53
4.9	Conclusion . . . . .	54
<b>5</b>	<b>Second Weight Estimate</b>	<b>56</b>
5.1	Fixed Quantities . . . . .	56
5.1.1	Method . . . . .	57
5.1.2	Revising Power and Wing loading . . . . .	57
<b>6</b>	<b>Wing and Airfoil Selection</b>	<b>60</b>
6.1	Wing's Vertical Location . . . . .	60
6.2	Airfoil Selection . . . . .	61
6.2.1	Calculating Reynolds number . . . . .	62
6.2.2	Deciding t/c ratio . . . . .	62
6.2.3	Airfoil type . . . . .	62
6.2.4	Wing sweep . . . . .	65
6.2.5	Taper ratio . . . . .	66
6.2.6	Winglet . . . . .	66
6.2.7	Wing twist . . . . .	67
6.2.8	Dihedral angle . . . . .	67
6.2.9	High lift devices . . . . .	67
6.2.10	Design of Control Surfaces . . . . .	69

6.2.11	Final Specifications . . . . .	71
<b>7</b>	<b>Fuselage and Tail Design</b>	<b>74</b>
7.1	Fuselage design . . . . .	74
7.1.1	Previous Aircraft Data . . . . .	74
7.1.2	Payload Dimensions and Characteristics . . . . .	76
7.2	Tail Configuration . . . . .	79
7.3	Horizontal Tail Configuration . . . . .	82
7.3.1	Horizontal Tail Arm and area . . . . .	82
7.3.2	Other Parameters . . . . .	84
7.3.3	Elevator . . . . .	84
7.4	Vertical Tail Configuration . . . . .	84
7.4.1	Rudder . . . . .	86
7.5	Final Parameters . . . . .	86
<b>8</b>	<b>Landing Gear Design</b>	<b>87</b>
8.1	Preliminary CG Location . . . . .	87
8.2	Comparison of Landing Gear Arrangements for UAV Mission . . . . .	88
8.2.1	Tricycle Landing Gear . . . . .	88
8.2.2	Tail-Dragger (Tailwheel) Landing Gear . . . . .	89
8.3	Steering for nose wing . . . . .	90
8.4	Landing Gear parameters . . . . .	92
8.4.1	Wheel Base . . . . .	95
8.4.2	Effect of crosswinds . . . . .	97
8.4.3	Tire Sizing . . . . .	98
8.4.4	Shock Absorber . . . . .	99
<b>9</b>	<b>CG Location and 3 View Diagram</b>	<b>102</b>
9.1	CG of the fuselage . . . . .	103
9.2	Payload CG . . . . .	103
9.2.1	Batteries . . . . .	104
9.2.2	Camera/Gimbal . . . . .	105
9.2.3	Seed dropping system . . . . .	105
9.2.4	Sensors . . . . .	106
9.2.5	Motor . . . . .	106
9.3	Final CG . . . . .	107
9.4	Verifying the empty weight . . . . .	107
9.4.1	Wing . . . . .	107
9.4.2	Horizontal Tail . . . . .	108
9.4.3	Vertical Tail . . . . .	108
9.4.4	Fuselage . . . . .	108

9.4.5	Landing gear . . . . .	108
9.5	Revised Landing gear Parameters . . . . .	109
9.5.1	Detailed View of Landing Gear . . . . .	110
9.6	Final CAD Model and 3 view Diagram . . . . .	110
<b>10</b>	<b>Static Stability Analysis</b>	<b>112</b>
10.1	Longitudinal Stability . . . . .	112
10.1.1	Contribution by wing . . . . .	113
10.1.2	Contribution of Fuselage to $C_{m_{\alpha cg}}$ . . . . .	113
10.1.3	Contribution of Tail to $C_{m_\alpha}$ . . . . .	114
10.1.4	Final Values . . . . .	115
10.1.5	Stick Fixed Neutral Point . . . . .	115
10.1.6	Longitudinal Control derivatives . . . . .	116
10.2	Directional Stability $C_{n_\beta}$ . . . . .	116
10.2.1	Contribution due to wing . . . . .	118
10.2.2	Contribution due to Fuselage . . . . .	118
10.2.3	Contribution due to Vertical Tail . . . . .	119
10.2.4	Directional Control . . . . .	119
10.3	Lateral Stability . . . . .	120
10.4	Control Surface Sizing . . . . .	122
10.4.1	Elevators . . . . .	122
10.4.2	Rudder . . . . .	122
10.4.3	Aileron . . . . .	123
10.5	High Lift Devices . . . . .	124
<b>11</b>	<b>Performance Analysis</b>	<b>125</b>
11.1	Drag Polar . . . . .	125
11.1.1	Calculation of $C_{D_0}$ . . . . .	125
11.1.2	Calculation of K . . . . .	127
11.1.3	Final Diagram . . . . .	128
11.2	Variation of Power vs Velocity . . . . .	128
11.3	V-n Diagram . . . . .	129
11.4	Range and Endurance . . . . .	131
11.5	Take off Distance . . . . .	132
11.6	Landing Distance . . . . .	135
11.7	Final Three view diagram . . . . .	136
<b>Appendix</b>		<b>138</b>
<b>A</b>	<b>Codes for weight estimation</b>	<b>139</b>
A.1	Linear model for weight estimation(empty weight ratio vs total weight) . . . . .	139

A.2 Logarithmic Model for weight estimation(empty weight ratio vs total weight) . . . .	140
A.3 Weight estimation Iteration . . . . .	141
A.4 Second wt estimation . . . . .	142
<b>B Code for Power Plant Estimation</b>	<b>144</b>
B.1 Motor/Propeller efficiency . . . . .	146
<b>C Calculation of Wing Loading</b>	<b>148</b>
<b>D Codes for fuselage length Estimation</b>	<b>150</b>
<b>E Python code for V-n Code</b>	<b>152</b>

# List of Figures

1.1	'Mission Profile'	14
1.6	Figures of aircrafts mentioned in literature review	18
2.1	'Direct Variation'	27
2.2	'Logarithmic Variation'	28
2.3	'Convergence plot'	29
2.4	'MTOW convergence'	29
3.1	'Power Calculations'	32
3.2	'Visualization representation of how Swet for fuselage was calculated'	34
3.3	'L/D variation with sqrt of wetted aspect ratio'	37
3.4	'L/D variation with wetted aspect ratio'	37
4.1	Coefficient of Friction Values	49
4.2	Selection of Takeoff Distance	50
4.3	Plot for Takeoff Parameter	51
4.4	W/P VS W/S	54
5.1	2nd weight estimation	57
6.1	Legend	63
6.2	Flap Types	67
6.3	Plain flap vs no flap	68
6.4	Flap area	69
6.5	Geometry of Aileron	71
6.6	Final Wing geometry	71
6.7	Lift distribution	72
6.8	Final Wing characteristics	73
7.1	Fuselage length variation with weight-linear regression	75
7.2	Fuselage length variation with span-linear regression	76
7.3	Full seed dispersal machinery	76
7.4	(a)Seed tank which will be inside the fuselage (b) seed tank attached in fuselage (c) servos used for plunging	77

7.5	Fuselage Preliminary Design . . . . .	78
7.6	Detailed view of fuselage . . . . .	79
7.7	Horizontal tail . . . . .	82
7.8	tail arm length . . . . .	82
7.9	NACA 0009 . . . . .	83
7.10	Vertical Tail Configuration . . . . .	84
8.1	Fuselage detailed dimensions . . . . .	87
8.2	Nose Gear Steering . . . . .	91
8.3	Take off phases . . . . .	92
8.4	Fowler flap effects on stall angle . . . . .	93
8.6	Landing Gear height . . . . .	94
8.7	Reference Aircraft . . . . .	94
8.8	Landing Gear base . . . . .	95
8.9	Landing Gear track . . . . .	96
8.10	Force balancing . . . . .	97
8.11	Tire Sizing Table from [8] . . . . .	98
8.12	Tire Notations [8] . . . . .	99
8.14	Levered Bungee shock absorber . . . . .	100
9.1	Distribution . . . . .	103
9.2	Slot to access the Payloads . . . . .	104
9.3	Battery Position . . . . .	104
9.4	Battery Position . . . . .	104
9.5	Camera/Gimbal Location . . . . .	105
9.6	Seed Dispersal Mechanism Position . . . . .	106
9.7	Sensors Location . . . . .	106
9.8	With landing gear CG . . . . .	109
9.9	Without landing gear CG . . . . .	109
9.10	Landing gear detailed view 1 . . . . .	110
9.11	Landing gear detailed view 2 . . . . .	110
9.12	Landing gear detailed view 3 . . . . .	110
10.1	Empirical Plot for $K_f$ . . . . .	114
10.2	Value of Tau . . . . .	116
10.3	Vertical tail role in the aircraft directional trim . . . . .	117
10.4	Empirical plots [8] . . . . .	121
10.5	One engine/Motor Fail scenario . . . . .	123
10.6	Empirical plots [8] . . . . .	123
10.7	Empirical plots [8] . . . . .	124
11.1	Turbulent-Laminar % [8] . . . . .	126

11.2 Drag Polar . . . . .	128
11.3 Power Velocity Bucket curve . . . . .	129
11.4 V-n diagram at Sea Level . . . . .	131
11.5 Coastal region . . . . .	132
11.6 Take off distance . . . . .	133
11.7 New battery location - brought ahead (towards nose) by 7cm in CAD to compensate for changed tail arm so that CG remains same in X axis . . . . .	136
11.8 Different Views of Final Airplane . . . . .	137
E.1 Motor Data Sheet . . . . .	159
E.2 Contribution1 . . . . .	162
E.3 Contribution2 . . . . .	162
E.4 Contribution3 . . . . .	162
E.5 Contribution4 . . . . .	163

# List of Tables

1.1	List of Equipment for Surveillance and Navigation Purposes . . . . .	13
1.2	Literature Review . . . . .	16
1.3	Additional Details . . . . .	17
1.4	Details of each segment . . . . .	17
2.1	Tentative Design Details for first weight estimation . . . . .	24
2.2	Segment details for battery weight . . . . .	24
2.3	Segment-wise Power consumption . . . . .	26
2.4	MTOW Estimation . . . . .	28
2.5	Total Weight Estimations . . . . .	29
3.1	Aircraft Data . . . . .	36
3.2	Total power Consumption of UAV . . . . .	40
3.3	Motor Specifications . . . . .	44
6.1	Comparison of Wing Configurations . . . . .	60
7.1	Previous Aircraft Reference data . . . . .	74
7.2	Previous Aircraft Reference data . . . . .	75
7.3	Sensor Specifications . . . . .	77
9.1	Payload exact CG location . . . . .	107
11.1	Component wise calculated parameters . . . . .	126
11.2	Component wise Calculated values . . . . .	127

# Chapter 1

## Introduction

---

Vast swathes of India's mountainous landscape hold immense potential for ecological restoration. However, their remoteness and inaccessibility pose significant challenges to traditional methods of seed dispersal and vegetation establishment. This report proposes a revolutionary approach - leveraging Unmanned Aerial Vehicles (UAVs) to sow seeds in these fertile but inaccessible regions, promoting vital greening efforts and contributing to a healthier planet.

This project focuses on four key regions with fertile pockets currently inaccessible to humans:

### 1. The Himalayas:

#### **Inner Himalayas:**

Fertility: Valleys like Lahaul-Spiti, Kinnaur, and parts of Uttarakhand have fertile soil due to glacial deposits and alluvial plains.

Challenges: High altitude (3,000-5,000 meters), extreme weather (-30°C to 30°C), limited infrastructure, and avalanches.

#### **Eastern Himalayas:**

Fertility: Valleys like Tawang and Munsiyari have fertile soil due to monsoon rains and organic matter.

Challenges: Dense forests, steep slopes (up to 70°), landslides, and limited accessibility.

### 2. The Western Ghats:

#### **Southern Western Ghats:**

Fertility: Plateaus like Nilgiri Hills and Shevaroy Hills have fertile soil due to volcanic activity and organic matter.

Challenges: Dense vegetation, steep slopes, and lack of proper roads.

### 3. The Eastern Ghats:

#### **Odisha Hills:**

Fertility: Plateaus like Koraput and Keonjhar have fertile red and black soils.

Challenges: Dense forests, lack of infrastructure, and tribal sensitivities.

## 1.1 Existing solutions

The following are the existing solutions for the given problem statement.

- One of the ways that afforestation/reforestation can be done is through manual labour which is highly labour intensive, time consuming and inefficient. Moreover these target areas are unreachable by humans. Hence using autonomy is the best solution for this.
- One way used by several companies worldwide is to use drones for seed dispersal in these target areas. However the endurance of the drones is far less compared to a fixed wing uav and it ensures difficulty in communication when the missions are led in places inaccessible by man.

The following companies use drone technology to assist mass afforestation/reforestation.

- In Australia, a company called AirSeed Technologies is aiming to restore natural forests cleared by logging, wildfires and flooding.
- In Africa, World Vision Kenya, in partnership with Kenya Flying Labs, is using drones to reseed degraded land in Tana River county with indigenous trees
- Companies and NGOs around the world are using drone seeding to reforest degraded land. U.K.-based environmental technology company Dendra Systems uses drones to drop seeds faster and more safely in remote areas.

## 1.2 Proposal

The seeds are typically planted over large areas. Manned reforestation/afforestation projects (often planted by hand) can become very dangerous for each worker, time consuming, and costly compared to the use of aerial drones.

Fixed-wing UAVs are more beneficial than most other types of drones as they can operate for long periods of time and can cover long distances without recharging/refuelling.

This is primarily due to the fact that they consume less energy to generate lift and most winged craft have a gliding capability, although the gliding capability is not often very efficient as the size and weight of fixed-wing aircraft used for this role are typically quite heavy.

Fixed-wing UAVs could not only be used in the reforestation process but could also be equipped with payloads such as electro-optical (EO) and LIDAR (Light Detection and Ranging) sensors enabling them to scope out the state of the target area beforehand whether it be for reforestation or afforestation.

### **1.2.1 The Mission Statement**

The mission of our fixed-wing UAV designed for afforestation in inaccessible areas is to contribute to ecological restoration by identifying fertile regions where vegetation can thrive without human access. The primary objective is to enhance biodiversity and green cover in areas that are challenging for humans to reach. The fixed-wing UAV will employ advanced sensors to survey and locate suitable terrain for afforestation, focusing on areas with optimal soil conditions and environmental viability.

The UAV will take off, navigate the target region, and utilize its sensor suite to assess the fertility of the soil, climate conditions, and other relevant factors for successful afforestation. Once identified, the UAV will deploy seeds in a precise and targeted manner to promote the growth of vegetation. The use of fixed-wing UAVs enables efficient coverage of larger areas, making it well-suited for afforestation initiatives in remote and inaccessible locations.

Our mission extends beyond the initial seed deployment. The UAV will periodically monitor the afforested areas, collecting data on vegetation growth, environmental conditions, and overall ecosystem health. This ongoing surveillance will inform adaptive strategies to optimize afforestation efforts, ensuring sustainable and resilient ecosystems.

### **1.2.2 Brief Overview of Desired Capabilities of the UAV**

- Ability to thoroughly navigate the area and deploy seeds if the target area is suitable of vegetation.
- Ability to carry payload(seeds) and have high range of 1-2 hrs and endurance of 80km.
- Ability to take off and land in short distance in a terrain where a polished take-off landing infrastructure is not available.
- Ability to carry sensors and camera to conduct detailed navigation and inspection of target area before dropping the seeds and after to check quality of growth.
- Equipped with essential machinery to drop the seeds from a height.
- The UAV will carry all essential sensors as mentioned in the table later, assisting it to collect data and perform its designated task.

### 1.2.3 Features and Functions

Equipments	Product Name	Features	Weight (g)
Camera	Sony Alpha A7R IV	<ul style="list-style-type: none"> <li>- With a 61-megapixel full-frame sensor capable of capturing 4 K video at up to 30 frames per second</li> <li>- High resolution, durable build and advanced connectivity</li> </ul>	665
Gimbal	Three-axis aluminium brushless gimbal	<ul style="list-style-type: none"> <li>- Stabilize and control the movement of cameras or other equipment.</li> <li>- Consists of three brushless motors that work together to eliminate unwanted motion and vibration, providing smooth and stable footage</li> </ul>	177.5
Flight controller	Pixhawk 4 Mini	Flight controller designed use in small UAVs that supports a wider range of sensors, including GPS, barometer, and other sensors	15
GPS Module	U-blox M8N	High accuracy, fast time-to-first-fix, and low power consumption	9
IMU	MPU-9250 IMU	A 9-axis IMU that combines accelerometers, gyroscopes, and a magnetometer, providing accurate data for flight control and navigation	2000-3000
Sensing Technology	LIDAR	<ul style="list-style-type: none"> <li>- Provides Highly accurate 3D mapping of the terrain, including elevation data.</li> <li>- Will be used to Map the terrain, identifying the land features and finding suitable location to plant the seed</li> </ul>	1000

Table 1.1: List of Equipment for Surveillance and Navigation Purposes

### 1.2.4 Mission Profile

As shown in the diagram above, we will mission profile will have the following sub components:

- Take off and climb-The UAV will take off (aimed to be a short take off landing)and climb to the cruising altitude.
- Cruise -The UAV will cruise to the location of interest at the specified cruise velocity. This covers majority of the flight time of the UAV.

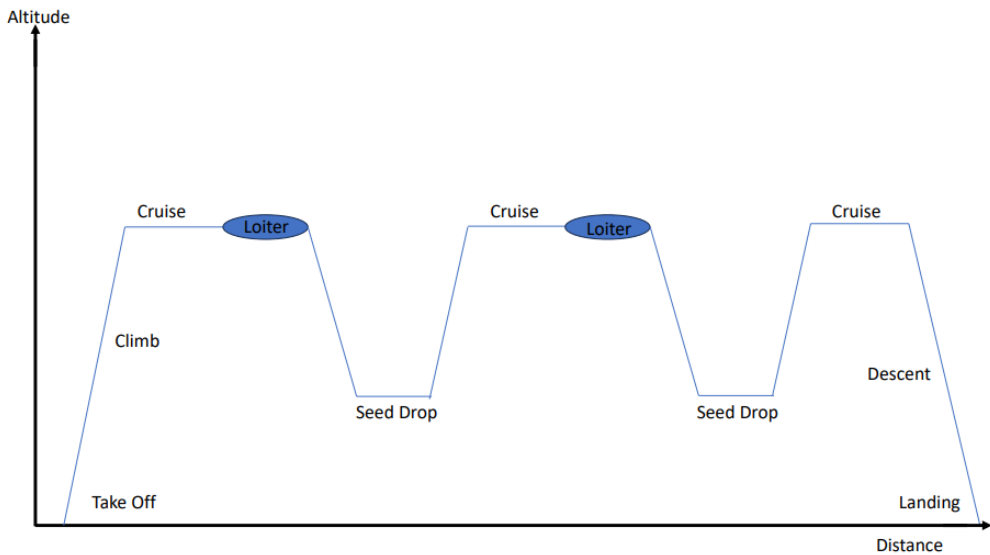


Figure 1.1: 'Mission Profile'

- Loiter- When the UAV reaches a target area, it loiters and checks whether that area is suitable for seed dispersal.
- Descend and seed dispersal- The UAV descends and disperses the seeds in the target area from a height which will be calculated as the safe height to disperse seeds effectively.
- Climb and cruise to next location and repeat the descend and seed dispersal- The same process is repeat once the uav has completing sowing seeds in one location, it will go to another similar location.
- Descend and Land- Once the UAV has completed its task of sowing seeds and the maximum endurance has been reached, it will perform the final segment which is landing(aimed to be a short landing) for refueling.

## 1.2.5 Desired Requirements and Mission Specifications

### Maximum Range

As per the literature survey of similar aircrafts the range of the UAV under consideration can be taken around 80-100km(calculated average from the literature survey).

### Absolute Ceiling

According to DGCA regulations, the absolute ceiling for all UAVs, including fixed-wing UAVs, in India is 400 feet above ground level (AGL), or if the UAV is equipped with a Remote Pilot Station, up to 400 feet above the highest obstacle within a radius of 5 km from the UAV. For the drone to operate within regulations, the absolute ceiling is set to 400 feet.

## **Minimum Height**

Depending upon the speed and the force with which we decide to air drop the seeds so that it does not affect the seeds but at the same time ensure effective planting, our minimum height will be decided. On an average the minimum height will be around 50-80 feet.

## **Cruise Velocity**

The cruise and loiter velocity will depend on number of factors like weight of the UAV and the type of sensors. Since we will need to map the area properly using LIDAR and the high performance camera, we will require a cruise velocity that can give high quality images but also generates enough lift for the UAV. The estimated cruise speed is around 20m/s and loiter is around 15m/s.

## **Endurance**

Depending upon the type of propulsion system that we choose later, the endurance will be anywhere between 3-8 hrs(calculated average from the literature survey).

## **Total Payload Weight**

The payload in our case will essentially consist of seed dispersal machinery, the seeds and the sensor details as mentioned above. The total payload is estimated to be around 6-7kg.

## **Landing and Take off method**

As mentioned earlier, we aim at having a short take off and landing in relatively rough/unpaved regions. The reason for choosing this method is:

- 1.The complexities that arise if more number of propellers are added in case of a vtol type UAV and chances of failure in an inaccessible region increase.
- 2.Using catapult launch increases the unsteadiness during take off and cause potential risk to the delicate sensors and dispersal machinery.

Hence we aim to use features in the aircraft which reduce the landing/take off distance as compared to a conventional runway length. The runway length is estimated to be around 10-15m.

## **Free weight**

The free weight of the aircraft will vary based on the material used for the structural part of the UAV. However, based on the literature review, the free weight will be around 8-10kgs.

## 1.3 Comparison with Similar Aircraft and Literature Survey

The major source of inspiration for this mission profile was taken from the following research papers [3]and [10]

Name of UAV	Purpose	MTOW	Payload weight	Range	Endurance	Engine	Span	Cruise Speed
Skyeye Sierra	ISR	12.5kg	5kg	500km	3hrs-elec 8hrs-gas	Gas/ Electric	3m	18m/s
Lancaster-5	Survey	4kg	2.4kg	1.93km	45 mins	Electric	1.5m	12- 16m/s
UAV Sitaria	Lidar scanning	35kg	4kg	60km	3 hrs	Electric	5.2m	20- 25m/s
The Tempest	Agriculture and Survey	4.5kg	3.2kg	80km	1.5hrs	Electric	3m	22m/s
Penguin BE		21.5kg	6.6kg	-	110 mins	Electric	3.3m	-
Albatross	Precision Agriculture and survey	10+kg	-	100km	4 hrs	Electric	3m	19m/s
Shabhal	ISR	17.5kg	5.5kg	12km	-	Electric	2.47m	36m/s
SkyrobotFX20	ISR	12kg	5kg	60km	4 hrs	Electric	3m	40m/s
Blackswift s2	Low altitude flight in confined space	9.5kg	2.3kg	110km	-	Electric	3m	18m/s
QODS Yasir	ISR	25kg	9kg	450km	24 hrs	Electric	3.11m	40m/s

Table 1.2: Literature Review

Some additional features of the above aircraft are given in the table below:

Name of UAV	Maximum Altitude	Maximum Speed	Fuselage length	Fuel/ Battery weight	Total weight (No payload)
SKYEYE Sierra	-	35m/s	-	-	-
Lancaster-5	2500m	22m/s	-	-	2.4kg
UAV Sitaria	6000m	38m/s	2.8m	13 kg	
The Tempest	-	-	-	-	-
Penguin BE	-	36.01m/s	-	14.9kg	-
Albatross	-	-	-	-	4kg
Shahbal	3000m	-	2.05m	-	9.5kg
SKYROBOT FX-20	4000m	-	1m	-	5kg
QODS Yadir	4575m	-	5.6m	-	16kg
Blackswift s2	6000m	-	6.3m	-	-

Table 1.3: Additional Details

As mentioned in the literature details above, according to the mission requirements, we will be aiming at designing an aircraft having the specifications similar to the following:

Segment	Altitude	Speed	Time	Distance
Take off and climb	0-300m	0-20m/s	10-15mins	15m+(2-5)km
Cruise	300m	20m/s	40-45mins	10-20km
Loiter	300m	15m/s	10-15mins	10km
Seed dispersal	25m	15m.s	10-15mins	10km
Descent and Landing	300-0m	20-0m/s	10-15mins	15m+(2-5km)

Table 1.4: Details of each segment

The below shows the pictures of the aircrafts discussed above:



(a) Lancaster



(b) Shahbal



(a) UAV Sitaria



(b) SkyrobbotFX20



(a) Albatross



(b) Penguin BE



(a) Skyeye Sierra



(b) Tempest



(a) QODS Yasir



(b) Blackswift S2l

Figure 1.6: Figures of aircrafts mentioned in literature review

In the preceding chapter (Week 1), we established a problem statement: to transport drones to inaccessible regions such as the Himalayas, eastern, and western ghats, at higher altitudes for the purpose of planting seeds to support afforestation/reforestation efforts. However, given the limitation that an STOL aircrafts cannot reach such high altitudes, we have opted to modify our target regions to more accessible lands that are in urgent need of reforestation/afforestation.

Here are some low-altitude regions in India that are in need of afforestation and are accessible for STOL drone seed ball sowing:

### **Coastal Plains**

#### **• Eastern Coast**

Stretching from Tamil Nadu to West Bengal, the east coast plains have witnessed significant deforestation for agriculture, aquaculture, and infrastructure development.

#### **• Western Coast**

The west coast plains, encompassing Gujarat, Maharashtra, Goa, Karnataka, and Kerala, have also seen their fair share of deforestation due to similar reasons.

Accessibility : Both the east and west coast plains are well-connected by road and rail networks, making them easily accessible for STOL drones and local communities.

Ecological Impact : Reforestation in these regions can help mitigate the effects of cyclones and floods, protect coastal ecosystems, and improve soil fertility.

Challenges :Hilly terrain and dense vegetation cover in some areas can be obstacles for drones.

### **Indo-Gangetic Plains**

Spanning across northern and eastern India, this vast plain suffers from deforestation due to intensive agriculture, fuelwood collection, and overgrazing.

Accessibility : The Indo-Gangetic Plains boast excellent accessibility with a dense network of roads and villages.

Ecological Impact : Afforestation efforts here can combat desertification, improve air quality, and provide habitat for diverse wildlife.

Challenges :Dust storms Might affect drone accuracy and seed dispersal.

### **River Deltas**

India's major river deltas, such as the Sundarbans, Mahanadi Delta, and Kaveri Delta, have experienced deforestation for agriculture, aquaculture, and settlements.

Accessibility : Accessibility can vary depending on the specific delta, but many areas are reachable by water transport and roads.

Ecological Impact : Reforestation in deltas helps prevent soil erosion, storm surges, and protects biodiversity-rich wetlands.

Challenges :Strong winds and high humidity near the coast can affect drone stability and seed

dispersal accuracy.

## Existing solutions

The following are the existing solutions for the given problem statement.

- One of the ways that afforestation/reforestation can be done is through manual labour which is highly labour intensive, time consuming and inefficient.
- One way used by several companies worldwide is to use drones for seed dispersal in these target areas. However the endurance of the drones is far less compared to a fixed wing uav.

The existing projects that utilize drone technology for afforestation/reforestation in India are:

- **Mahanadi Delta Mangrove Restoration Project:** This project, led by the Odisha Forest Department and Wildlife Institute of India, uses drones to plant native mangrove species in degraded areas of the Mahanadi delta.
- **Andhra Pradesh Coastal Greening Project:** This project by the Andhra Pradesh Forest Department employs drones to plant native tree species across degraded coastal areas, aiming to mitigate climate change and conserve biodiversity.
- **Haryana Afforestation Initiative:** This collaborative effort by the Haryana Forest Department and NGOs utilizes drones to plant drought-resistant trees in critical areas of the Indo-Gangetic plains, promoting water conservation and climate resilience.

## The Mission Statement

The mission of our fixed-wing UAV designed for afforestation is to contribute to ecological restoration by identifying fertile regions where vegetation can thrive. The primary objective is to enhance biodiversity and green cover in these areas. The fixed-wing UAV will employ advanced sensors to survey and locate suitable terrain for afforestation, focusing on areas with optimal soil conditions and environmental viability.

The UAV will take off, navigate the target region, and utilize its sensor suite to assess the fertility of the soil, climate conditions, and other relevant factors for successful afforestation. Once identified, the UAV will deploy seeds in a precise and targeted manner to promote the growth of vegetation. The use of fixed-wing UAVs enables efficient coverage of larger areas, making it well-suited for afforestation initiatives in remote and inaccessible locations.

Our mission extends beyond the initial seed deployment. The UAV will periodically monitor the afforested areas, collecting data on vegetation growth, environmental conditions, and overall ecosystem health. This ongoing surveillance will inform adaptive strategies to optimize afforestation efforts, ensuring sustainable and resilient ecosystems.

# Chapter 2

## First Weight Estimation

Weight is an important consideration in the performance and design of an aircraft. The design experience has shown that the lowest-weight design is also the lowest-cost and most efficient design. Every addition to the weight results in an increment in the wing area, thrust, and fuel consumed leading to further increase in weight and adversely affecting performance and costs. Therefore, weight estimation holds a very significant role in design. The preliminary design phase of an aircraft consists of estimating the fundamental parameters like aircraft maximum take-off weight (MTOW or  $W_0$ ), wing reference area ( $S_w$  or  $S_{ref}$ ), and engine power ( $P_E$ ). These three parameters govern the aircraft size and manufacturing cost. The weight estimation is generally done by breaking the total weight into several parts and calculating the individual weights. The four essential elements are:

- Payload Weight ( $W_P$ )
- Crew Weight ( $W_C$ )
- Battery Weight ( $W_B$ )
- Empty Weight ( $W_E$ )

The payload and crew weight are mostly known from the mission requirement and data available. These are not dependent on aircraft take-off weight. However, the fuel weight and empty weights are both functions of MTOW. The following calculations are carried out.

$$W_0 = W_P + W_C + W_B + W_E \quad (2.1)$$

The crew weight of the UAV is zero. Thus,

$$W_0 = W_P + \frac{W_B}{W_0}W_0 + \frac{W_E}{W_0}W_0 \quad (2.2)$$

From Equation (2.2),  $W_0$  can be written as,

$$W_0 = \frac{W_P}{1 - \left( \frac{W_B}{W_0} + \frac{W_E}{W_0} \right)} \quad (2.3)$$

Since the UAV conceptualized has an electric propulsive system, the fuel weight is taken to be zero.

## 2.1 Payload Weight Estimation

This table has been mentioned above but we will also be mentioning it here for easier access and better topic alignment.

Equipment	Product Name	Weight	Quantity
Camera	Sony Alpha A7R IV	665g	1
Gimbal	Three axis Aluminium brushless Gimbal	177.5g	1
Flight Controller	Pixhawk 4 mini	15g	1
GPS Module	u-Blox M8N	9g	1
IMU	MPU-9250 IMU	2000-3000g	1
Sensing Technology	LIDAR	1000g	1

The payload in our case will essentially consist of seed dispersal machinery, the seeds and the sensor details as mentioned above. The total payload is estimated to be around 6-7kg.

### 2.1.1 Choice of Power Plant

We believe that using an electric motor rather than a fuel engine would benefit us and here are a few reasons why:

#### Environmental benefits:

- **Reduced emissions:** Electric motors produce zero tailpipe emissions, unlike fuel-powered engines which emit greenhouse gases and pollutants. This aligns perfectly with the mission's goals of ecological restoration and enhancing biodiversity.
- **Quieter operation:** Electric motors are significantly quieter than fuel engines, minimizing noise pollution that can disturb wildlife and local communities.

#### Mission efficiency:

- **Lower operating costs:** Electricity can be cheaper than fuel, especially in the long run, reducing the overall operational costs of the UAV mission.
- **Increased payload capacity:** Electric motors typically weigh less than fuel engines, allowing the UAV to carry more seeds or other equipment for monitoring and data collection.
- **Improved efficiency:** Electric motors generally have higher efficiency than fuel engines, meaning they convert more of the energy stored in the battery into useful work, resulting in longer flight times and increased coverage area.

### Safety and reliability:

- **Reduced fire risk:** Electric motors eliminate the risk of fuel leaks and fires, making the UAV safer to operate in sensitive environments.
- **Simplified maintenance:** Electric motors have fewer moving parts and require less maintenance compared to fuel engines, reducing downtime and increasing mission reliability.

Note that we will be using a Lithium ion battery for our purpose as they have higher energy density and last longer on an average as compared to lithium polymer batteries. The temperature of the batteries is not of concern to us as we will not be performing our mission under extreme weather conditions.

## 2.2 Battery Weight Estimation

The battery weight estimate is done on basis of the power required to generate the required thrust in each segment. Each segment of the flight is analysed with a set of general assumptions. To estimate the weight of the battery, we first need to estimate the total energy required by the aircraft to complete the specified mission. This will give us the total energy required to be stored by the battery.

The energy required to complete the mission can be split up into the energy required for each phase of the mission as shown in equation below.

$$E_{\text{total}} = E_{T/O} + E_{\text{climb}} + E_{\text{cruise}} + E_{\text{loiter}} + E_{\text{seed dispersal}} + E_{\text{descent}} + E_{\text{landing}}$$

The following assumptions common to all the segments are:

- The aircraft is considered as a point mass and the performance parameters are studies using this assumption.
- Since most part of the flight is steady, the entire segment calculation will be done considering steady flight.
- The lift coefficient is considered a constant as a result of the velocity pitch angle being constant and small(steady flight assumption)( +/- 5 degrees). Thus wherever necessary the lift is taken same as the total weight of the aircraft.
- Specific to our case, the weight of the airplane before/after the seed dispersal is considered a constant as seeds account for very less part of the payload and individually way very less relative to the whole aircraft. Majority of the payload weight is due to the sensors and the seed dispersal machinery.

Average span	3.5m
Mean chord	0.0855m
Cl/Cd ratio	0.866(CL/CD MAX)=15
Parasite Drag	0.047
Wing Area	$0.31 \text{ m}^2$
Density at sea level	$1.225 \text{ kg/m}^3$
Ostwald efficiency factor	0.85

Table 2.1: Tentative Design Details for first weight estimation

The following values as per the literature are taken while calculating the power for each segment:

Under the light of , lift to drag ratios for cruise and loiter were decided for maximum performance. As per the reference,[8] (pg.33)( $L/D$ )<sub>Cruise</sub> = 0.866( $L/D$ )<sub>max</sub> = 15(aprrox.) The factor of 15 in the equation is replaced by 17 in case of loiter, however we assume it to be 15 in the power estimation done further for adding some extra leverage to the battery weight incase of emergency or if the aircraft does not fly at the velocity which gives best performance for loiter and cruise.

The wing specifications were taken from [7] Note that these values are subject to change after detailed wing specification study. These are tentative averaged values. Based on these values the lift coefficient is calculated to be:

$$C_l = \frac{2L = W_0}{\rho \times V^2 \times A}$$

$$C_l = 0.01316W_0$$

Name of segment	time	distance	altitude from MSL	initial vel(m/s)	final vel(m/s)
take off	90 s	0	0 m	0	2
climb	15 min	-	0-200m m	2	20
cruise (forward)	45 min.	50 km	200m m	20	20
loiter	15 min.	1 km	200m m	10	10
descent	15 min.	50 km	200 – 0 m	20	2
seed dispersal	15 min	-	50m m	10	10
landing	90 s	0	0 m	2	0

Table 2.2: Segment details for battery weight

## 2.2.1 Power required-Cruise

For cruise  $T = D$  and  $L = W_0$

Thus thrust in terms of  $W_0$  is

$$C_d = \frac{D}{\rho AV^2/2}$$

$$C_d = Cd_0 + \frac{C_l^2}{\pi A Re}$$

$$D = T = 5.063 * C_l = 0.066W_0$$

Thus power required:

$$P = T * V_{\text{cruise}} = 1.32W_0$$

## 2.2.2 Power required-Take off and Landing

This is a highly unsteady region, with the velocity angle of attack and the velocity pitch angle changing rapidly till the transition phase. Moreover, the ground effect will have to be modelled in this phase, thus the power required for this section is considered within climb/descent where we take the velocity range from 0-20m/s rather than the transition to cruise velocity. Since our aircraft aims at a short take off and landing, this region will now account for much of the power consumption.

## 2.2.3 Power required-Climb/Descent

### Climb

For climb a part of the thrust is also used in balancing the weight. However as per the previous assumption that the velocity pitch angle is small, we will be using the same  $C_l$  value as in cruise. Since we are looking at steady flight, the velocity of climb is taken as 17m/s at a rate of climb of 2m/s which gives us an angle of 7 degrees. However to account for the take off and landing power, we will be using 20m/s as the velocity to over compensate for the power required. These values of rate of climb are taken as the maximum values for a propeller type UAV. Thus

$$T = D + W_0 * \sin \gamma$$

$$P = T * V_{\text{avg climb}} = 1.5W_0$$

### Descent

The similar set of assumptions are made for the descent part:

for descent,  $T = D - W_0 * \sin \gamma$  and  $T = 0.0277w_0$

$$P = T * V_{\text{avg descent}} = 0.33W_0$$

However, for descent part, a lot of the flight will be in glide motion thus not much power will be utilized.

## 2.2.4 Power Required-Loiter

The speed while loiter mode is less than cruise, hence we can approximate the power required per unit time in loiter as that of cruise which would give a safety margin as in reality the power required in loiter will be lesser than climb.

$$D = T = 5.063 * C_l = 0.066W_0$$

$$P = T * V_{\text{loiter}} = 0.66W_0$$

## 2.2.5 Power required-Seed Dispersal

The power required during seed dispersal will depend on the seed dispersal machinery and the number of seeds to be dispersed depending on the area of the target location. However, it will not consume a huge part of the battery power and can be considered within the 10% extra margin of the battery power for emergency purposes.

## 2.2.6 Total Battery weight

All the codes for the given sections are given in Appendix A.

Segment	Power
Take off/Land	-
Cruise	$1.32W_0$
Climb/Descent	$1.5W_0$
Seed dispersal	$1.1E_{\text{initial}}$
Loiter	$0.66W_0$

Table 2.3: Segment-wise Power consumption

Now that we have the power consumed by each section of the mission segment, we can use the approximate endurance of each segment and calculate the battery weight in terms of the total weight. Let  $E_{\text{total}}$  be the total energy required.

$$E_{\text{initial}} = P_{R_{\text{cruise}}} \times E + P_{R_{\text{climb}}} \times E + P_{R_{\text{loiter}}} \times E + P_{R_{\text{descent}}} \times E + P_{R_{\text{t/o}}} \times E + P_{R_{\text{landing}}} \times E$$

Here E is the respective endurance of that segment as taken from Table1.2.

As mentioned in the seed dispersal and the landing take off section, we will be adding a further 10% safety margin to the total energy. Thus,  $E_{\text{Total}} = 1.1 \times E_{\text{initial}}$

$$W_{\text{battery}} = \frac{E_{\text{total}}}{\eta_{\text{total}} \times SED}$$

$$\eta_{\text{total}} = \eta_{\text{propeller}} \times \eta_{\text{motor}} \times \eta_{\text{discharge}}$$

$$\eta_{\text{propeller}} = 0.85$$

$$\eta_{\text{motor}} = 0.85$$

$$\eta_{\text{discharge}} = 0.95$$

$$SED = 200 \text{ Wh/kg}$$

Hence  $W_{\text{battery}} = 0.33w_0$

## 2.3 Empty Weight Estimation

The following aircraft data was used in the plots:

UAV	$W_0$	$W_e$
Swallow Electric	9	3.3
Atlas II	10	3
SkyEye II	15	6.5
Shahbal	17.5	9.5
Arya UAV	9.75	5.5
Lancaster 5	3.55	2.4
Warmate	5.7	4
Avian Puma AE UAV	7	5.9

Using the data of the previous air crafts, the following regression curves were obtained. Thus the value of A and L are taken as 1.08012 and -0.3329 respectively.

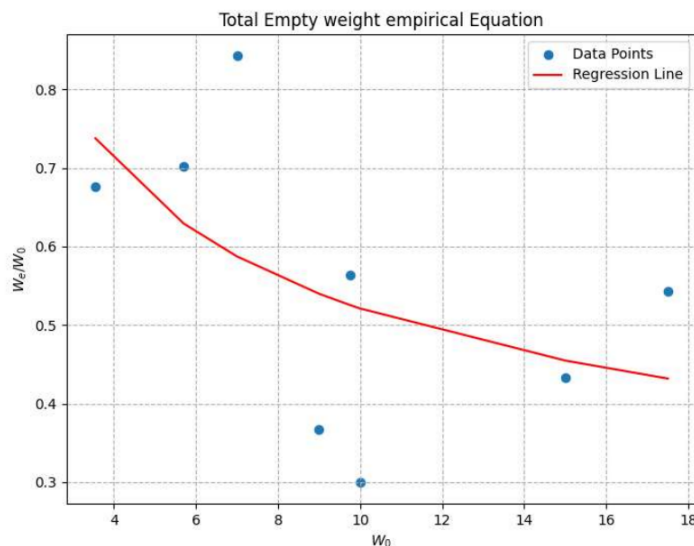


Figure 2.1: 'Direct Variation'

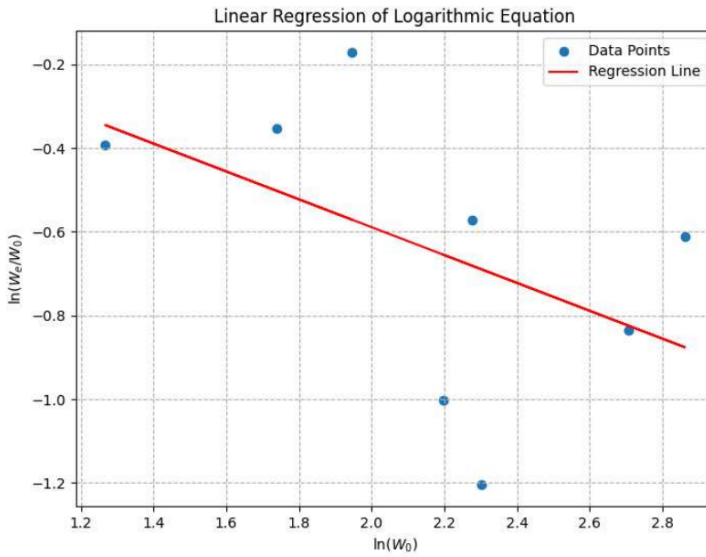


Figure 2.2: 'Logarithmic Variation'

## 2.4 Maximum Takeoff Weight Estimation

Using the slope and intercept values obtained from the logarithmic plots above, we run an iteration loop to find the maximum weight of the aircraft based on power requirements, endurance and the

$$W_o = \frac{W_{\text{payload}}}{1 - \frac{W_b}{W_o} - \frac{W_e}{W_o}}$$

$$\frac{W_e}{W_o} = A(W_o)^{-L}$$

Here  $A=1.08012$  and  $L=-0.3329$ . The iterations converged with a tolerance of 0.0001 after 17 iterations giving the maximum take off weight as 21.3882kg. The table below shows the values generated at certain iterations upto convergence.

Iteration	MTOW	$W_{\text{battery}}$	$W_e/w_0$
1	25.8	10.32	0.438
3	22.245	8.898	0.4003
8	21.567	8.632	0.3886
12	21.3880	8.555	0.3895
14	21.3883	8.555	0.3895
17	21.3882	8.555	0.3895

Table 2.4: MTOW Estimation

Hence, we can finalize the following weight estimations,

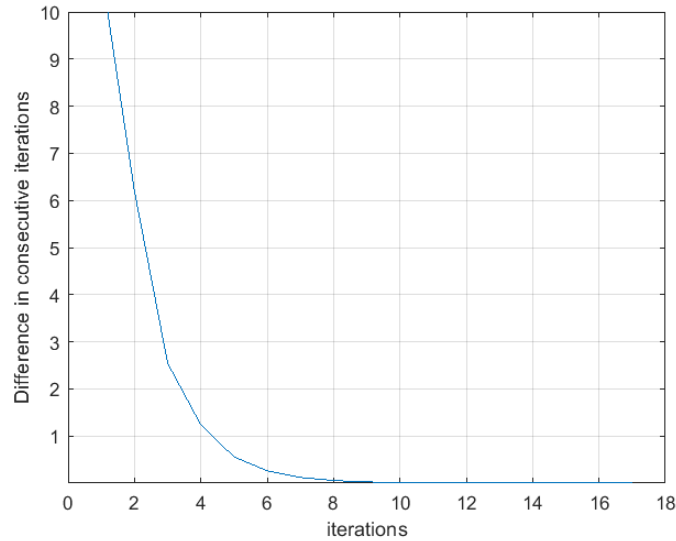


Figure 2.3: 'Convergence plot'

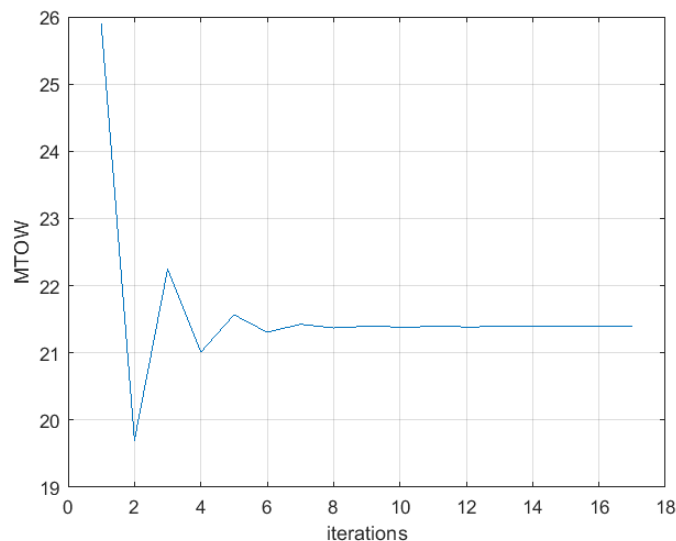


Figure 2.4: 'MTOW convergence'

Component	Estimated Weight
1	Payload weight: 6 kg
2	Battery weight: 8.55kg
3	Empty weight: 8.311 kg
MTOW	21.388kg

Table 2.5: Total Weight Estimations

NOTE: Note that this is the first weight estimate and is subject to change based on the further considerations that will be incorporated in future:

- Prospective use of Canard to increase the lift and further reduce the runway distance.

- Change in the airfoil selection for the wing which may alter the ratio of coefficient of lift and drag.

In previous Chapter, there was a mistake in accounting for the power during climb. Assuming steady climb, we calculated the power for unsteady flight and neglected the W term. The mistake has been rectified in section 2.2.4. However the battery weight remains the same as this was a mistake in documenting not calculations.

# Chapter 3

## Power Plant Specifications

Taking a closer look into the values of the aerodynamic coefficients of previous aircrafts, in this section , we find the drag coefficients and the power requirements based on our First weight estimation. Then we proceed to do the selection of the propeller and the motor based on the maximum power requirements. The motor and propeller should be able to give maximum power /thrust in the segment which requires the highest power. They should also meet the endurance requirements of the mission thus have enough weight and energy requirements.

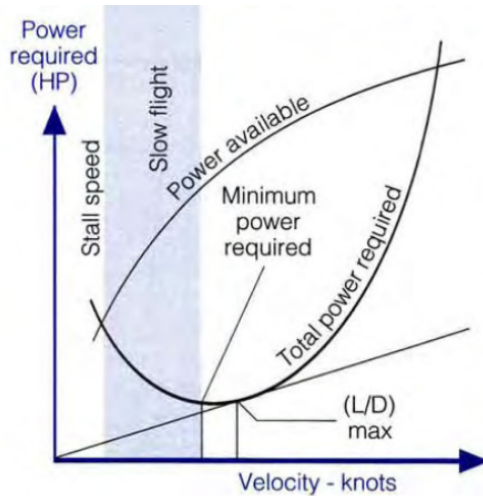


Figure 3.1: 'Power Calculations'

As per the above plot, we will calculate the power required for each segment. The power that the motor/propeller can provide(power available) should be higher than that.

### 3.1 Calculating $C_{D_0}$

The primary equation used in the calculation of  $C_{D_0}$  is as given in [8] Pg. 281 as follows:

$$(C_{D_0})_{\text{subsonic}} = \frac{\sum (C_{f_c} F F_c Q_c S_{\text{wet } c})}{S_{\text{ref}}} + C_{D_{\text{misc}}} + C_{D_{L\&P}}$$

Here, FF is the form factor and Q is taken to be 1. The Cd0 of each aircraft is found using this formula and thus the L/D of each aircraft is found, the formula of which requires CD0 of each aircrafts. Note that, as explained before we take the ratio of Swet by Sref as a constant as 2.01 for wings but varying for each aircrafts and will be calculated as discussed below.

$$S_{\text{wet-total}} = S_{\text{wet-wing}} + S_{\text{wet-fuselage}} + S_{\text{wet-tail}}$$

Assumptions:

1. The miscellaneous Drag was neglected.
2. Thus essentially the total parasite drag is the combination of parasite drag due to the wing and the fuselage, the calculations for which are discussed below.
3. The Swet formula for the wing was calculated as given in [8](discussed below).
4. The Swet formula for the fuselage is estimated using a formula and image processing, which is also discussed further below.
5. For  $C_f$ , we have used the turbulent equations as the Reynolds number in each case turns out to be in the turbulent regime.  $C_f = \frac{0.074}{Re_L^{1/5}}$
6. For the Reynolds Number of Wing, the mean chord is taken as the reference parameter, and for the fuselage, the length of the aircraft is used.

$$R_e = \frac{\rho u l}{\nu}$$

Where

$$\rho = 1.22552 \text{ kg/m}^3$$

$$u = 20 \text{ m/s (cruise speed)}$$

$l$  = is the characteristic length taken as the fuselage diameter for Re of the fuselage and as mean chord for re of the wing.

$$\nu = 1.8 \times 10^{-5} \text{ Pa.s}$$

### 3.1.1 $S_{\text{wet}}$ for wing

The Swet of the wing was calculated using the formula:

$$S_{\text{wet}} = S_{\text{exposed}} [1.977 + 0.52(t/c)]$$

as taken from [8]

The value of t/c was taken as 0.1 as seen from literature review and similar aircrafts.(Note that this is a value bound to be changed after the wing specifications are calculated. The maximum value is taken right now to prevent less estimation of power required).

The  $S_{\text{exposed}}$  is taken as  $S_{\text{ref}}$  for a wing found using image processing websites. Thus this value is 2.01.

### 3.1.2 Swet for fuselage

The Swet formula for fuselage as give in Raymer is:

$$S_{\text{wet}} \cong 3.4 \left( \frac{A_{\text{top}} + A_{\text{side}}}{2} \right)$$

However, finding the  $A_{\text{top}}$  and  $A_{\text{side}}$  from oblique view pictures of previous aircrafts would lead to inaccuracies and maybe lead to lesser power consumption due to less drag value.

Hence it was decided to rather go with a formula that gives an approximate for the fuselage wetted area based on the lengths found using pixel counting method.

Thus the fuselage was broken down into conical front, cylindrical middle and again a conical end, and thus the surface area of each section was calculated. This will be overestimating the Swet for fuselage. An image of one example is given below.

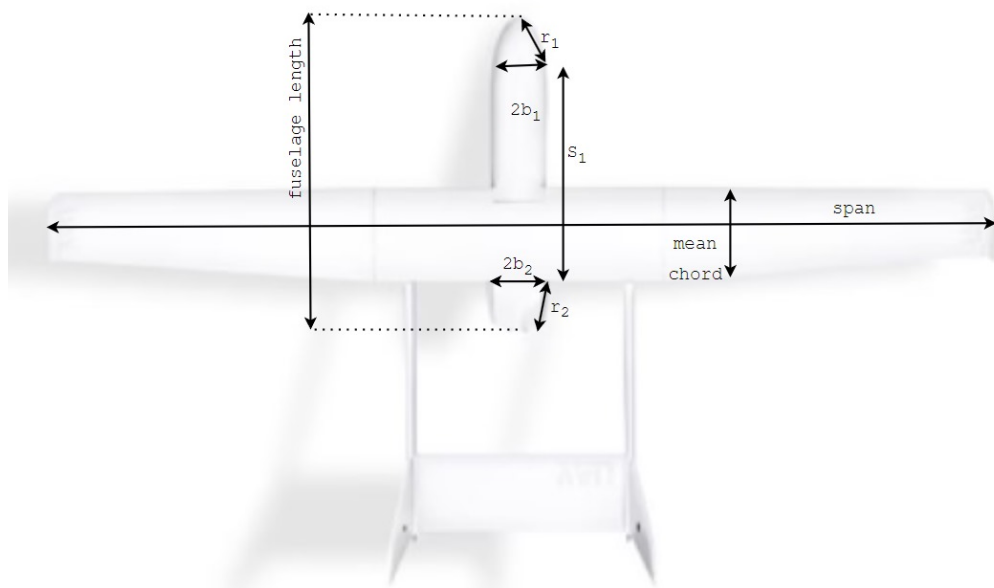


Figure 3.2: 'Visualization representation of how Swet for fuselage was calculated'

The formula for the same is:

$$S_{\text{wet-fuselage}} = \pi * r1 * b1 + \pi * r2 * b2 + \pi * s1 * (b1 + b2)/2$$

### 3.1.3 Swet for horizontal/Vertical Tail

The horizontal and vertical tail will not account for much of the wetted area and this can be accounted for in the extra fuselage area that we are calculating as explained above or in the motor specification when we use a motor which is capable of providing 10% extra max power than what is needed.

## Calculation of FF- Form factor

This is only for fuselage of the aircrafts, for wing this term is taken as 1. As mentioned in two different editions of [8], For aircrafts having  $l/d$  lesser than 6, the following formula gives a good approximate of form factor for fuselage:

$$FF = \left( 1 + \frac{60}{f^3} + \frac{f}{400} \right)$$

For aircrafts having  $l/d$  greater than 6, the following formula gives a good approximate of form factor for fuselage:

$$FF = \left( 0.9 + \frac{5}{f^{1.5}} + \frac{f}{400} \right)$$

Here  $f = l/d$ , where  $l$  is the fuselage length and  $d$  is the maximum fuselage diameter.

### 3.1.4 Previous aircraft data

We use image processing to find the required lengths for the aircrafts. The method explained above was adopted to find the coefficient of parasitic drag and thereby the  $C_l/C_d$  relations were used to find the Lift to Drag ratio at which each of these aircrafts fly. After finding the  $C_d 0$  for each airplane using the swet calculations as explained above, the wetted aspect ratio is calculated using:

$$AR_{\text{wet}} = \frac{AR_{\text{normal}}}{\frac{S_{\text{wet}}}{S_{\text{ref}}}}$$

The entire code is well written and documented in Appendix B.

## Image Processing

- To know the dimensions of the aircraft we used a web application known as "ImageJ.js". It is an open source image processing package. ImageJ.js is a JavaScript library that provides functionality for image processing and analysis within web applications. It is based on the popular ImageJ software, which is widely used for scientific image analysis. ImageJ.js brings the capabilities of ImageJ to the web platform, allowing developers to perform various image processing tasks directly in the browser.
- To measure the various parts of aircraft length, We first Uploaded the image which is in top view and then set a reference scale (like the known length of aircraft's wing span). After that we measured the dimensions like mean chord (by averaging the minimum chord length and maximum chord length), fuselage length, and other relevant parameters.

Table 3.1: Aircraft Data

Aircrafts	Span (m)	Chord_max (m)	Length (m)	Planform area (m <sup>2</sup> )	Fuselage diameter (m)	Mean chord (m)	l/d
SKYEYE Sierra	3	0.299	1.52	0.815562	0.182	0.2615	8.35
Lancaster-5	1.5	0.227	0.982	0.328354	0.115	0.22	4.463
UAV Sitaria	5.16	0.39	1.939	1.314104	0.357	0.274	5.431
Penguin BE	3.3	0.24	2.27	0.79	0.288	0.2265	7.88
Albatross	3	0.28	-	0.6069	0.193	0.217	
SKYROBOT FX-20	3.16	0.397	1.05	0.5929	0.157	0.274	6.68
Blackswift s2	3	0.23	1.673	0.604032	0.188	0.208	8.89
Atlas II	2.1	0.266	1.15	0.539232	0.099	0.274	11.61
Shahbal	3.22	0.237	1.921	0.76314	0.223	0.237	8.244
Arya UAV	3.22	0.345	2.093	1.11484	0.139	0.345	15.05
Warmate	1.6	0.217	1.1	0.259128	0.126	0.177	8.73
Avian Puma AE UAV	2.8	0.383	1.657	0.8358	0.177	0.2985	9.36

Aircrafts	s1	b1	b2	r1	r2	l2	l1	l3	Fuselage Area
SKYEYE Sierra	0.79	0.167	0.153	0.205	0	0	0.054	0.397	0.451
Lancaster-5	0.468	0.102	0.095	0	0.041	0.006	0	0.145	0.151
UAV Sitaria	0.591	0.358	0.333	0.877	0.522	0.273	0.493	0.641	1.408
Penguin BE	0.4	0.278	0.254	0.514	0.198	0.079	0.224	0.334	0.638
Albatross	0.289	0.195	0.168	0.422	0	0	0.129	0.165	0.294
SKYROBOT FX-20	1.194	0.21	0.112	0.188	0.097	0.017	0.062	0.604	0.683
Blackswift s2	0.517	0.158	0.176	0.136	0.318	0.088	0.034	0.271	0.393
Atlas II	0.576	0.092	0.083	0	0.074	0.01	0	0.158	0.168
Shahbal	0.43	0.225	0.177	0.44	0.222	0.062	0.156	0.272	0.489
Arya UAV	0.585	0.118	0.12	0.16	0.105	0.02	0.03	0.219	0.268
Warmate	0.623	0.12	0.103	0.146	0.307	0.05	0.028	0.218	0.295
AvianPuma AE UAV	0.589	0.157	0.164	0.107	0.819	0.211	0.026	0.297	0.534

$$\bullet \quad l1 = r1 \times b1 \times \pi \quad \bullet \quad l3 = s2 \times \pi \times b_{mean} \quad \bullet \quad l2 = r2 \times b2 \times \pi$$

Since we are using a propeller based engine rather than a jet engine, the quantity we are most concerned about is the lift by drag ratio at minimum power consumption. This will be the ratio of lift to drag at which the aircraft will be cruising.

Minimum power occurs when the quantity  $\left(\frac{C_L^{3/2}}{C_D}\right)_{\max}$  is achieved. Using drag polar and differentiating, we find that:

$$\left(\frac{C_L^{3/2}}{C_D}\right)_{\max} = \frac{(3C_{D,0}\pi e AR)^{3/4}}{4C_{D,0}}$$

Thus  $\frac{L}{D}$  at the above relation is  $\sqrt{\frac{3\pi e AR}{16*C_{D,0}}}$

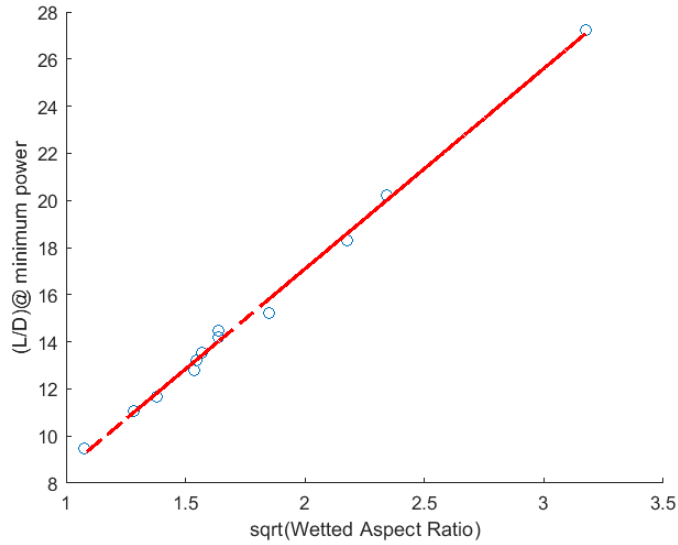


Figure 3.3: 'L/D variation with sqrt of wetted aspect ratio'

From the above plot, we can see the the ratio of lift to drag at minimum power consumption is the linearly varying with the square root of wetted aspect ratio. This is a good fit with the previous aircraft data. The value of slope and the intercept is: 8.51 and 0.089 respectively.

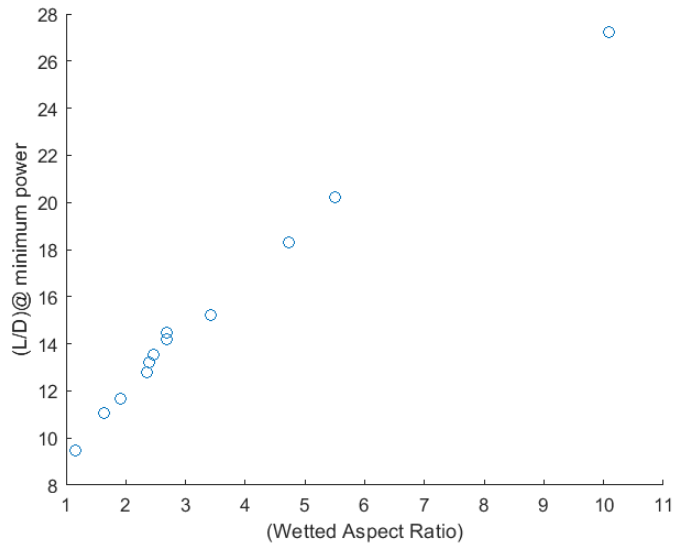


Figure 3.4: 'L/D variation with wetted aspect ratio'

## 3.2 P/W Calculation for each segment

Using the average value of L/D and using the straight line equation via the linear regression plot, we can find the averaged values for the quantities that we will need for power estimation of each segment of the aircraft. The following table shows the values that will be used for further calculations.

L/D	15.1144
AR_wet	2.6
Swet/Sref	3
Sref	1.9 m <sup>2</sup>
AR	8
span	3m
Cd <sub>0</sub>	0.0130

For the oswalds efficiency factor, the following formula from [8] will be used.

$$e = 1.78(1 - 0.045(AR)^{0.68}) - 0.64 \text{ On applying AR}=8, \text{ the } e \text{ value turns out to be } 0.81.$$

### 3.2.1 Cruise

The L/D at cruise is the maximum L/D at which the propeller based aircraft flies. The L/D at minimum power is taken as the average values from the previous aircraft data as formulated above. The average is 15.11. Thus the L/D for cruise is 17.45 Corresponding to 17.45 L/D at cruise we get an aspect ratio wetted and normal aspect ratio as thus,

$$\frac{T}{W} = \frac{D}{L}$$

$$\frac{P}{W} = \eta \times \left( \frac{T}{W} \right) \times v$$

Using propeller efficiency as 0.85(as used in the previous Chapter 2 aswell) and velocity of the cruise as 20m/s. we get P/W as 0.92 for the cruise section.

### 3.2.2 Loiter

At loiter, for a propeller based engine, the aircraft is flying at minimum power. This occurs at (L/D)<sub>min</sub> power.

$$\left( \frac{C_L}{C_D} \right)_{\max} = \frac{(C_{D,0}\pi e AR)^{1/2}}{2C_{D,0}}$$

Thus we can see that for a propeller based aircraft,

$$\left( \frac{L}{D} \right)_{\text{Loiter}} = 0.866 \left( \frac{L}{D} \right)_{\text{Cruise}}$$

The velocity in loiter is approximated as 10m/s.

Thus based on this the P/W for loiter is 0.53.

### 3.2.3 Take off and Landing

$$v_{\text{stall}} = \sqrt{\frac{W}{0.5\rho C_{L_{\max}} S}}$$

$V_{stall}$  is the lowest velocity that the aircraft can go till. It is calculated to be around 9.3m/s According to the NACA series of airfoils (which we will be using for our purpose) the average  $C_{lmax}$  is 1.5 and so we have used that in the calculation of  $V_{stall}$ .

$$P_{T/O} = \left( \frac{1}{2} \rho v_{L/O}^2 S C_D + \mu m g \right) v_{L/O}$$

$v_{L/O}$  is taken as 1.2 times  $v_{stall}$ . Value of  $\mu$  is taken as 0.02 and  $C_D$  as 0.04 (considering ground effects and maximizing the possible Drag coefficient at take off). Thus P/W for take off comes out to be 0.5. The Weight in this formula is taken based on the FIRST WEIGHT ESTIMATE in chapter 2.

### 3.2.4 Climb

During climb, as assumed before, the velocity pitch angle is taken to be 7 degrees and the velocity during climb as 17m/s. This is assuming a steady climb segment. Thus rate of climb, which is the vertical velocity of the aircraft, is taken as 2m/s. This is in accordance with the general rate of climb for the propeller based uavs.

$$P = (W \sin \gamma + D) v_{climb}$$

Using the Rate of Climb formula (from [1] we can find the power to weight ratio of the aircraft,

$$(R/C)_{max} = \frac{\eta_{pr} P}{W} - V_{(R/C)_{max}} \left[ \sqrt{\frac{K C_{D,0}}{3}} + \sqrt{3 K C_{D,0}} \right]$$

here,  $K = \frac{1}{\pi e A R}$  and propeller efficiency is taken as 0.85 as in earlier cases. Thus the P/W for climb is 3.5204.

### 3.2.5 Descent

Not much power will be used for descent as majority part of the descent will be in glide mode and the rest will be accounted as redundancy as we will take 10-15% extra energy and power while calculating the battery weight and the motor.

## 3.3 Total Power

Thus we have revised P/W of each segments. We can use the formula in chapter two to find new energy in terms of the aircraft weight to find the new total weight of the aircraft.

Segment	P/W	P	Velocity	Thrust
Cruise	0.91	236.2W	20m/s	11.81N
Climb	3.52	739.2W	17m/s	43.48N
Loiter	0.53	136.5W	10m/s	13.65N
Takeoff	0.5245	110.145W	9.6m/s	11.47N

Table 3.2: Total power Consumption of UAV

## 3.4 Selection of Configuration and Motor

### 3.4.1 Configuration of the UAV

In a propeller-driven UAV, two distinct configurations are apparent. The plane is propelled forward by a front nose-driven propeller, also referred to as a "Tractor". Another type of propeller is a rear-driven propeller, known as a "Pusher", since it has a motor and a propeller nose pointing backward to provide push thrust. To fully utilize the performance of the selected motor and propeller configuration, the configuration is crucial and it depends on the mission profile of the UAV and the mode of take off and landing of the UAV.

#### Tractor Configuration:

##### Advantages:

- The tractor configurations are silent. They don't make much noise, unlike the pusher, because the front propeller receives direct "clean" un-disturbed airflow from the front, causing the air to flow through the blades more smoothly and balanced on each side of the propeller blade, which is why they don't make much noise due to low vibration incident to the blade.
- The clean air then pushes to the back along the main wings, giving more direct airflow to the aileron control, elevator, and rudder control, allowing better maneuverability at low speed because each control surface receives constant steady airflow from the propellers even if the forward airspeed is at minimum.
- On the performance side, Tractor setup on FPV/UAV models doesn't require long take-off and landing space. Some are almost STOL (Short Take Off and Landing) capable when proper wing surface control receives a full amount of airflow along the main wings.

##### Disadvantages:

- The cockpit view on Tractor driven plane aren't much an appealing for forward viewing because the front are mostly obstructed by big propellers.
- In FPV flights, the majority of pilots dislike it because it obstructs camera viewing, especially during recording.

- Scale planes with bigger and heavier propellers, having huge inertial weight on their propeller blades that will “torque roll” the whole plane fuselage if it suddenly takes off without getting enough airspeed to allow airflow around the wings to counter the effect.

## **Pusher Configuration:**

### Advantages:

- Pusher planes are usually ideal for FPV because the propellers are located at the back and don't obstruct the camera's forward viewing and recording.
- They are very popular for hand-launched and belly landing style flying platforms, and the pilot can also safely catch these planes during landing in the air because there's nothing in the nose to hurt their hands.

### Disadvantages:

- The pusher configurations are definitely a very noisy setup because pusher propellers receive “unclean” or disturbed airflow that runs through various surfaces on the airframe before it reaches the propeller blades. Clean forward air bumps along the fuselage nose, windshields, cameras, wing leading edges, and other surfaces, causing an unstable ripple of wavy air and then hits the propeller blades at the final destination.
- The uneven wave of "disturbed" air from slammed from various sides causes each propeller blade to flex/vibrate unevenly throughout the RPM, causing noisy pitching sounds. It's like the different amplitude of waves in the ocean hitting differently on each side of your boat.
- Because of being slammed by different forces of airflow into the blades, pusher airframe owners always use hard type composite blades such as APC type blades to counter flexy pitch blade problem, thus reducing bleed of thrust performance. Smaller blade pitch and length help to minimize the problem and ease fast rotation to generate thrust.
- The pusher only pushes airflow through the elevator and rudder surface control because the pusher motor is usually located behind the main wing. To take off, the pusher plane has to speed forward fast to get more wind/airflow under the wings, thus requiring a longer runway to take off and land. However, this can be compensated by having a bigger and longer wingspan to generate short lift-off capability but with added weight for an extra inch of wing extension. This can be seen on glider-type pusher props.

As concerned with the mission profile of the our UAV, the seeds are needed to be dropped during the cruise. The estimated payload for the UAV is found to be 6 kgs, which is substantial and almost equal to the empty weight of the UAV.

- If we go with the pusher configuration, the majority of the power plant weight is concentrated on the middle section of the UAV, which leaves us to place the battery in the front of the plane and payload at the back of the plane.
- If we go with the tractor configuration, the battery and the motor is placed at the nose of the plane, to counter this weight the payload and the sensors are placed at the end of the plane, accounting for the required location of center of gravity.
- We need to reduce the vibrations on the plane for precise dropping of the seeds and to get accurate data from the LIDAR sensor, for which the tractor configuration is more suitable.
- Since, the UAV for our mission profile is required to take off and land in inaccessible area, where a proper runway is unavailable, and more over the UAV has a landing gear. So, the tractor configuration is optimal for our use.

**The selected configuration of our UAV is Tractor configuration**

### 3.4.2 Motor Selection

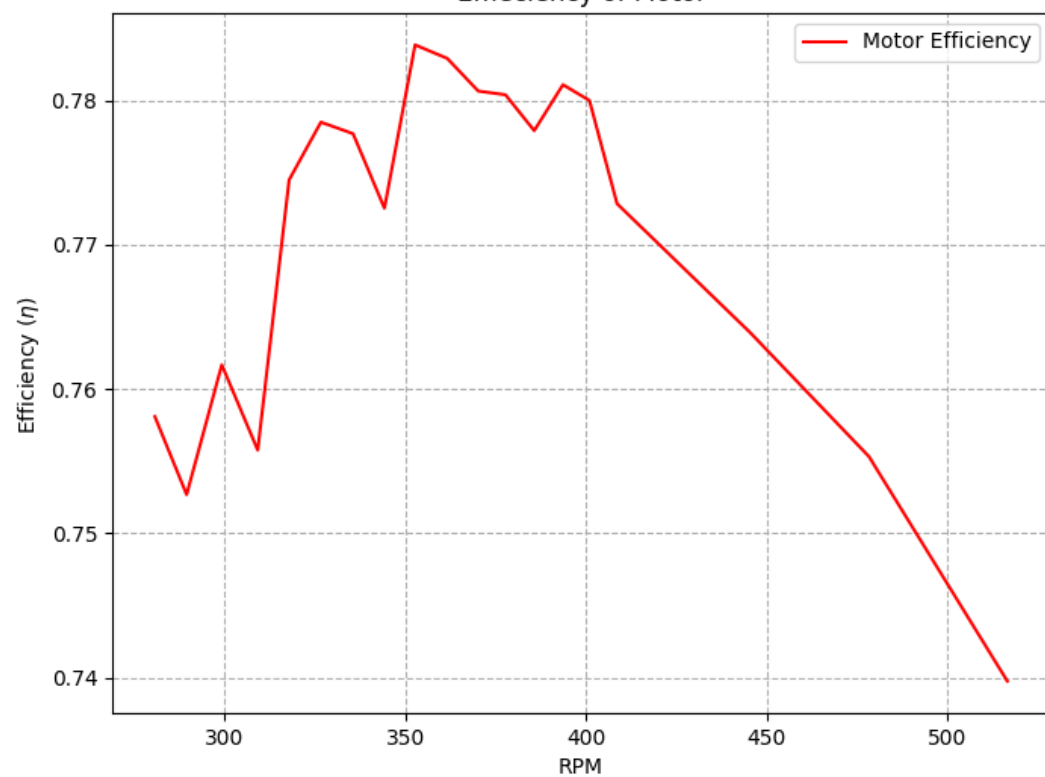
The selection of Motor and propeller depends on the maximum power utilized by the UAV during the mission. Based on the power estimation we got, [3.2](#) the maximum power is consumed during the climb (739.2 W) and also the maximum thrust required (43.48 N). Based on the power, thrust estimation and the data available on the motors specification [3.3](#), the best suitable for my UAV will be **Antigravity MN6007 KV320**, which can generate a maximum thrust of 53.995 N. Using the motor specifications, [E.1](#) given in the Appendix, we can calculate the propeller efficiency and motor efficiency using the following formulas

$$\eta_{motor} = \frac{\text{Mechanical Power output}}{\text{Electrical Power input}} = \frac{\text{Torque} \times \text{RPM (in rad/s)}}{\text{Power (W)}}$$

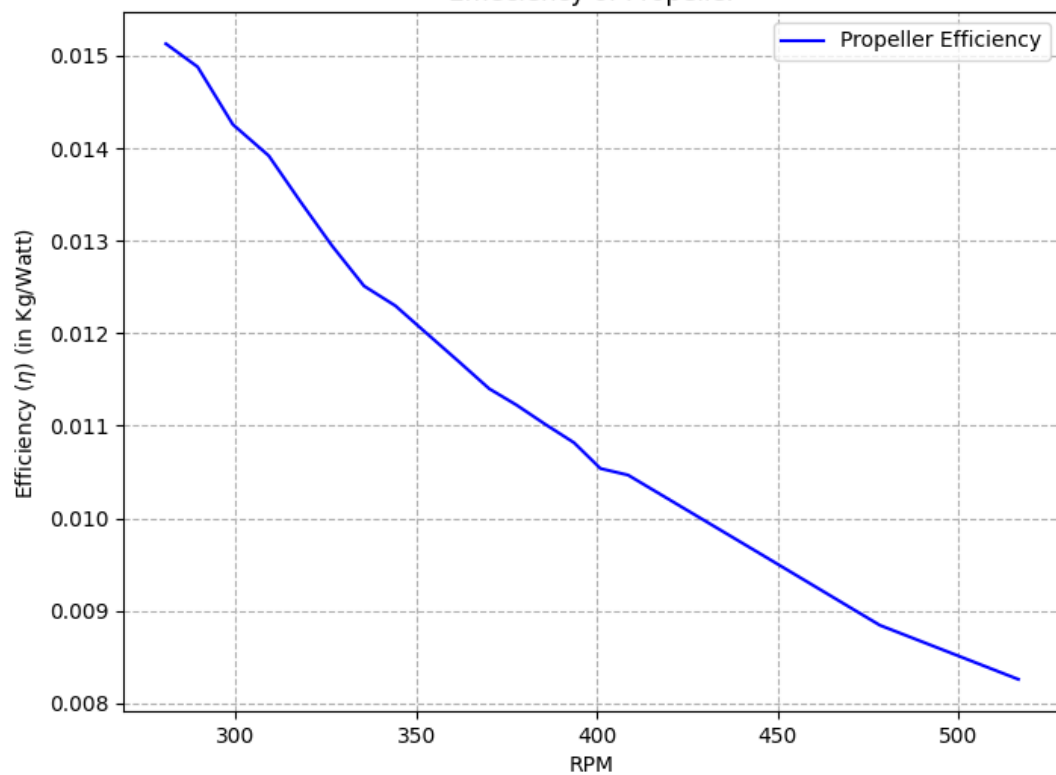
$$\eta_{propeller} = \frac{\text{Thrust} \times \text{velocity (in m/s)}}{\text{Mechanical power output}}$$

From the graph below, we can see the variation of the motor efficiency with RPM, considering the optimal and for safe conditions, we are considering the motor efficiency to be  $\eta_{motor} = 0.74$ . As per the data sheet, the efficiency of the propeller P22\*6.6 Propeller will be close to  $\eta_{propeller} = 0.8$ .

Efficiency of Motor



Efficiency of Propeller



Motor Name	Thrust (N)	Torque (N.m)	Motor Weight (g)	Propeller (inches)	Voltage Rating (V)	Current (A)
Antigravity MN8014 KV100	125.79	4.19	392	9.5	50.4	52
Antigravity MN6007 KV320	53.955	1.3	172	21 - 22	50	38.31
ALTUS X60 Uno 120kv	99.23	3.23	403	28	44	46.5
Tarot TL96020 5008 340KV	36.297	3.7	168	12-15	25.2	26.5
Tiger Motor MN701S KV280	92.55735	2.66	340	24 - 26	22	80.60
T-Motor AM670 KV480	91.7	2.28	416.1	18-10	21.65	109.93
T-Motor MN801-S KV120	80	4.16	470	28 - 29	47.8	48.79
T-Motor U10 Plus 80kv	65.3346	2.734	511	26 - 29	40	22.38
Hobbywing X9 motor 110kv	188.4	-	1400	34.7	46	82.7
ALTUS X60 Duo	172.9	3.53	403	30	67.2	120

Table 3.3: Motor Specifications

For our design, we have decided to mount two Antigravity MN6007 KV320, on the UAV for the following reasons,

- For reliability issues, incase of failure of one motor, we can still get back our UAV using the other motor in full capacity.
- using two motors, we don't have to put full load on the single motor which reduces its life span.
- Using two motors running at 55% throttle, we can **produced the required thrust which just 20 A current supply**, where as with one motor to produced the power required, we have supply a total of 39 A and need to keep the motor running at maximum capacity.
- The total flight time can be increased

### 3.4.3 LiPo Battery calculations:

For a Lithium ion batteries used in UAV, the following specification are crucial for deciding the appropriate battery for the mission

- **Battery Voltage:** Generally LiPo batteries are a pack of single batteries connected in series, with voltage of 3.7 V. A 3S 11.1 V LiPo is a pack of 3 3.7 V LiPo batteries connected in series together to get 11.1 V.
- **Battery Capacity (in mAh) :** For the computation to work, you must convert your battery's capacity (often measured in milliampere-hours) into amp-hours. To convert milliampere-hours to amp-hours (mAh to Ah), divide your battery capacity by 1,000.
- **Battery steady Current Rate (C-rating) :** The C rating will appear as two digits separated by a slash, such as 60/90 or 40/120. The first number denotes the constant current it can deliver. This is the amount of current that the lipo battery can deliver on a continuous basis without significantly dropping voltage (and killing the battery).

The second number is the burst current, or the amount of current that the lipo battery can produce in a short period of time; normally, this is much higher current, and the voltage will begin to drop rapidly as well.

- **Battery Discharge:** You cannot fly with a LiPo battery unless it is totally flat. This is because there is a limit to the number of amp-hours that may be discharged before the battery cannot be recharged. This means that a LiPo's effective capacity is only 80% of the total amp-hours. It is recommended that Lithium Ion batteries are not operated below SOH = 0.8.

- **Flight Time** = 
$$\frac{\text{Battery Capacity} \times \text{Battery Discharge}}{\text{Average Amp Draw}} \times 60$$
 (in minutes)

Based on the motor power consumption, and power consumption of other electronic components on board, we can decide the suitable battery for our UAV. According to the motor specification ([motor specifications](#)), the current drawn is 9.61 A at 52% throttle, which will be the most suitable operating conditions to produce the required thrust and the battery for this specific motor is 6s lipo battery, which is 22.2 V battery.

The other electronic components Lidar sensor, servo motors, IMU sensor, camera draws current less than 250 mA - 500 mA. In total, we will take the total power drawn by these components to be 2 A. Therefore the total current drawn by the UAV in extreme condition is 22 A.

With a TATTU 22.2V 25C 6S 22000MAH Lipo Battery, the flight time we can get is

$$\text{Flight Time} = \frac{22Ah \times 0.8}{22A} \times 60\text{min} = 48\text{mins}$$

Flight time = 48 minutes, to increase the flight time, we can connect two or three similar Lipo batteries in parallel connection. This is in accordance to the battery weight fraction that we got in chapter 2 in first weight estimation(battery weight can be about 7kg) In total, we will get **Flight time = 144 minutes** with three TATTU 22.2V Lipo Batteries

The selected configuration for the UAV,

- Motor : Two Antigravity MN6007 KV320
- Propellers : P22\*6.6
- LiPo Battery : Two-Three 22.2V 25C 6S 22000MAH Lipo Battery

In previous chapter, we mentioned that the propeller driven aircraft will fly with minimum power at cruise. However, since we are using a propeller driven aircraft, loiter will occur at minimum power and the cruise will occur at maximum value of  $L/D$ . These values have been corrected in chapter 3. However the values for battery, motor and propeller selection remain unchanged as they are calculated based on maximum power loading which occurs in climb condition.

# Chapter 4

## Wing Loading

Using the Power loading found in previous chapter, we will now find the wing loading for different segments and for different constraints during the flight. The following constraints are essential to consider while calculating the wing loading. Using this wing loading, an optimal wing shape and specifications will be decided.

- Stall Velocity
- Cruise
- Climb with maximum ROC
- Maximum ceiling
- Sustained turn(loiter)
- Maximum Velocity

### 4.1 Constraint Based on Stall Velocity ( $V_{stall}$ )

#### 4.1.1 Calculating $V_{stall}$

Since our mission profile requires us to have a short take off landing(runway constraints) we will decide on  $V_{stall}$  based on the runway requirements. Using the formula that relates the take off speed and the take off distance:

$$s_{LO} = \frac{(V_{LO}^2)(W/g)}{2 \{T - [D + \mu_r(W - L)]_{av}\}}$$

Writing  $T = P/V$  and using  $[D + \mu_r(W - L)]_{av} = [D + \mu_r(W - L)]_{0.7v_{LO}}$  we get an approximate relation between lift off velocity and the take off distance. Take off speed( $V_{LO}$ ) is taken as 1.1 times the stall speed.

Surface	$\mu$ -typical values	
	Rolling (brakes off)	Brakes on
Dry concrete/asphalt	0.03–0.05	0.3–0.5
Wet concrete/asphalt	0.05	0.15–0.3
Icy concrete/asphalt	0.02	0.06–0.10
Hard turf	0.05	0.4
Firm dirt	0.04	0.3
Soft turf	0.07	0.2
Wet grass	0.08	0.2

Figure 4.1: Coefficient of Friction Values

Thus using the stall speed we can find the maximum  $C_{l\max}$  for our aircraft.

$$v_{\text{stall}} = \sqrt{\frac{W}{0.5\rho C_{L\max} S}}$$

According to [8] the  $C_{l\max}$  should be around 3.5 for a short take off landing aircraft which we will verify using the mentioned formula and steps.

Note that we have taken the maximum possible runway distance without rotation. Short take off landing aircrafts rotate after a certain runway distance to accelerate lift. However, we consider the worst possible case here.

#### 4.1.2 Determining the Take off distance and roughness value

Using the table given in [8], we take the typical roughness coefficient value for our mission to be 0.045.(rolling distance- brakes off). The following plot taken from [6] shows the variations of the take off distance of a normal fixed wing UAV with the payload.

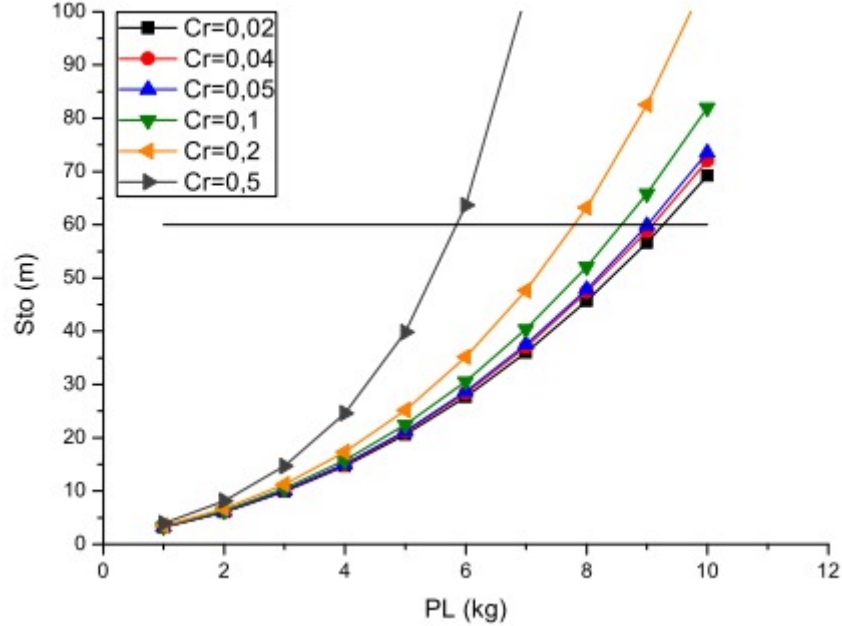


Figure 4.2: Selection of Takeoff Distance

Note that as mentioned earlier we are considering no rotation for this iteration of the runway distance. Hence according to this plot, the runway distance is around 50m

Thus plugging in the values in equation, we get the following values:

S_take off	53.69m
V_take off	7.20m/s
Cl_max	3.7
V_stall	6.6m/s
$\mu$	0.045

## 4.2 Wing Loading for Take off

Using the take off distance decided above, we use the plot in [8] to find the TOP(take off parameter) to find the wing loading for take off segment of the flight.

$$\begin{aligned} \text{Prop: } (W/S) &= (\text{TOP})\sigma C_{L_{TO}}(\text{hp}/W) \\ \text{Jet: } (W/S) &= (\text{TOP})\sigma C_{L_{TO}}(T/W) \end{aligned} \quad (4.1)$$

Thus we take the TOP as 100 and  $C_{L_{TO}}$  as 3.30 based on the take off velocity. The P/W is taken as what was derived in Chapter 3 for the P/W for take off.

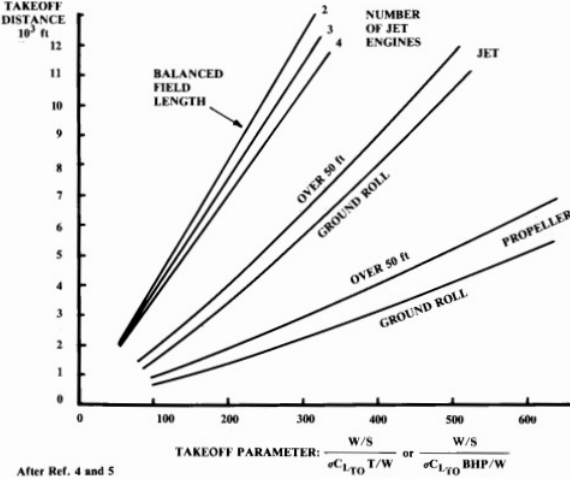


Figure 4.3: Plot for Takeoff Parameter

## 4.3 Wing loading for Stall speed

In a cruising flight with the stall speed, the aircraft weight must be balanced with the lift ( $L$ ) :

$$L = W = \frac{1}{2} \rho v_{stall}^2 S C_{L_{max}}$$

Here,  $C_{L_{max}}$  is the aircraft maximum lift coefficient. By dividing both sides in the above equation by  $S$ , we get:

$$\left( \frac{W}{S} \right)_{v_{stall}} = \frac{1}{2} \rho v_{stall}^2 C_{L_{max}}$$

For our case, we use the values found and mentioned in table in section 4.1.2 based on the runway constraint.

## 4.4 Wing loading for Maximum speed

We consider a propeller-driven aircraft flying at maximum speed at the cruise altitude. The aircraft is in longitudinal trim; hence, the maximum available engine power ( $P_{max}$ ) must be equal to the maximum required power ( $P_{req}$ ), which is thrust multiplied by maximum speed:

$$\eta_P P_{max} = T V_{max} \quad (4.2)$$

If we denote power at the cruise altitude as  $P_{alt}$  and the power at sea level as  $P_{SL}$ , we can write:

$$P_{alt} = P_{SL} \left( \frac{\rho}{\rho_0} \right) = P_{SL} \sigma \quad (4.3)$$

In the trim condition, the thrust is equal to the drag, and the lift is equal to the weight. Using this fact and the expression for the drag polar, we can write:

$$\eta_P P_{SL} \sigma = \frac{1}{2} \rho v_{max}^3 S \left( C_{D_0} + K \left( \frac{2W}{\rho v_{max}^2 S} \right)^2 \right) \quad (4.4)$$

Dividing by weight, W, and inverting the equation, we get the final relation:

$$\left( \frac{W}{P_{SL}} \right)_{v_{max}} = \frac{\sigma \eta_P}{\frac{1}{2} \rho v_{max}^3 C_{D_0} \left( \frac{1}{\frac{W}{S}} \right) + \frac{2K}{\rho v_{max}} \left( \frac{W}{S} \right)} \quad (4.5)$$

Using the fact given in equation 4.58 in [9]

$$V_{max} = (1.2 - 1.3) V_{Cruise}$$

Thus we use maximum velocity as 25m/s. Since our aircraft will be going at a maximum altitude above mean sea level of 200-300m we take the value of  $\sigma$  as 0.9

## 4.5 Wing loading for Cruise

In the same way, we derived the relation for maximum speed; we derive the relation for cruise velocity as:

$$\left( \frac{W}{P_{SL}} \right)_{v_{cruise}} = \frac{\sigma \eta_P}{\frac{1}{2} \rho v_{cruise}^3 C_{D_0} \left( \frac{1}{\frac{W}{S}} \right) + \frac{2K}{\rho v_{cruise}} \left( \frac{W}{S} \right)}$$

Velocity for cruise is taken as 20m/s and the value of  $\sigma$  as mentioned is taken as 0.9 as not much difference in densities is observed within 200-300 metres.

## 4.6 Wing loading for Climb

In the previous chapter, we have used the maximum rate of climb and the velocity corresponding to that to find the power loading for climb. We use the same quantities here. On calculating the Velocity at maximum roc, we get 17 m/s using a pitch angle of 7 degrees and the rate of climb as 2.03m/s.

$$(ROC) = \frac{P_a - P_{req}}{W} = \frac{\eta_{pr} P - DV}{W} \quad (4.6)$$

$$P_R = DV = \frac{W}{C_L/C_D} \sqrt{\frac{2 \frac{W \cos \gamma}{S}}{\rho C_L}} \quad (4.7)$$

For maximum rate of climb, power required should be minimum.

$$P_R \propto \frac{C_D}{C_L^{3/2}} \quad (4.8)$$

Hence, minimum power required occurs when the airplane is flying such that  $\frac{C_L^{3/2}}{C_D}$  is a maximum value.

$$C_{L_{\frac{C_L^{3/2}}{C_D}}} = \sqrt{\frac{3C_{D_0}}{k}} \quad (4.9)$$

The velocity at which  $P_R$  is a minimum occurs at:

$$V_{\frac{C_D}{C_L^{3/2}}} = V(R/C_{\max}) = V(P_{R_{\min}}) = \sqrt{\frac{2W \cos \gamma}{\rho_\infty S_{\text{ref}} \sqrt{\frac{3C_{D_0}}{k}}}} \quad (4.10)$$

$$V(R/C_{\max}) = V(P_{R_{\min}}) = \sqrt{\frac{2W \cos \gamma}{\rho_\infty S_{\text{ref}} \sqrt{\frac{3C_{D_0}}{k}}}} \quad (4.11)$$

Thus substituting all in equation 4.6

$$\begin{aligned} ROC_{\max} &= \frac{\eta_P P_{\max}}{W} - \sqrt{\frac{2}{\rho \sqrt{\frac{3C_{D_0}}{K}}} \frac{W}{S} \frac{1.155}{(L/D)_{\max}}} \\ \left(\frac{W}{P}\right)_{ROC} &= \frac{1}{\frac{ROC}{\eta_P} + \sqrt{\frac{2}{\rho \sqrt{\frac{3C_{D_0}}{K}}} \frac{W}{S} \frac{1.155}{(L/D)_{\max}}} \eta_P}} \end{aligned}$$

## 4.7 Wing loading for Maximum Ceiling

At the absolute ceiling, the rate of climb is zero. From this fact, we get:

$$\begin{aligned} (R/C)_{\max} &= \frac{\eta_{\text{pr}} P}{W} - \frac{D}{W} \sqrt{\frac{2W}{\rho_\infty S_{\text{ref}} \sqrt{\frac{3C_{D_0}}{k}}}} = 0 \quad (\text{as it is maximum ceiling}) \quad (4.12) \\ \left(\frac{W}{P_{SL}}\right)_{AC} &= \frac{\sigma_{AC}}{\sqrt{\frac{2}{\rho_{AC} \sqrt{\frac{3C_{D_0}}{K}}} \frac{W}{S} \frac{1.155}{(L/D)_{\max}}} \eta_P}} \end{aligned}$$

Here  $\sigma_{AC}$  is the ratio of the densities at sea level and the absolute ceiling.

## 4.8 Wing loading for Sustained turn

As given in [8], for a sustained turn during loiter, we will be using the given formulas. However for a sustained turn, an additional consideration of load factor comes into picture and the load factor for a particular aircraft, can take only a certain range of values. The constraint on  $n$ (load factor) is given below. Thus for our aircraft we chose the value of  $n$  to be 2.5(as seen from literature) and the value of  $T/W$  corresponding to this  $n$  has to be greater than 0.13.

We take T/W as the below equation which comes out to be 0.534 for the parameters of our aircraft.

$$\frac{T}{W} = \frac{qC_{D_0}}{W/S} + \frac{W}{S} \left( \frac{n^2}{q\pi Ae} \right)$$

$$\frac{W}{S} = \frac{(T/W) \pm \sqrt{(T/W)^2 - (4n^2 C_{D_0}/\pi Ae)}}{2n^2/q\pi Ae}$$

Constraint:

$$\frac{T}{W} \geq 2n\sqrt{\frac{C_{D_0}}{\pi Ae}}$$

## 4.9 Conclusion

Segment/Constraint	W/S
Cruise	173.006
Climb	128.17
Max. Ceiling	1360
Stall speed	91.8
Loiter	104.8
Max. Speed	345.2
Take off	135.6

The following plot shows the variation of W/P with W/S for each segment for a more qualitative understanding.

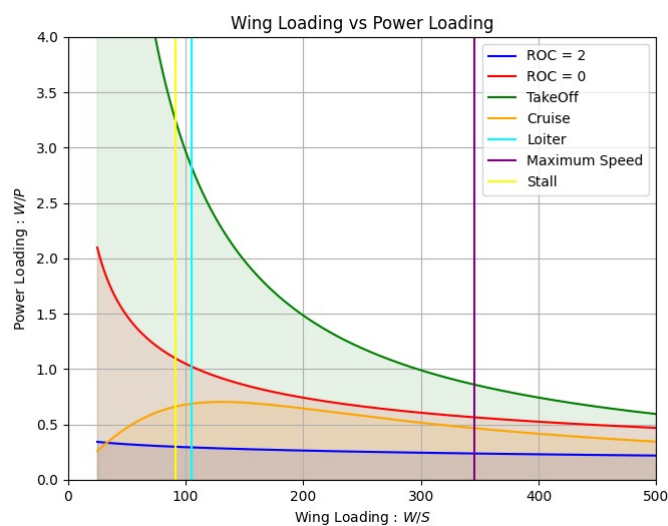


Figure 4.4: W/P VS W/S

We have to choose the W/S which gives the least value in a particular segment. Lower wing loading for an aircraft signifies lesser speed to take off and land and turning is also faster

for a wing with lesser wing loading. Aircrafts with higher wing loading are usually meant for higher speeds. Since our mission does not aim for higher speeds, but for less runway distance, low altitude and medium speed, we have to particularly choose the wing loading that is the least which will eventually meet the requirements of the other segments as well. From the table we can see that stall speed constraint has the lowest wing loading.

Thus the chosen value of  $W/S$  is 91.8. The wing design will be done based on this. Based on first weight estimate, then span area should be  $2.28m^2$

# Chapter 5

## Second Weight Estimate

Now that we have the wing loading estimate and the power consumption for each section, we can find a better estimate of the weight for our aircraft.

### 5.1 Fixed Quantities

From the above Chapter 3 and 4, the following quantities remain fixed irrespective of the fractional or total weight:

- $\frac{L}{D}$  during loiter and cruise remains constant(since it is taken from the plot made from previous aircraft data), hence the power loading in loiter and cruise remains constant.
- $AR/AR_{wet}$ , ostwalds efficiency factor is fixed as the corresponding  $\frac{L}{D}$  is fixed.
- The value of A and L obtained from regression using previous aircraft data for first weight estimation remains the same.

The following quantities depend on weight of the aircraft:

- Power loading during Take off, Power loading during climb.
- The wing loading for each segment will depend on Power loading for that section, however, the segment with least wing loading is the segment of our interest, thus only the wing loading for the stall speed constraint will be considered while estimating the second weight.

Assumptions:

- The take off distance and thus the stall speed and the maximum lift coefficient are considered as a constant as the value is same as calculated in chapter 4 for simplicity and since it matches with the data from previous aircraft.

### 5.1.1 Method

In chapter 3, we have selected the battery to give us the required endurance. We will be using the TATTU 22.2V Lipo Batteries which each weight 2.49kg. Hence the total battery weight is taken as 7.5kg. Using the weight fraction formula used in chapter 2, we will find revised weight of the aircraft.

$$W_o = \frac{W_{\text{payload}} + W_{\text{battery}}}{1 - \frac{W_e}{W_o}}$$

$$\frac{W_e}{W_o} = A(W_0)^{-L}$$

This is the fixed weight of the aircraft and will be used for further calculations.

Thus iterating this gives us a final weight of 21.98kg, with battery weight of 7.5kg and payload weight as 6kg and empty weight as 8.48kg

Using this weight we will revise the power and the wing loading to get an optimal span for the wing specifications in further chapters.

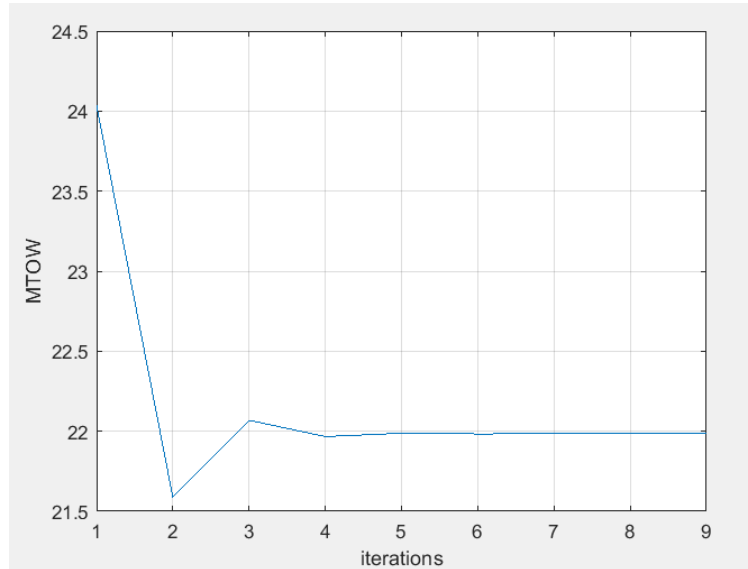


Figure 5.1: 2nd weight estimation

### 5.1.2 Revising Power and Wing loading

Just like for weight estimate, to estimate optimal span, we will have to run an iterative loop. The code for the same can be found in the appendix. Since the planform area is decided based on the wing loading and the minimum wing loading occurs at stall, to calculate optimal planform area, we will only use  $W/S$  at stalling velocity constraint. The stalling velocity, at constant weight of aircraft, itself depends on the planform area.

Thus the optimal area comes out to be  $2.20m^2$ .

Using this fixed weight and wing area, the other quantities are calculated.

Segment	W/S	P/W	Power(W)	Thrust(N)
Cruise	173.8	0.91	169.2	8.45
Climb	138	3.03	665.9	47.5
Max. Ceiling	1000	-	-	
Stall speed	84.5	-	-	
Loiter	135	0.53	98.53	9.85
Max. Speed	345	-	-	
Take off	104	0.3788	68.78	9.7
Cl_max=3.7, planform area = 2.20 m ^2				
Vstall	6.1069m/s			
R0C	1.5 m/s			

Since the maximum power is within the range of the motor we selected in chapter 3, the motor remains the same. The codes for the weight estimate is in APPENDIX A4.

In previous chapter, we decided the wing loading based on the stall and take off distance constraints, however the planform area found using those will be the extended planform area by the high lift devices. Thus the wing loading used for optimal lift coefficient is used as the Cruise wing loading, and it should have a planform area around  $1.5m^2$  in accordance to the cruise wing loading of  $150N/m^2$

# Chapter 6

## Wing and Airfoil Selection

### 6.1 Wing's Vertical Location

Table 6.1: Comparison of Wing Configurations

Configuration	Advantages	Disadvantages
High Wing	<b>Stability:</b> Better inherent stability, especially in roll.	<b>Stability in Turbulence:</b> More prone to turbulence effects.
	<b>Visibility:</b> Better downward visibility for observation.	<b>Visibility During Turns:</b> May offer poorer visibility during turns.
	<b>Ease of Access:</b> Easier access to cabin/cargo area.	<b>Structural Complexity:</b> May require complex structures.
	<b>Ground Clearance:</b> Better ground clearance for wings and engines.	<b>Ground Handling:</b> More challenging ground handling characteristics.
Low Wing	<b>Performance:</b> Better aerodynamic efficiency and reduced drag.	<b>Ground Clearance:</b> Reduced ground clearance.
	<b>Visibility:</b> Better upward visibility.	<b>Access to Cabin/Cargo:</b> Less convenient access.
	<b>Stability in Turbulence:</b> May exhibit better stability.	<b>Stability During Ground Operations:</b> More prone to tipping.
	<b>Ease of Refueling:</b> Easier refueling with accessible fuel tanks.	<b>Visibility During Taxiing:</b> May offer poorer visibility.
Mid Wing	<b>Aerodynamic Efficiency:</b> Good aerodynamic efficiency.	<b>Payload Integration:</b> Challenging integration of payloads.
	<b>Structural Simplicity:</b> Simpler structurally in some cases.	<b>Access to Cabin/Cargo:</b> More difficult access.
	<b>Visibility:</b> Good upward and downward visibility.	<b>Stability During Ground Operations:</b> Challenges in stability.
	<b>Ground Clearance:</b> Adequate ground clearance.	<b>Manufacturing Complexity:</b> May require complex manufacturing.

Based on our mission statement, a **high-wing configuration** would likely be more suitable for the fixed-wing UAV designed for afforestation. Here's why:

1. **Stability and Visibility:** High-wing configurations typically offer better stability, especially in turbulent conditions. Since our UAV will be surveying and navigating target regions, including remote and possibly rough terrain, stability is crucial for reliable flight performance. Additionally, the high-wing configuration provides better downward visibility, which is essential for assessing the terrain and identifying suitable locations for afforestation.
2. **Ease of Access and Payload Deployment:** High-wing aircraft allow for easier access to the cabin or cargo area, which facilitates the deployment of seeds in a precise and targeted manner. Our mission involves deploying seeds to promote vegetation growth, and a high-wing configuration simplifies the process of accessing and deploying payloads from the UAV.
3. **Ground Clearance:** High-wing designs offer better ground clearance for the wings and engines. This is particularly beneficial when operating in remote and potentially uneven terrain, as it reduces the risk of damage to the aircraft during takeoff, landing, and ground operations.
4. **Efficient Coverage of Larger Areas:** The use of fixed-wing UAVs with high-wing configurations enables efficient coverage of larger areas. This is crucial for afforestation initiatives, especially in remote and inaccessible locations, as it allows for comprehensive surveying and monitoring of the target regions to identify suitable terrain for afforestation and assess vegetation growth over time.

## 6.2 Airfoil Selection

For selecting the airfoil, the following considerations are kept in mind.

1. L/D at cruise is kept constant as found in chapter 4 from previous aircraft data.
2. Corresponding AR is also kept a constant due to direct variation between AR and L/D.
3. The planform area is a constant as found from wing loading. The planform area is taken as  $1.8m^2$ .
4. As a first assumption, the Coefficient of lift for the airplane and the airfoil are taken to be the same.

### 6.2.1 Calculating Reynolds number

The airfoil characteristics vary with varying Reynolds number. The Reynolds's number for our specific aircraft depends on the wing chord. Since the Aspect Ratio of the planform area is fixed, the span is also fixed at 3.7m. Using this information, and approximating the mean aerodynamic chord(MAC) length (using taper ratio varying from 0.4-0.60), we find the mean chord to be 0.45m. Thus we find the Reynolds's number using the characteristic length as MAC.

For most segment of the flight the aircraft will be cruising or loitering, thus the Reynolds's number corresponding to these stages are found and the airfoil standard characteristics are taken around Reynolds's number of 500,000.

### 6.2.2 Deciding t/c ratio

The t/c ratio has direct implications on the lift and drag. According to [8], thickness ratio affects the maximum lift and stall characteristics mainly by the effect on nose shape. For a wing of fairly high aspect ratio, a greater nose radius provides a higher maximum lift and stall angle. As per fig4.3 in [8], the maximum lift coefficient in most airfoil series is achieved with thickness ratio between 12-15%. Hence we will be looking at airfoils with the same range.

#### Cruise life-drag ratio

Since maximum part of the mission segment will be based on cruise, the optimum Cl that the chosen airfoil should be able to provide has to match with the Cl for cruise for our mission profile and requirements. the wing loading is increased to 150 as compared to what is mentioned in previous chapters, as the wing loading constraints for take off and landing will be taken care by the high lift devices as mentioned later on.

$$C_{L\text{design}} = \frac{W}{0.5\rho S v_{\text{cruise}}^2} = 0.62$$

### 6.2.3 Airfoil type

The following airfoils were shortlisted based on the requirements mentioned above:

Airfoil	Cl_max	Cl_cruise	Cl/Cd_max	AOA_cruise	stall AOA
NACA 2412	1.35	0.703	47.7	5	12
ONERA OA212	1.34	0.86	36	7	14
EPPLER EA 8	0.74	0.617	46.8	5.5	10.5
GOE 444	0.57	0.567	47.8	5.5	5.5
GOE 704	1.41	0.995	39.9	8	14

The following plots comparing the performance at different airfoils are given below. These plots

are for airfoils with a standard NACA roughness and Mach 0 (compressibility effects neglected). These plots are generated using BIGFOIL.

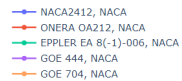
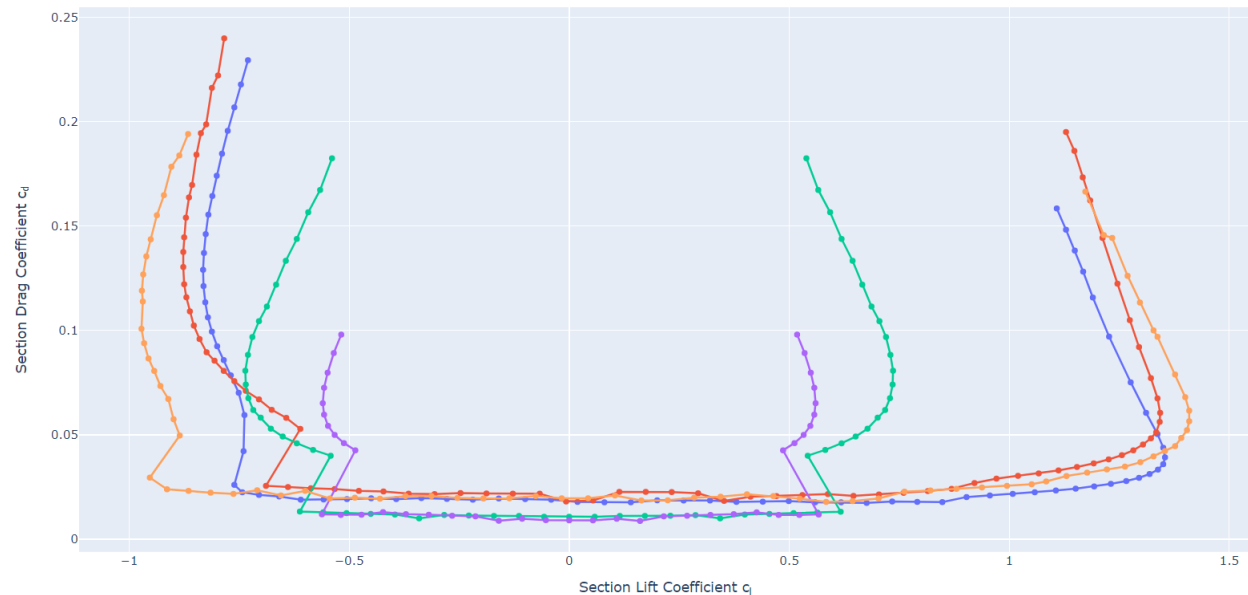
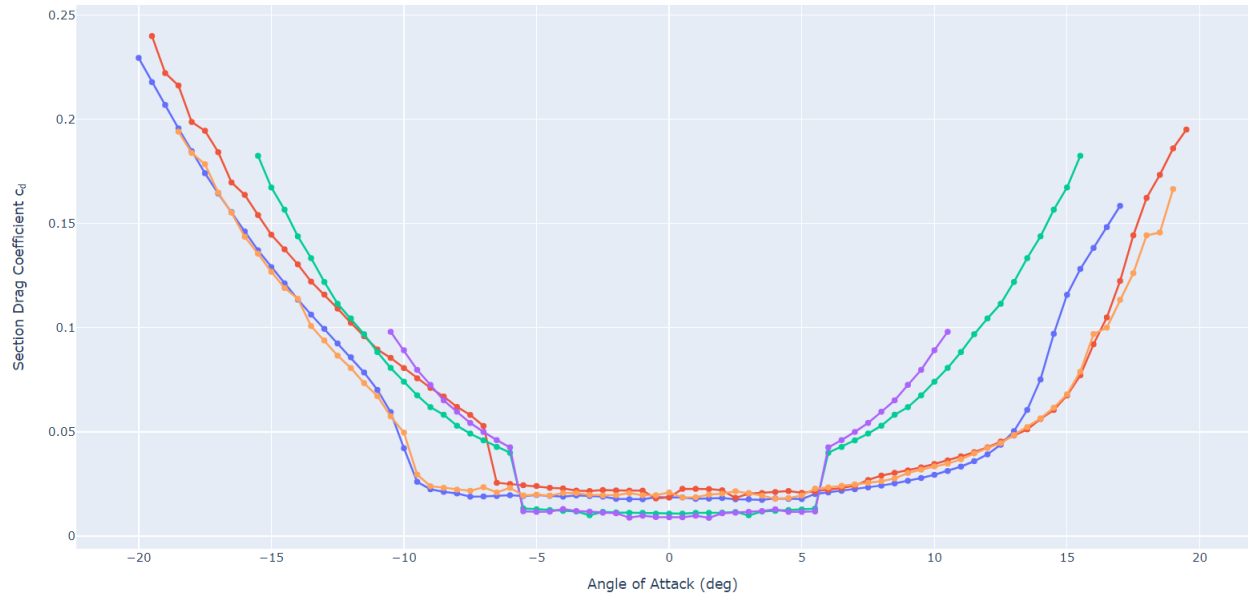
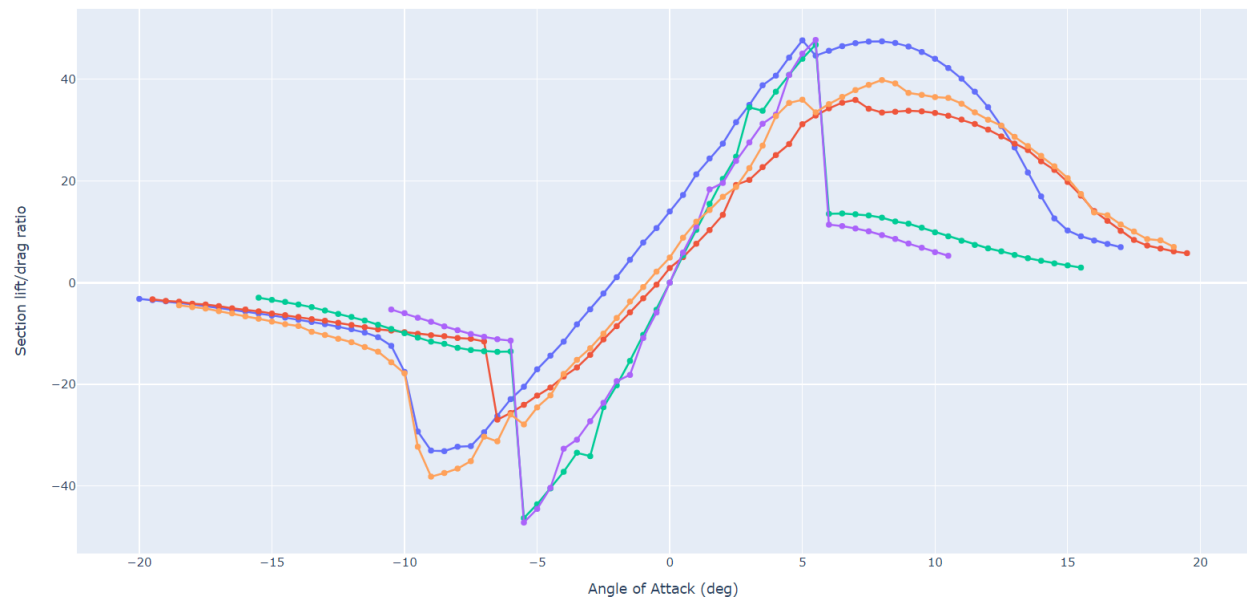
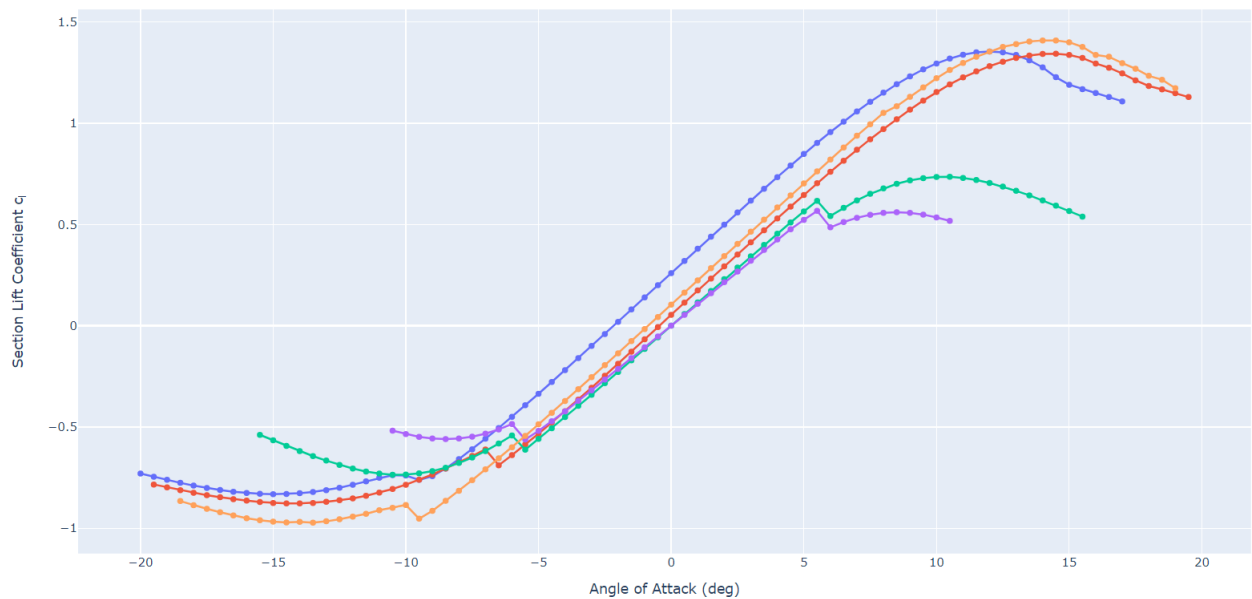
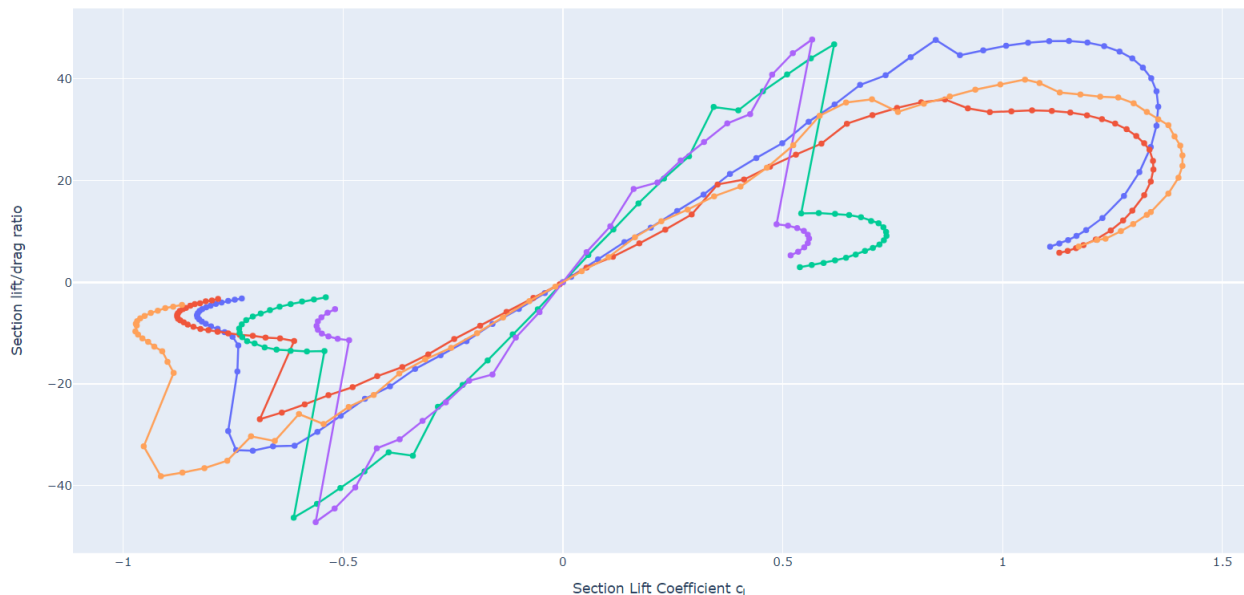


Figure 6.1: Legend







The following steps were followed while selecting the airfoil:

1. Airfoils having nearby value for optimum C (the value of Cl where the tangent of the drag polar has the highest slope) are chosen.
2. Amongst these airfoils, the airfoil having the highest lift to drag ratio for the required Cl is chosen to ensure least drag.
3. The angle of attack at the optimal Cl is verified to ensure that the angle of attack at the cruise conditions is much lower than at stall.
4. The setting angle of the wing is decided based on this angle of attack at the cruise conditions.

Even though EPPLER EA 8 gives the closest Cl at cl to the optimum value, the maximum Cl given by Eppler EA is very low and thus we decide to go ahead with NACA 2412 (higher lift drag ratio compared to ONERA OA212). Moreover, choosing an airfoil giving higher lift than what we need at cruise is beneficial as higher lift will be needed to counter balance the negative lift produced by the tail during the cruise.

Wing setting angle = 5° during cruise, velocity pitch is equal to zero.

#### 6.2.4 Wing sweep

Since we are operating at low speeds, drag divergence is not an issue, hence we will not be using an sweep for the aircraft. Due to high wing configuration, we already have enough roll stability hence we do not need wing sweep for roll stability either.

### 6.2.5 Taper ratio

From Prandtl wing theory, the taper ratio affects the lift along the span of the wing. The tapered wing will eliminate the undesired effect of a constant chord wing. Further, it influences the following qualities:

- Induced drag
- Structural weight
- Ease of fabrication

The induced drag is minimum in an elliptical wing configuration. A rectangular wing has 7% higher induced drag than an elliptical wing. Choosing a taper ratio,  $\lambda = 0.45$  almost eliminates those effects for an unswept attachment, and the lift distribution produced is very close to an elliptical wing.<sup>[8]</sup> For a tapered wing, the span loading is concentrated in the inboard portions of the wing, and the airfoil at the root is thicker than near the tip. Further, tip stalling is also not an issue for a taper ratio between 0.3 – 0.5. The only drawback is that the manufacturing cost is higher for a tapered wing than a rectangular one.

$$\lambda = 0.45$$

We can calculate the tip and root chord length using this value and the wing reference area(based on wing loading).

$$S = \frac{b}{2} (c_t + c_r) = 1.66$$

We now use the Aspect Ratio,  $\text{AR}$ , that we found in chapter3 to calculate the mean aerodynamic chord,  $\bar{c}$ . Since the wing is tapered, we shall apply the following formula for aspect ratio,

$$AR = \frac{b}{\bar{c}}$$

Where  $\bar{c}$  is the Mean Aerodynamic Chord (MAC). It is given by:

$$\bar{c} = \frac{2}{S} \int_0^{\frac{b}{2}} c(y)^2 dy$$

Where  $y$  is the length along the span of the wing and  $b$  is the span. We know that the value of  $c(y) = c_t$  at  $y = 0$  and  $c(y) = c_r$  at  $y = b/2$ . Using this to solve the equation for mean chord and substituting it along with the value of  $\text{AR}$  in the equation for aspect ratio, we get the equation

$$8 = \frac{3S}{c_t c_r + c_r^2 - c_t^2}$$

### 6.2.6 Winglet

Winglets are used to reduce wing tip vortices and the losses associated with them. Since we aim at a short take off landing aircraft, according to literature survey<sup>[5]</sup> Drooped wing tips are used in STOLs however they come with a weight penalty since they need to be added to the wing.

### 6.2.7 Wing twist

A wing twist is used to prevent tip stall and revise the lift distribution to approximate an ellipse.

However, for the preliminary design of our UAV, we have opted for a wing without any twist.

### 6.2.8 Dihedral angle

High wing configuration already ensures roll stability due to differential angle of attack. Hence there is no requirement for extra dihedral angle for stability as it may reduce the maneuverability of the aircraft. However, in order to further reduce roll stability, anhedral angle can be used. But in the preliminary wing design, we do not consider any anhedral or dihedral and will be added later on depending on the requirements of stability coefficients.

### 6.2.9 High lift devices

As calculated in chapter 4, during take off and landing, we need a wing loading ranging from  $91 - 105 N/m^2$ . Thus according to iterations carried out in previous chapter, we need a planform area of  $2.20 m^2$ . The flaps and slats have to thus extend enough to increase the planform area from  $1.66 m^2$  which is the optimum span for the weight during cruise.

#### Flaps

Flaps are used to increase the lift coefficient during take off, and in certain cases, the area of the wing. Since our mission profile has a constraint on runway distance and the stall velocity, we need to use high lift devices like flaps to increase the lift coefficient to 3+ during take off. Comparative study on types of flaps:

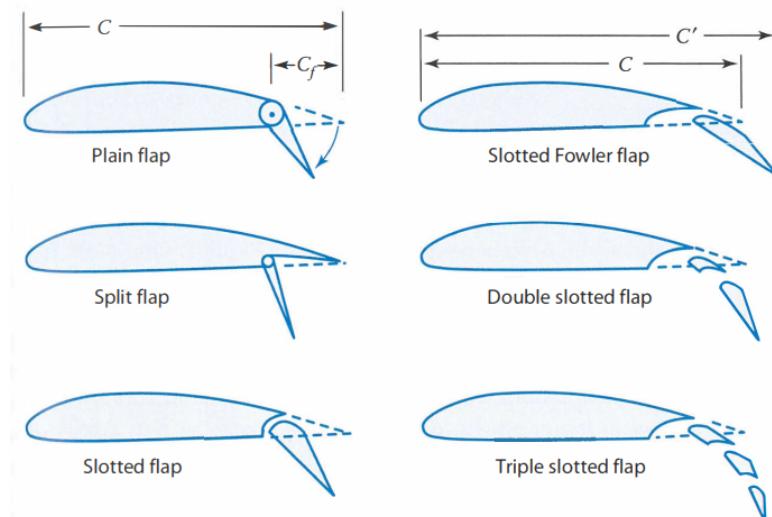


Figure 6.2: Flap Types

High-lift Device	$\Delta C_{l_{\max}}$
Flaps	
Plain and split	0.9
Slotted	1.3
Fowler	$1.3c'/c$
Double slotted	$1.6c'/c$
Triple slotted	$1.9c'/c$
Leading-edge devices	
Fixed slot	0.2
Leading-edge flap	0.3
Kruger flap	0.3
Slat	$0.4c'/c$

The fig6.3 shows the comparison between the lift generated by plain flap NACA2412 airfoil at 70% chord, 50 % chord thickness, at maximum flap deflection angle 45 degrees(orange line) and NACA2412 without any flap(green line). A plain flap can generate coefficient of lift only upto 2, without any change in surface area of the airfoil. However, we need a flap which gives a lift coefficient of higher than 3 along with the required change in surface area of the wing to balance the wing loading derived in chapter 4 and the necessary stall speed based on the runway distance.

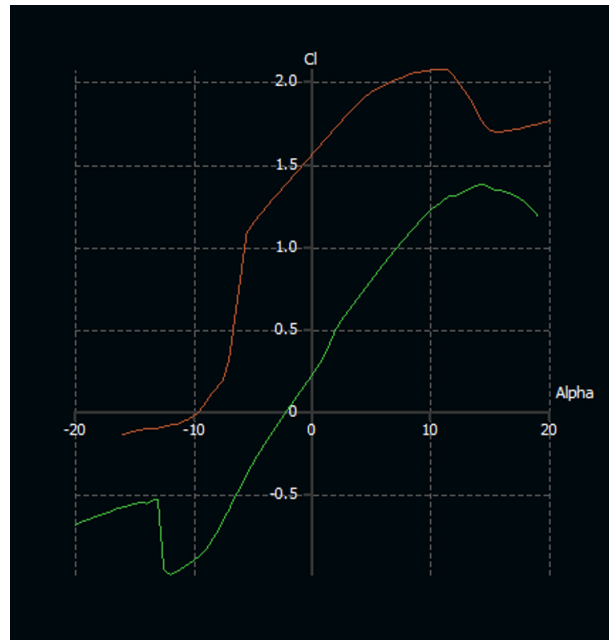


Figure 6.3: Plain flap vs no flap

The following table from section 12.4.6 of [8] shows the comparison in the change in lift coefficient in different flap types.

Thus, we have decided to go with a double slotted FOWLER flap which is attached at 30%

of the chord, thus increasing the chord length by 1.3 times at max deflection.

$$\Delta C_{L_{\max}} = 0.9 \Delta C_{\ell_{\max}} \left( \frac{S_{\text{flapped}}}{S_{\text{ref}}} \right) \cos \Lambda_{\text{H.L.}}$$

Using the formula given above, we can find the

$$\left( \frac{S_{\text{flapped}}}{S_{\text{ref}}} \right)$$

to get a desired change in the surface area of the wing to get a lift coefficient of 3 at take off. The following values are obtained:

$$\left( \frac{S_{\text{flapped}}}{S_{\text{ref}}} \right) = 1.5$$

$$\Delta C_{L_{\max}} = 2$$

$$\Delta C_{\ell_{\max}} = 1.6 * 1.3$$

Max flap deflection=  $45^\circ$ ,  $c'/c = 1.3$

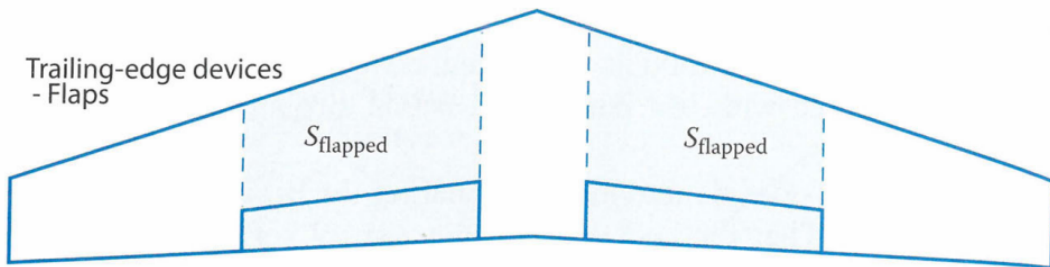


Figure 6.4: Flap area

## Slats

Similar to flaps, we have decided to go ahead with slats which help in increasing the lift by increasing camber. We use slats at maximum deflection of 20 degrees attached at 20% of the chord.

### 6.2.10 Design of Control Surfaces

The directional changes such as roll, pitch and yaw are brought about by the control surfaces. Accurate sizing of the control surfaces ensures safe operation of the UAV within the aerodynamic parameters such as bank angle, pitch angle, angle of attack. The ailerons located on the back of the trailing end of each wing cause movement or roll of the aircraft around its longitudinal axis. The elevator located on the horizontal tail takes care of the pitching motion on its transverse axis. Finally, the rudder mounted on rear of the vertical tail causes a movement of

the UAV about its vertical axis. Each of these control surfaces is actuated by a servo motor.

The values for pitch, roll and yaw coefficient are to be found out from the graphical data from the wing design model. These data are then utilized to determine the required roll, yaw and pitch rates, and the approximate required area of the control surfaces is decided to provide the UAV with appropriate roll, pitch and yaw authority. Finally, 10% of the excess area calculated is added to compensate for the empirical or manufacturing errors.

The control surface efficiencies are evaluated using the following equation, where  $C_{l\delta_a}$  is the control authority,  $y_1, y_2$  refer the control surface distance from the root and  $C_{l\alpha_w}$  is the lift curve slope of the control surfaces.

$$C_{l\delta_a} = 2C_{l\alpha_w} \int_{y_1}^{y_2} cy dy$$

$$\Rightarrow C_{l\delta_a} = \frac{2C_{l\alpha_w} \tau C_r}{Sb} \left[ \frac{y^2}{2} + \frac{2}{3} \left( \frac{\lambda - 1}{b} \right) y^3 \right]_{y_i}^{y_0}$$

Where  $\tau$  is the aileron effectiveness parameter,  $C_r$  is the wing root. The above expression is obtained by integrating  $C$ , the wing chord as the function of  $y$  along the span. The span and chord of the ailerons are approximated at 15% and 30% of the wing of the UAV, in most of the package delivering and dropping UAVs. The main factor governing the location and size of the ailerons is the desired maneuverability of the UAV. The location of ailerons also plays a major part in the structural aspect of the wing as outboard ailerons cause more twist to the wing, leading to fluttering on low aspect ratio wing.

## Aileron

In the design process of an aileron, four parameters need to be determined. They are: (i) aileron planform area ( $S_a$ ), (ii) aileron chord/span ( $C_a/b_a$ ), (iii) maximum up and down aileron deflection ( $\pm\delta_{A_{max}}$ ), and (iv) location of inner edge of the aileron along the wing span ( $b_{ai}$ ). As a general guidance, the typical values for these parameters are as follows:  $S_a/S = 0.05\text{--}0.1$ ,  $b_a/b = 0.2\text{--}0.3$ ,  $C_a/C = 0.15\text{--}0.25$ ,  $b_{ai}/b = 0.6\text{--}0.8$ , and  $\delta_{A_{max}} = \pm 30^\circ$ . Based on this, about 5–10% of the wing area is devoted to the aileron, the aileron-to-wing-chord ratio is about 15–25%, the aileron-to-wing-span ratio is about 20–30%, and the inboard aileron span is about 60–80% of the wing span.

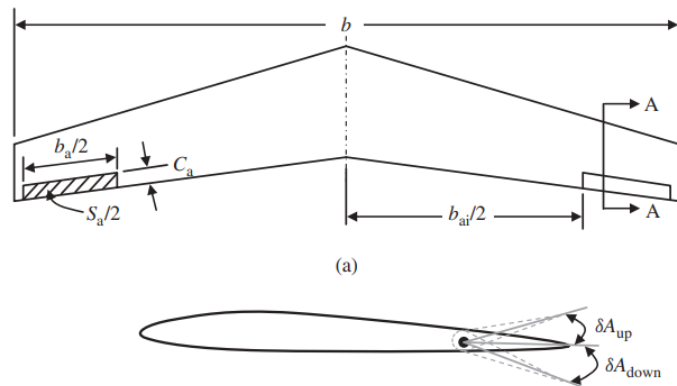


Figure 6.5: Geometry of Aileron

### 6.2.11 Final Specifications

Property	Table
Airfoil Type	NACA2412
Planform area	1.66 m <sup>2</sup>
Aspect Ratio	8
Taper ratio	0.45
Sweep	0
Dihedral	0
span	3.64m
tip chord	0.45m
root chord	0.63m
mean chord	0.48m
winglet type	Drooped
C <sub>m</sub> _alpha	negative
C <sub>m</sub> _0	negative

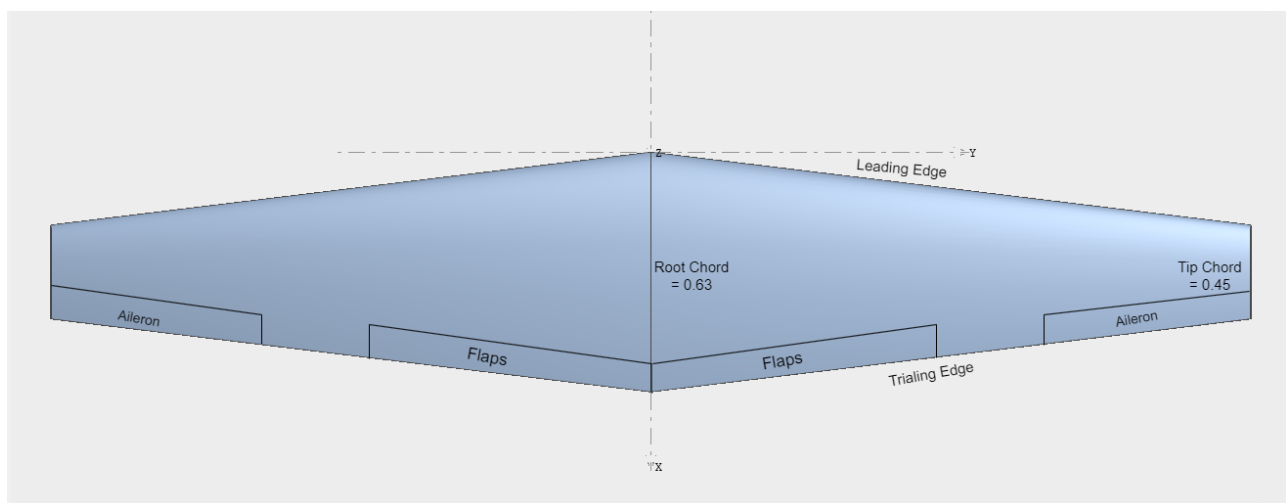


Figure 6.6: Final Wing geometry

The figure below shows the lift distribution obtained at different angles of attack for the wing only for cruise condition. The lift distribution is similar to elliptic distribution hence the efficiency of the wing will be pretty high.

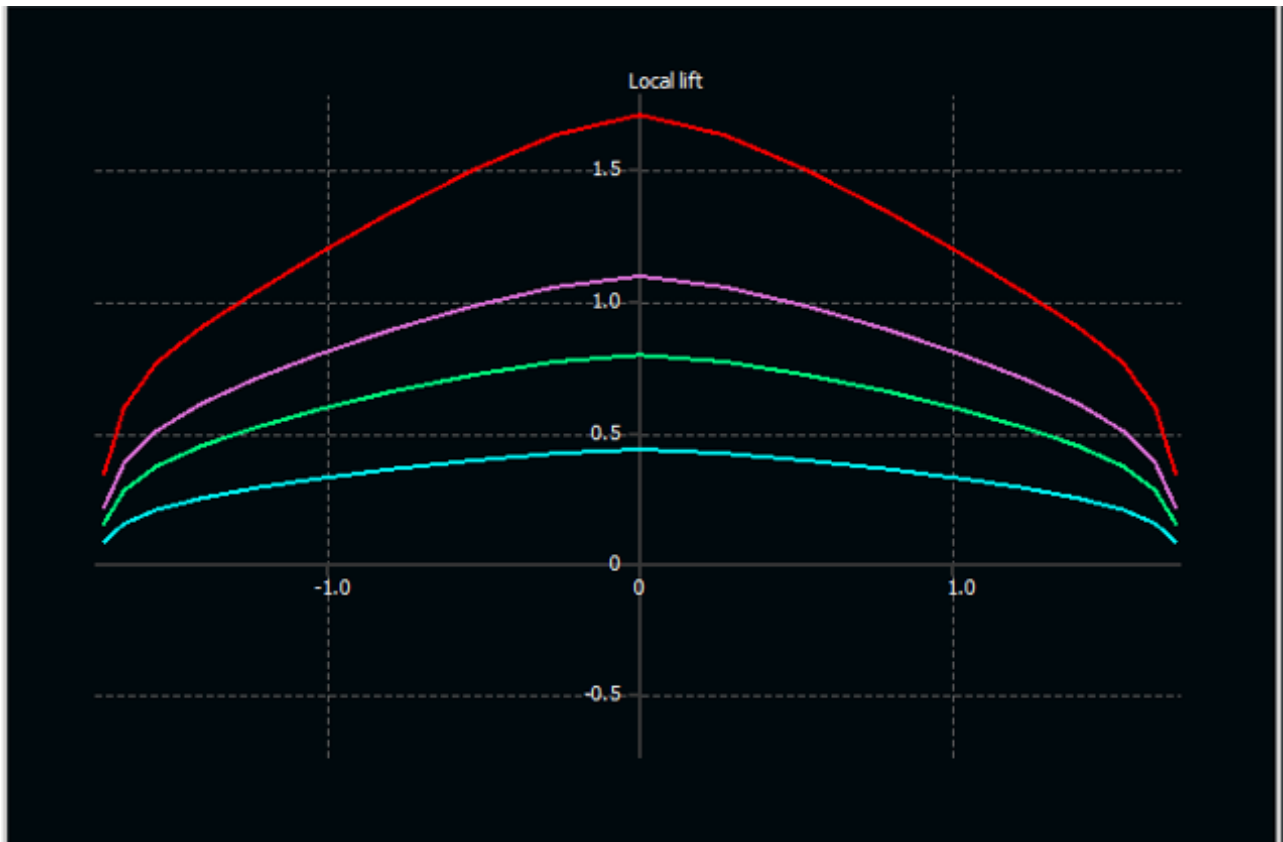


Figure 6.7: Lift distribution

The red line shows Local lift profile at  $15^\circ$ , blue is at  $2^\circ$ , pink is at  $8^\circ$  and green is a  $5^\circ$  Angle of attack. The characteristics of the wing in cruise are shown below: Note that the  $Cm_o$  is negative and will have to be made positive for static stability in the tail design chapter.

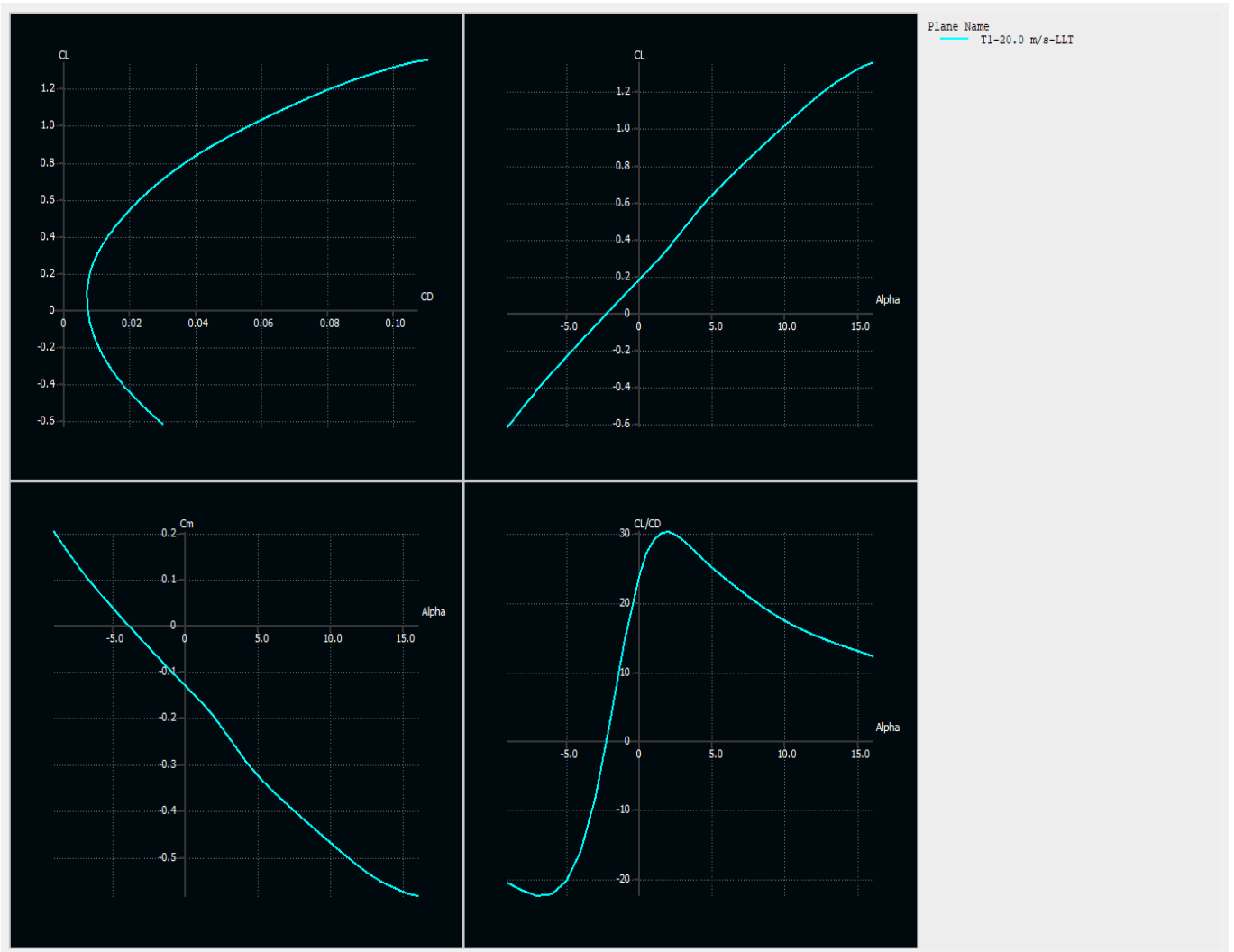


Figure 6.8: Final Wing characteristics

# Chapter 7

## Fuselage and Tail Design

### 7.1 Fuselage design

#### 7.1.1 Previous Aircraft Data

From the previous aircraft data as mentioned in table 3.5 and , we find the relation between Fuselage length and the weight of the aircraft. Since span, wing loading is also a constraint, we find the variation of fuselage length with span from previous aircraft data aswell.

#### Weight variation

$$\text{Fuselage length} = aW_0^c$$

Table 7.1: Previous Aircraft Reference data

Name	Weight(kg)	Fuselage length(m)
Atlas 2	10	1.15
Shahbal	17.5	1.921
Arya UAV	9.75	2.093
Lancaster-5	3.55	0.982
Warmate	5.7	1.1
Avian Puma AE	7	1.657
Blackswift S2	9.5	1.673
Skyrobot FX-20	12	1.05

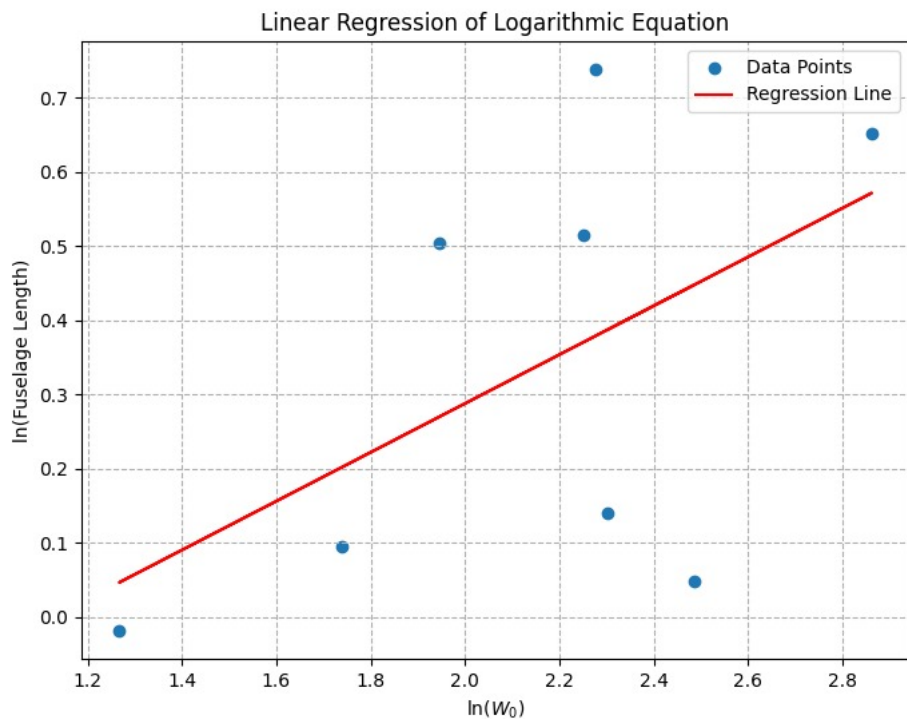


Figure 7.1: Fuselage length variation with weight-linear regression

From this, corresponding to weight of 21.98kg(from second weight estimate), we get fuselage length of 1.909m

## Span variation

Table 7.2: Previous Aircraft Reference data

Name	Span(m)	Fuselage length(m)
Atlas 2	2.1	1.15
Shahbal	3.22	1.921
Arya UAV	3.22	2.093
Lancaster-5	1.5	0.982
Warmate	1.6	1.1
Avian Puma AE	2.8	1.657
Blacksift S2	3	1.673

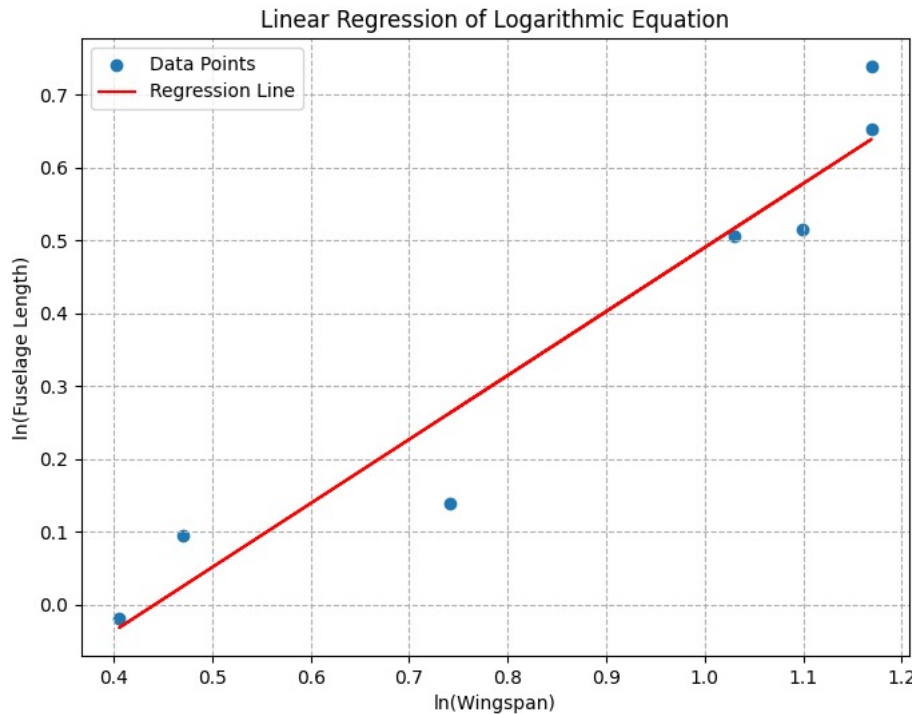


Figure 7.2: Fuselage length variation with span-linear regression

From this, corresponding to span of 3.64m, we get fuselage length of 1.8m. Taking an average of the two, the final fuselage length is 1.85m.

### 7.1.2 Payload Dimensions and Characteristics

The below pictures show the seed dropping machinery which will be used. Only the seed tank( $2000\text{cm}^2$ ) will be inside the fuselage. The remaining parts(seed dispersal) will be attached to the fuselage but not inside it. All images are taken from [10]

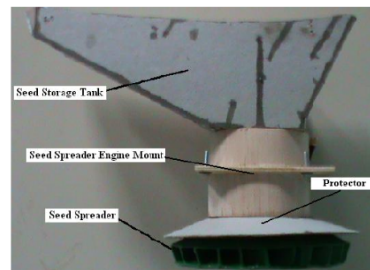


Figure 7.3: Full seed dispersal machinery

Sensor	Length (mm)	Width (mm)	Height (mm)	Comments	Source
Sony Alpha A7R	77.5	128.9	96.4		<a href="#">Link</a>
Pixhawk 4 mini	55	38	15.5		<a href="#">Link</a>
Ublox NEO-M8N	54	22	54	Diameter = 54 mm	<a href="#">Link</a>
MPU-9250 IMU	14.3	-	20.5		<a href="#">Link</a>
Three-axis aluminium brushless gimbal	90	140	110	(Length, Width are packing Dimensions, actual dimensions are close to it)	<a href="#">Link</a>
NDVI sensor	30.5	37	30.5	Diameter = 30.5	<a href="#">Link</a>
MN6007 Antigravity KV3200	67	30.1	67	Diameter = 67 mm	<a href="#">Link</a>
Tattu 22.2V 25C 22000 mah	210	90	60		<a href="#">Link</a>
Payload Dropping Mechanics	-	-	-	As per [10], we will be using the same seed dispersal system. The total volume of the seed tank is 2000 cm <sup>3</sup> and will house 9000 seeds.	

Table 7.3: Sensor Specifications

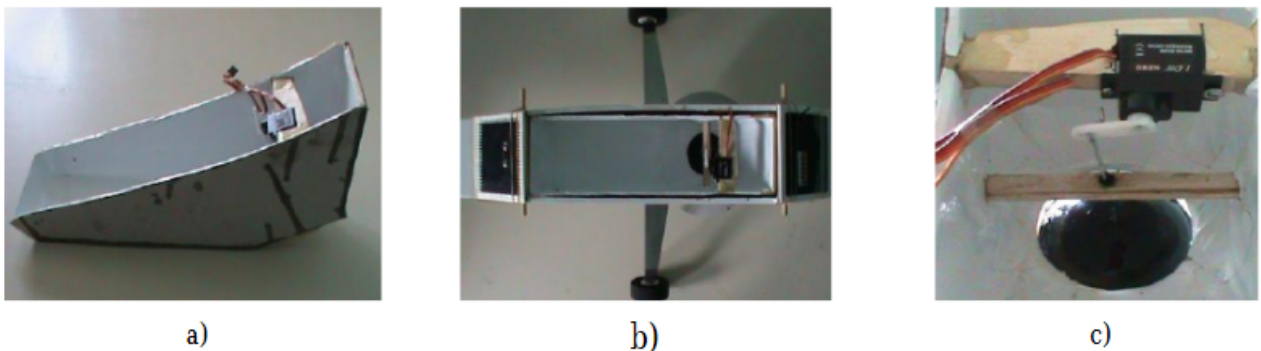


Figure 7.4: (a)Seed tank which will be inside the fuselage (b) seed tank attached in fuselage (c) servos used for plunging

The following things have to be kept in mind while deciding the arrangement of payload in the fuselage:

- The seed tank will be at the lowest position.
- The batteries have to be in front due to chosen double tractor configuration.
- The camera and gimbal have to be on bottom besides the dispersal system.
- There should be an easily accessible slot in the fuselage to access the different payloads/sensors and refill seeds into the tank etc.

- The motors, sensors should be placed such a way that least wiring is used.

Based on the above considerations, the following configuration for the fuselage was decided.

- The nose of the fuselage is taken as spherical for simplicity and for decreased drag.
- The tail boom must be approximately 50-60% of the total fuselage length. It was obtained by subtracting the total fuselage length from the length required to keep all the sensors and it came to be around 1.127 m
- The sensors are placed such that they can be used optimally.

Final Lengths:

1. Fuselage Diameter: 0.350m
2. Fuselage Length: 1.85m
3. Tail Boom Length: 1.127m

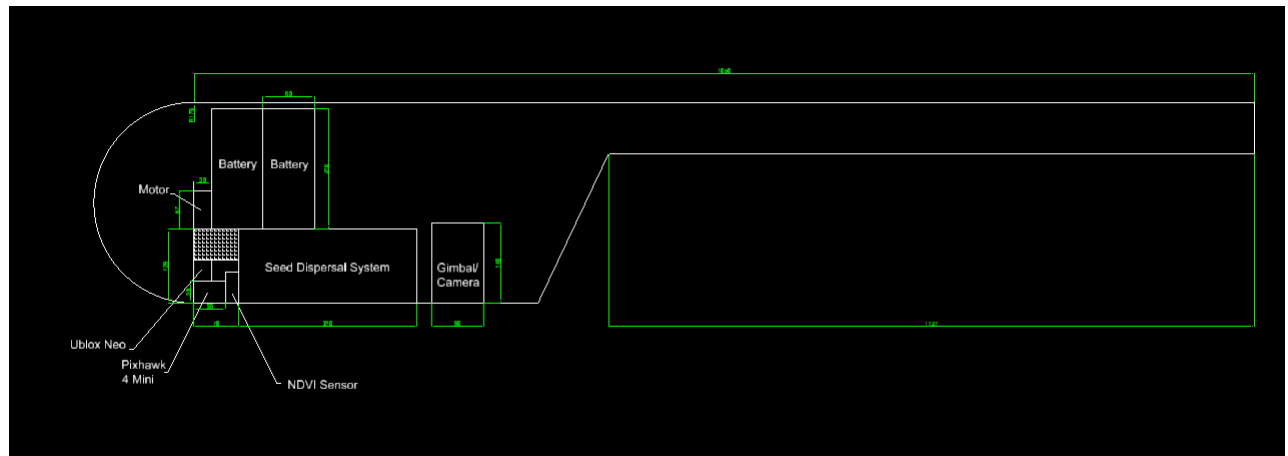


Figure 7.5: Fuselage Preliminary Design

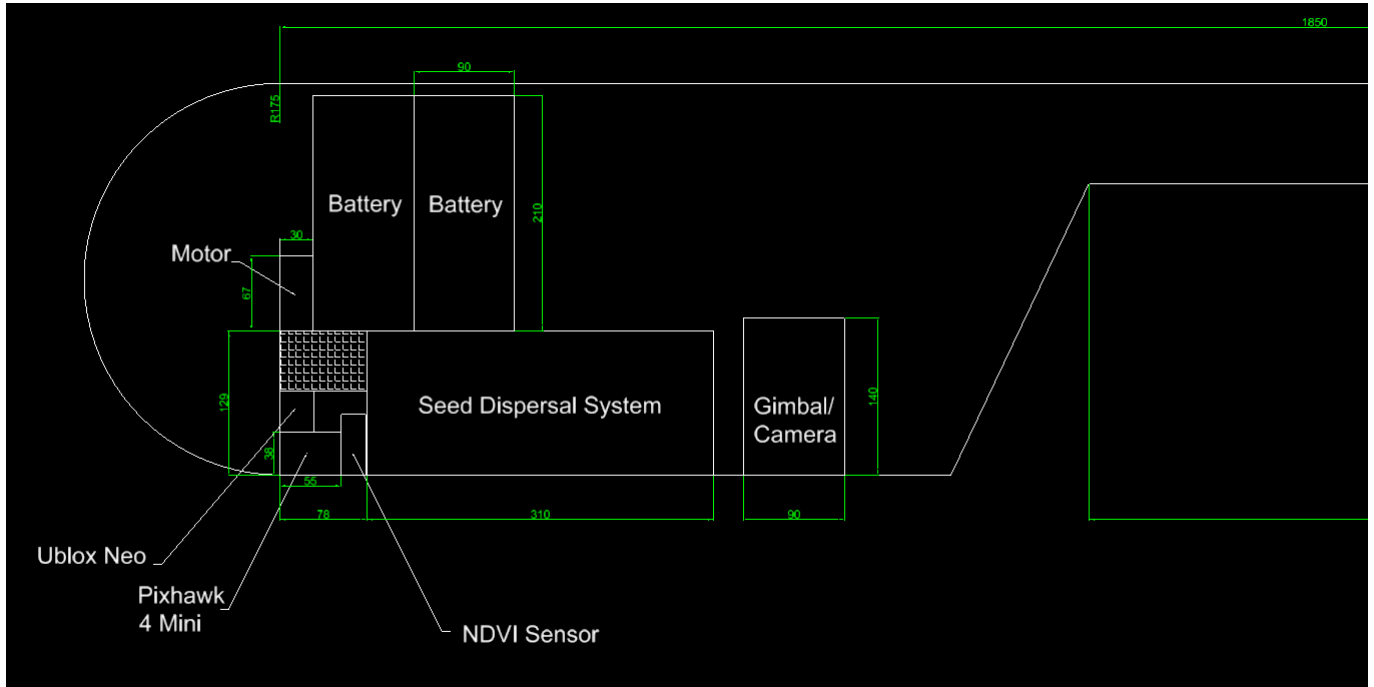


Figure 7.6: Detailed view of fuselage

## 7.2 Tail Configuration

### Types of AFT Tail Configuration

#### V-tail

##### Advantages

- Reduced total tail area, leading to potential weight savings and improved overall aerodynamic efficiency
- Simplified control system with combined ruddervators, reducing mechanical complexity and weight
- Can provide satisfactory longitudinal and directional trim, especially in applications where minimizing tail area is a priority

##### Disadvantages

- Less effective in maintaining longitudinal and directional stability compared to conventional tail configurations, especially in certain flight conditions
- More susceptible to Dutch-roll tendencies, which can affect overall stability and control
- Complex control system with potential adverse roll/yaw coupling, requiring careful design and pilot technique

## **Y-tail**

### **Advantages**

- Reduced tail contribution to aircraft dihedral effect, improving directional controllability
- Tail surfaces kept out of wing wake at high angles of attack, potentially improving stability and control characteristics

### **Disadvantages**

- The lower section of the tail may limit aircraft performance during takeoff and landing, requiring careful operational considerations
- Structural considerations regarding tail clearance from the ground and aerodynamic interference with the fuselage and wings

## **Conventional (or) Inverted T-tail**

### **Advantages**

- Simple and straight-forward design making it perform all tail functions (i.e., trim, stability, and control)
- Lightweight, efficient, and commonly used in a wide range of aircraft because of its performance under regular flight conditions

### **Disadvantages**

- Limited to moderate performance in extreme flight conditions or specialized applications
- May not offer the same level of efficiency or specific advantages as more complex tail configurations in certain scenarios

## **T-tail**

### **Advantages**

- Higher efficiency and safety due to being out of the regions of wing wake, downwash, vortices, and engine exhaust, leading to reduced tail vibration and structural stress
- Positive end-plate effect resulting in a smaller vertical tail area and improved overall aerodynamic performance

### **Disadvantages**

- Heavier vertical tail structure due to the need to transfer bending moments from the horizontal tail, leading to increased weight
- Susceptibility to deep stall conditions, especially if not designed and operated correctly, which can result in dangerous pitching moment instabilities

## H-tail

### Advantages

- Improved performance at high angles of attack due to reduced influence from turbulent flow and better engine exhaust concealment in military applications
- Enhanced lateral control and shorter vertical tail span, leading to improved maneuverability and aerodynamic characteristics

### Disadvantages

- Slightly heavier than conventional and T-tail configurations due to the need for a strong horizontal tail to support two vertical tails
- More complex structural design and engineering compared to conventional configurations, requiring careful consideration of weight and balance

### Advantages

- By mounting the tail at the end of booms, the interference between the propeller flow (in prop-driven aircraft) and the tail is minimized, leading to improved aerodynamic efficiency and reduced drag
- The use of booms allows for a shorter fuselage design, which can reduce weight, improve maneuverability, and potentially lead to cost savings in manufacturing and maintenance

### Disadvantages

- The overall weight of the aircraft may be slightly heavier due to the addition of booms to support the tail structure, affecting fuel efficiency and overall performance, especially in terms of payload capacity and range
- The structural design and engineering of boom-mounted tails can be more complex compared to conventional tail configurations, requiring careful analysis and design considerations
- Depending on the specific design and aircraft type, the boom-mounted tail configuration may require careful attention to ground clearance during takeoff, landing, and ground operations, ensuring sufficient clearance to avoid tail strikes or other ground-related issues

Due to simplicity of the design and no issues of deep stalling, we consider inverted T tail, or the conventional tail configuration for our aircraft.

## 7.3 Horizontal Tail Configuration

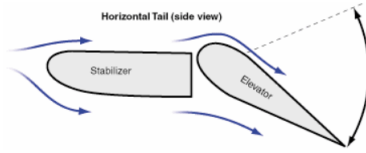


Figure 7.7: Horizontal tail

The horizontal tail sections are made up of the elevator and the stabilizer. Both these sections are unique and developed specifically for maximum effectiveness at low speeds and at high angles of attack. The stabilizer is an inverted airfoil section to maximize downward lift to help achieve high angles of attack required for short take-off and landing performance. The elevator is an actual airfoil section, and provides a ‘virtual venturi’ effect when deflected down, as illustrated below. The unique tail sections provide maximum effectiveness for short take-off and landing performance – while also minimizing the actual size of the tail sections.

### 7.3.1 Horizontal Tail Arm and area

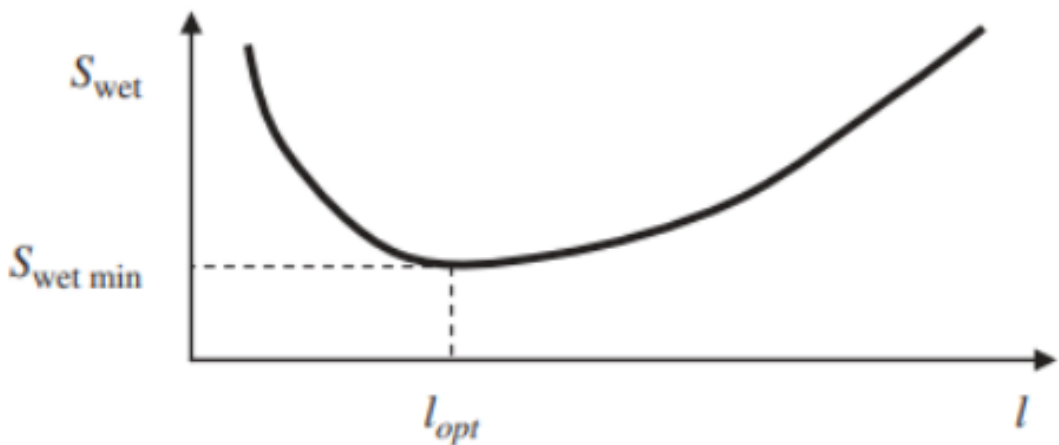


Figure 7.8: tail arm length

Using the formula in [9], we find the optimum tail area.

$$l_{opt} = K_c \sqrt{\frac{4\bar{C}S\bar{V}_H}{\pi D_f}}$$

where  $K_c$  is a correction factor,  $\bar{C}$  is the mean aerodynamic chord of the wing.  $S$  is the surface area of the wing,  $\bar{V}_H$  is volume coefficient,  $D_f$  is the maximum fuselage diameter. By substi-

tuting the values we get the optimum tail arm as: 1.259m

The volume ratio for horizontal tail, for a conventional aircraft is usually, 0.5 (acc to [8]).

$$S_{ht} = V_{ht} \frac{S_w}{l_{ht}} \bar{c}_w = 0.28 m^2$$

## Airfoil type

For the horizontal and vertical tail, usually a symmetric airfoil is used since the tail is required to produce both positive and negative lift thus should behave the same in positive and negative angle of attack. Also, The t/c ratio of the tail airfoils must be approximately 90% of the the t/c for the wing. The chosen airfoil type is NACA0009.

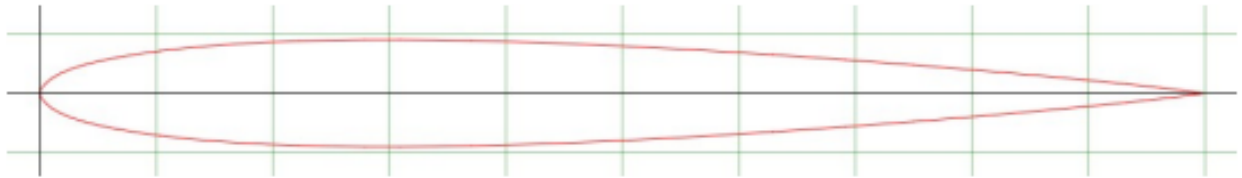


Figure 7.9: NACA 0009

## Aspect Ratio

Aspect ratio is the ratio of the span to the mean aerodynamic Chord. The tail Aspect ratio tends to have direct effect on the tail lift-curve slope. As the tail aspect ratio is increased, the tail lift curve slope is increased. The initial value of the aspect ratio can be determined as follows

$$AR_H = \frac{2}{3} * AR_w$$

Thus the wing aspect ratio is 5.33. This is consistent with that is given in [8] which is that for subsonic aircraft, the aspect ratio is typically taken to be around 5 for the horizontal tail. The final value for the tail aspect ratio will be determined based on the aircraft stability and control, cost, and performance analysis evaluations after the other aircraft components have been designed.

## Taper ratio

According to [8], some general aviation aircraft use untapered horizontal tails ( $\lambda = 1.0$ ) to reduce manufacturing costs. Hence, the selected taper ratio for horizontal tail is 1.

## Sweep

Leading-edge sweep of the horizontal tail is usually set to about 5 deg more than the wing sweep. For low-speed aircraft, the horizontal tail sweep is frequently set to provide a straight

hinge line for the elevator, which usually has the left and right sides connected to reduce flutter tendencies.

### 7.3.2 Other Parameters

The span of the horizontal tail can be obtained as follows

$$b_h = \sqrt{AR_h \cdot S_h} = 1.22m$$

The chord length can be obtained as

$$\bar{C}_h = \frac{b_h}{AR_h} = 0.22m$$

### 7.3.3 Elevator

The typical values of the area, span and chord of the elevator seen below are taken from the reference book [9]

$$S_e/S_h : 0.15 - 0.4$$

$$b_e/b_h : 0.8 - 1$$

$$c_e/c_h : 0.2 - 0.4$$

## 7.4 Vertical Tail Configuration

Take from [5] and [2],

The aircraft features an all-flying vertical tail (rudder) section for excellent effectiveness and control, especially at low speeds. The all-flying rudder provides responsive rudder control, while also minimizing weight and complexity (there's only one vertical tail section). Two rudder bearings bolt to the rear fuselage to fix the rudder to the fuselage.

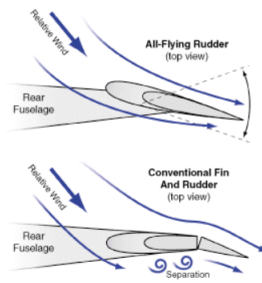


Figure 7.10: Vertical Tail Configuration

### Vertical Tail Arm

The vertical moment arm plays very important when dealing with a phenomena called spin, similar to how stall is. for the horizontal tail. Increasing the vertical tail moment arm increases

the values of the derivatives  $C_{n\beta}$  and  $C_{nr}$  and thus makes the aircraft directionally more stable. An increase in the vertical tail moment arm improves the directional and lateral control. In the early stage of the vertical tail design, where other aircraft components have not been designed, the vertical tail moment arm is selected to be equal to the horizontal tail moment arm. This assumption means that the vertical tail is located at the same distance from the wing as the horizontal tail. The assumption will be modified in the later design stage, when the aircraft directional and lateral stability, control, and trim are analyzed.

## Area

According to [8] the volume ratio for the vertical tail for general uavs is about 0.05. Using this, we find the area of the vertical tail as following:

$$S_{vt} = V_{vt} \frac{S_w}{l_{vt}} b_w = 0.206 m^2$$

## Airfoil type

The same airfoil as the horizontal tail will be used for the vertical tail, NACA0009.

## Aspect Ratio

Similar to those of horizontal tail, increasing aspect ratio of vertical tail have the following effects:

higher lift curve slope

lower drag and

higher structural weight.

In addition to these, an increase in the aspect ratio of the vertical tail also has the following effects: 1. Increases the height of vertical tail and in turn the height of the airplane 2. Lower lateral control as the moment of inertia about longitudinal axis increases. 3. Higher directional control as the moment arm ( $I_{vt}$ ) increases

Compromising the above parameters, subsonic aircrafts have conventional tails with vertical tail aspect ratio between 1 to 2 .

## Taper ratio

Typical values for an UAV are around 0.4-0.6. At the preliminary stage we take it to be 1 meaning both the root chord and tip chord are same and equal to mean aerodynamic chord.

## Sweep

As per [8], Vertical-tail sweep varies between about 35 and 55 deg. For a low-speed aircraft, there is little reason for vertical-tail sweep beyond about 20 deg other than aesthetics. Hence the chosen vertical sweep is 20 degrees.

## Other Parameters

$$b_v = \sqrt{AR_v \cdot S_v} = 0.558m$$

The chord length can be obtained as

$$C_{\text{root}} = \frac{2 * b_v}{(1 + \lambda) * AR_v} = 0.461m$$

$$C_{\text{tip}} = \lambda * C_{\text{root}} = 0.27m$$

### 7.4.1 Rudder

The typical values of the area, span and chord of the Rudder seen below are taken from the reference book [9]

$$S_r/S_v : 0.15 - 0.35$$

$$b_r/b_v : 0.7 - 1$$

$$c_r/c_v : 0.15 - 0.4$$

However, this holds if we go for a conventional rudder configuration and not an all flying vertical tail as mentioned in figure 7.10. The final selection will be done on basis of stability derivatives.

## 7.5 Final Parameters

Parameters	Horizontal Tail	Vertical Tail
Aspect Ratio	5	1-2
Taper Ratio	1	0.4-0.6
Sweep	5 degrees	20 degrees
Airfoil	NACA 0009	NACA 0009
Volume Coefficient	0.5 7	0.005
Tail Arm	1.259 m	1.259 m
Area	$0.28m^2$	$0.206 m^2$
Span	1.22 m	0.558m
Root Chord	0.22m	0.27m
Tip chord	0.22m	0.27m
Mean Chord	0.22m	0.365m

# Chapter 8

## Landing Gear Design

### 8.1 Preliminary CG Location

Using the 2-D CAD model and the position of the components as decided in chapter 7, we will make a rough estimate of the CG. We have assumed throughout that the aircraft is symmetric, thus the CG lies on the mid plane of the aircraft.

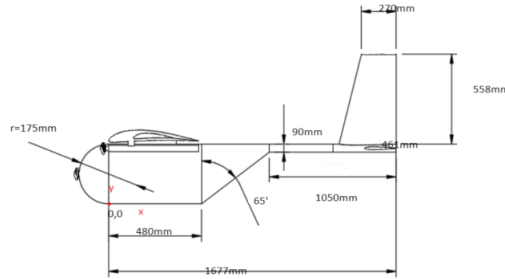


Figure 8.1: Fuselage detailed dimensions

The X(horizontal) and Y(vertical) axis and the origin of the coordinate system are as shown in the figure above. Based on the component placement decided in chapter 7, Fig 7.6, the following was calculated for CG.

(Note that this is subject to change after the 3D CAD model is made)

Component	X(mm)	Y(mm)	Mass(kg)
Fuselage	853.08	375.24	8.35
Battery1	75	234	3.8
Battery2	165	234	3.8
Camera	433	70	0.665
Flight controller	27.5	19	0.0024
NDVI sensor	64.5	25	0.05
Seed dispersal	233	64.5	3
Neo	15	58	0.023
Motor	15	162.5	0.4

Hence, the CG location based on first estimate is

1.  $X_{CG} = 447.55mm$
2.  $Y_{CG} = 259.88m$
3.  $Z_{CG} = 0$

## 8.2 Comparison of Landing Gear Arrangements for UAV Mission

### 8.2.1 Tricycle Landing Gear

The tricycle landing gear configuration consists of three landing gear units: two main wheels located towards the front of the aircraft under the wings and a single nose wheel positioned at the front under the fuselage. This arrangement offers several advantages for UAV missions focused on afforestation. Firstly, tricycle gear provides enhanced ground stability and maneuverability, making it well-suited for operations in varied or rugged terrains. The nose wheel placement enhances visibility during critical phases like takeoff and landing, aiding in precise navigation and assessment of target areas for afforestation. Additionally, tricycle gear facilitates smoother ground operations, including taxiing and ground handling, which is beneficial for autonomous UAV operations. However, tricycle landing gear can result in slightly increased aerodynamic drag and may require a heavier and more complex nose gear system compared to tail-dragger configurations.

#### Advantages:

1. **Ground Stability and Maneuverability:** Tricycle landing gear provides enhanced ground stability, making it easier to take off and land, especially in varied or rugged terrain.
2. **Improved Ground Clearance for Payload:** Tricycle gear offers higher ground clearance for sensors and payload deployment mechanisms, minimizing the risk of damage on rough surfaces.
3. **Enhanced Visibility for Takeoff and Landing:** Nose wheel placement improves visibility for sensors and cameras during critical mission phases.
4. **Simplified Ground Operations:** Tricycle gear facilitates smoother taxiing and reduces operational complexities, suitable for autonomous UAV operations.
5. **Adaptability to Various Terrains:** Tricycle gear offers better adaptability to different terrains and weather conditions, enhancing reliability and versatility.

#### **Disadvantages:**

1. **Increased Drag:** Tricycle landing gear can create slightly more aerodynamic drag compared to a tail-dragger design.
2. **Heavier Nose Gear:** The nose gear of tricycle landing gear systems tends to be heavier and more complex.

### **8.2.2 Tail-Dragger (Tailwheel) Landing Gear**

The tail-dragger landing gear arrangement features two main wheels positioned towards the front under the wings and a smaller tailwheel located at the rear of the fuselage. This design offers advantages such as lower aerodynamic drag, potentially improving speed and fuel efficiency, which could be beneficial for long-duration missions. Tail-dragger configurations also tend to have a lighter and simpler landing gear system, reducing overall aircraft weight. However, they present challenges related to ground handling, including reduced ground visibility during takeoff, landing, and taxiing. Tail-draggers require more skill and attention from pilots during ground operations, which may increase operational complexity and training requirements. Overall, while tail-dragger landing gear offers certain aerodynamic benefits, tricycle landing gear is often preferred for UAV missions due to its stability, visibility, and suitability for autonomous operations in diverse terrains.

#### **Advantages:**

1. **Lower Drag:** Tail-dragger configurations generally offer lower aerodynamic drag, potentially improving speed and fuel efficiency.
2. **Lighter Weight:** Tailwheel designs have a simpler and lighter landing gear system, reducing overall aircraft weight.
3. **Better Propeller Clearance:** Some tailwheel configurations offer better propeller clearance, advantageous in rough or unimproved runway conditions.

#### **Disadvantages:**

1. **Limited Ground Visibility:** Tail-draggers have reduced ground visibility, posing challenges during takeoff, landing, and taxiing.
2. **Complex Ground Handling:** Tail-draggers require more skill and attention during ground operations, increasing operational complexity.
3. **Training and Operational Familiarity:** Tailwheel designs may require more training and experience for pilots due to handling characteristics.

#### **Advantages of Tricycle Landing Gear for UAV Mission:**

- 1. Ground Stability and Maneuverability:** Tricycle landing gear provides enhanced ground stability, crucial for safe takeoff and landing in remote or rugged terrains.
- 2. Improved Ground Clearance for Payload:** Higher ground clearance of tricycle gear minimizes risk of equipment damage during operations on uneven surfaces.
- 3. Enhanced Visibility for Takeoff and Landing:** Nose wheel placement improves visibility for sensors and cameras during critical mission phases.
- 4. Simplified Ground Operations:** Tricycle gear facilitates smoother taxiing and reduces operational complexities, ideal for autonomous UAV operations.
- 5. Adaptability to Various Terrains:** Tricycle gear offers better adaptability to different terrains and weather conditions, enhancing reliability and versatility.

#### **Comparison with Tail-Dragger for UAV Mission:**

- 1. Limited Ground Visibility:** Tail-dragger configurations have reduced ground visibility, posing challenges during takeoff, landing, and taxiing.
- 2. Complex Ground Handling:** Tail-draggers require more skill and attention during ground operations, increasing operational complexity.
- 3. Training and Operational Familiarity:** Tricycle gear is more commonly used in modern aircraft and UAV designs, reducing training requirements.

There are other landing gear configurations such as quatercycle etc, however due to their irrelevance and lack of prominence in use, we have not considered those.

Based on the above considerations, even though tail dragger is used for conventional short take off landing aircraft, the tail dragger has disadvantages of stability and also is complex to calculate the transition phase. Modern stols like STOL CH701 are able to achieve the same short take off landing with a tricycle arrangement via high lift devices. Hence we intend to do the same and use TRICYCLE ARRANGEMENT as the chosen landing gear configuration.

### **8.3 Steering for nose wing**

Since we will be operating in regions which may have high crosswind effects, it is necessary to incorporate their effects in our design. We will consider the effects of crosswinds in the landing gear track length and rudder design. However, it is necessary to see how the nose gear design can help in cross winds.

Nose wheel steering plays a crucial role in managing crosswinds during ground operations, particularly during takeoff and landing. Here's how it helps:

**Directional Control During Takeoff Roll:** In crosswind conditions, the aircraft is subject to lateral forces that can push it off the centerline of the runway. Nose wheel steering allows the pilot to counteract these forces, maintaining a straight path until the aircraft reaches a speed where aerodynamic controls (rudder) become effective.

**Landing Roll:** After touchdown in crosswind conditions, the aircraft's speed decreases, and the effectiveness of the aerodynamic controls reduces. Nose wheel steering becomes essential for maintaining directional control as the aircraft slows down, preventing it from veering off the runway.

**Taxiing in Crosswinds:** During taxiing, crosswinds can push the aircraft sideways. Nose wheel steering provides the necessary control to counteract this lateral force, ensuring the aircraft remains on the intended taxiway path.

**Ground Handling:** In strong crosswinds, nose wheel steering aids ground handling by allowing more precise maneuvering when parking, turning, or aligning with ground facilities. This is especially important in avoiding collisions and ensuring safe ground operations.

The following picture shows how the steering system for nose gear will look like:



Figure 8.2: Nose Gear Steering

## 8.4 Landing Gear parameters

### Landing Gear height

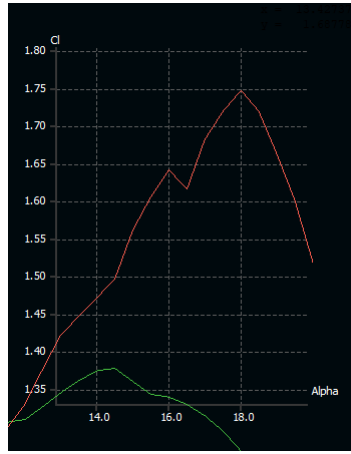
As mentioned in chapter 6, the wing setting angle is taken to be  $5^\circ$ . Now, since we aim at a short take off landing, using a tricycle landing gear system, we have to rotate the airplane to an angle where the wing (with full fowler flaps and slats) give the required lift coefficient of 3.5. Hence, the exact pitch angle at rotation will be decided based on the camber that the flaps and slats provide and the angle required for the maximum lift to be generated at take off. Since the flaps and slats will be deployed at maximum during rotation and lift off, we have to make sure that the angle of attack for the wing does not cross the stall angle of attack. Thus should be kept in mind while choosing  $\alpha_{TO}$



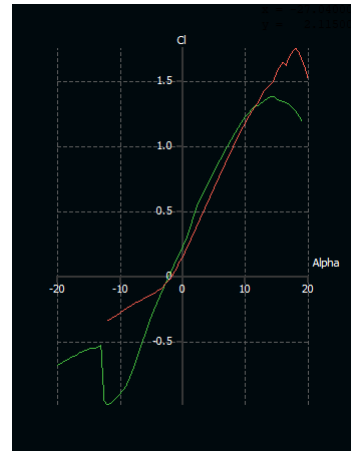
Figure 8.3: Take off phases

### Effect of Flaps on stall angle

As mentioned in Chapter 6, we will be using double slotted Fowler flaps to generate a lift coefficient of 3.5 for a short take off. However, experimental data shows that fowler flaps do not change in stall angle of attack or the angle of attack which the aircraft will lift off at. The below picture shows the effect of different fowler flaps.



(a)  $C_l$  vs  $\alpha$



(b)  $C_l$  vs  $\alpha$

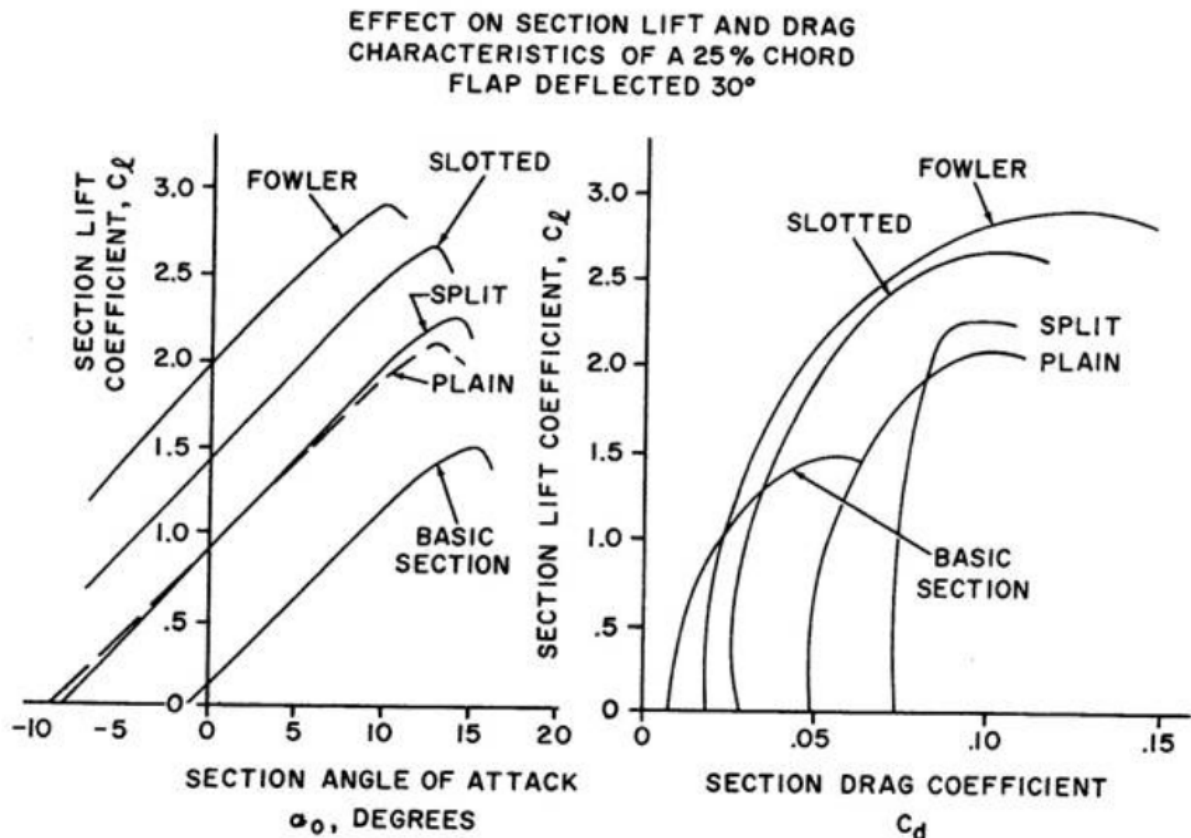


Figure 8.4: Fowler flap effects on stall angle

### Effect of slats on stall angle

During take off, the slats will be deployed at  $20^\circ$  as mentioned in chapter 6. Slats tend to increase the stall angle of attack. For our case, using NACA2412, at full slat deflection, we get an increase in stall angle of 4.5 degrees as can be seen from the plots generated on XFLR5 below.

$$\alpha_{wing} = \alpha_{\text{Inclination angle}} + \alpha_{\text{take off}}$$

Note that this is only because the velocity is taken nearly horizontal at the rotation and lift off phase. After this phase the aircraft will have a pitch angle corresponding to the rate of climb requirements are mentioned before.

As mentioned previously, the inclination angle is taken to be  $5^\circ$ . Hence, the  $\alpha_{\text{take off}}$  should be such that the the  $\alpha_{\text{wing}}$  does not cross the stall angle of attack. From the data of NACA2412 and the extra stall that slats provide, we decide an  $\alpha_{\text{take off}}$  of  $12^\circ$ .

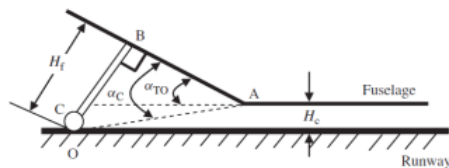


Figure 8.6: Landing Gear height

$$H_f = AB \tan(\alpha_{TO}) + \frac{H_c}{\cos(\alpha_{TO})}$$

Thus, as mentioned above, the  $\alpha_{TO}$  is a design choice, based on runway constraints in the calculation of landing gear height.

Based on previous aircraft data of Lancaster-5, Penguin C and Penguin BE (as obtained from image processing), we have decided the ground clearance to be 150mm and AB to be 50mm. The value of AB should be such that the main landing gear is after the CG location even at the highest pitch of the aircraft. The below picture shows the reference for Penguin C.

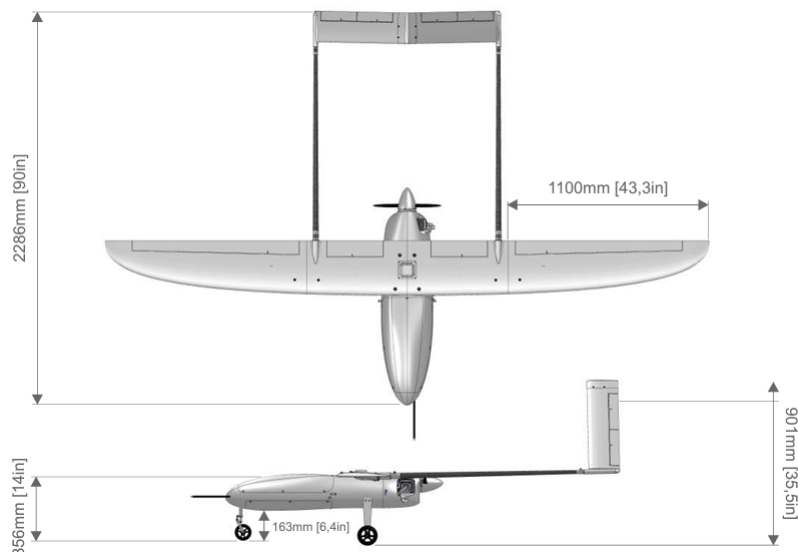


Figure 8.7: Reference Aircraft

Thus putting all these values in, we get the landing gear height as 163.97m.

## Clearance angle

The take-off rotation ground clearance requirement to prevent a fuselage hit is as follows:

$$\alpha_C \geq \alpha_{TO}$$

where the clearance angle is:

$$\alpha_C = \tan^{-1} \left( \frac{H_f}{AB} \right)$$

In other words, if the clearance angle is less than the aircraft rotation angle during take-off, the fuselage will strike the ground. Based on the above values, the clearance angle is  $61^\circ$ , which is much greater than the take off angle.

### 8.4.1 Wheel Base

The wheel base decides the load carried by the nose and the main landing gear. It is important from a structural point of view to have the loads distributed properly. We have to decide the portion of the load carried by the landing gear and we shall obtain the distance between the nose and main landing gear. According to [8] typically, the main tires carry about 90% of the total aircraft weight. Nose tires carry only about 10% of the static load but experience higher dynamic loads during landing. Just like for a motorcycle, when the brakes are applied the nose dips down. The torque caused by the braking force is pushing the nose wheel downward. It has to be able to withstand that extra force. This will also be taken into consideration during the tire sizing.

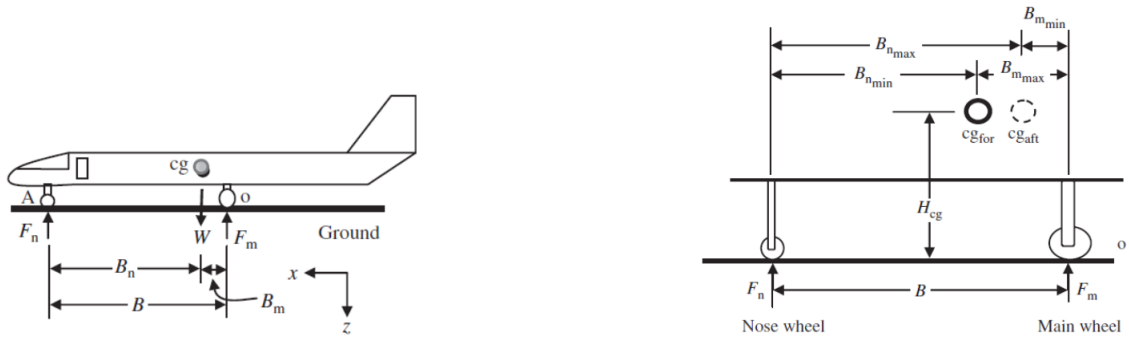


Figure 8.8: Landing Gear base

Let  $F_n$  and  $F_m$  be the weight carried by the nose and main landing gear, respectively. We have

$$F_n + F_m = W = 219.8N$$

Let  $B$  be the base distance. From the moment balance equation, we have

$$\sum M_0 = 0 \implies F_n B - W B_m = 0$$

Therefore we have,

$$F_n = \frac{B_m}{B}W \quad F_m = \frac{B_n}{B}W$$

The  $CG_{aft}$  and  $CG_{for}$  will be the same for our case. From  $AB=170\text{mm}$  from the landing gear height section and  $X_cg = 447.8\text{mm}$ ,  $B_m$  is found to be  $25\text{mm}$ .

Since the Nose gear takes about 10-20% of the static load, the value of  $\frac{F_n}{W}$  is taken to be 0.15.

Using this, we get

$$B = 166.66\text{mm}$$

## Wheel track

Since we have chosen a tricycle landing gear, we will have two landing points for the main landing. The distance is determined using the height of the CG from the ground and ground controllability. This could have been obtained using other factors like maximum structural bending or ground stability, which would require numerical values of complex parameters. Hence we avoid that approach.

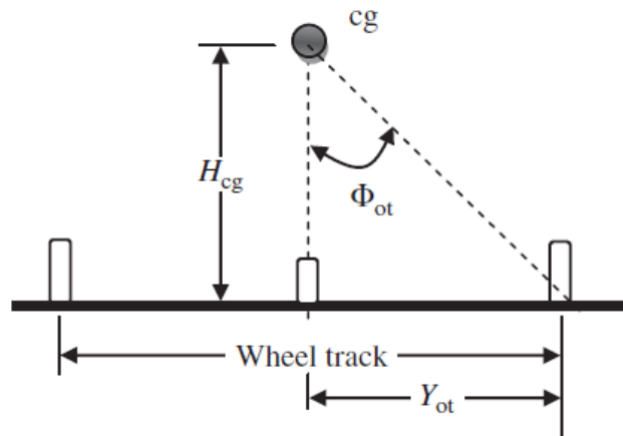


Figure 8.9: Landing Gear track

$$T = 2 \times Y_{ot} = 2 \times H_{CG} \times \tan \phi_{ot}$$

From figure 11.11, we can write

$$\sum M_o = 0 \implies F_c \cdot H_{cg} + W \cdot Y_{ot} = 0$$

, where

$$F_c = m \frac{V^2}{R}$$

We shall assume safe values of  $V = 5 \text{ m/s}$  and  $R = 3 \text{ m}$ .

Another constraint we have is that :

$$T > 2Y_{ot}$$

Hence taking  $T = 2.1$  times  $Y_{ot}$ , we have

$$\phi_{ot} = \arctan \left( \frac{1.05 \times F_c}{mg} \right) = 41.741^\circ$$

Hence we have

$$T = 2 * H_{cg} \times \tan 41.741^\circ = 782.35 \text{ mm}$$

$$H_{cg} = Y_{cg} + \text{Landing gear height} = 448\text{mm}$$

Since  $\phi_{ot} > 25^\circ$ , the wheel track satisfies the rule of thumb for overturn prevention requirement.

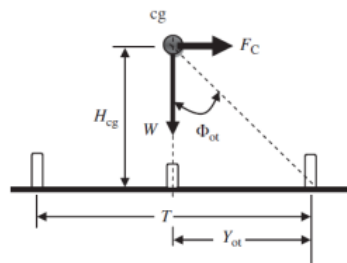


Figure 8.10: Force balancing

### 8.4.2 Effect of crosswinds

One of the atmospheric phenomena affecting the aircraft ground stability is the wind. The most noticeable wind affecting an aircraft on the ground is the cross-wind, where it is perpendicular to the aircraft ground path or fuselage center line. A cross-wind creates a force on an aircraft at the ground, which in turn generates a moment that is capable of overturning the aircraft. The restoring moment is the aircraft weight times its corresponding arm (half of the wheel track). Thus, the wheel track ( $T$ ) plays an important role in the aircraft ground stability. It must be large enough to prevent the aircraft rolling over when on the ground due to a cross-wind.

### 8.4.3 Tire Sizing

Aircraft Type	Diameter		Width	
	A	B	A	B
<b>British units: Main wheels diameter or width (in.) = <math>A W_W^B</math></b>				
General aviation	1.51	0.349	0.7150	0.312
Business twin	2.69	0.251	1.170	0.216
Transport/bomber	1.63	0.315	0.1043	0.480
Jet fighter/trainer	1.59	0.302	0.0980	0.467
<b>Metric units: Main wheels diameter or width (cm) = <math>A W_W^B</math></b>				
General aviation	5.1	0.349	2.3	0.312
Business twin	8.3	0.251	3.5	0.216
Transport/bomber	5.3	0.315	0.39	0.480
Jet fighter/trainer	5.1	0.302	0.36	0.467

$W_W$  = Weight on wheel.

Figure 8.11: Tire Sizing Table from [8]

Since, the main tires takes 90% of the weight of the aircraft and the other 10% is carried by the nose tyre, the Weight considered on each of the main tires is 9.8kg. Thus using the emperical relation in the table above, we get the diameter of the main tire as 11.311cm and width as 4.668cm. Since, we will be working on rough surfaces in coastal regions, according to [8], the diameter and width of the tire should be increased by 30%. Hence the final values for main tire are:

1. Diameter-14.7043cm
2. Width- 6.068cm

Nose tires can be assumed to be about 60-100% the size of the main tires. According to table 11.3 in [8], the recommended pressure for operating over hard soil/dry grass/unpaved roads is 45-60psi.

$$W_w = P A_p$$

$$A_p = 2.3\sqrt{wd} \left( \frac{d}{2} - R_r \right)$$

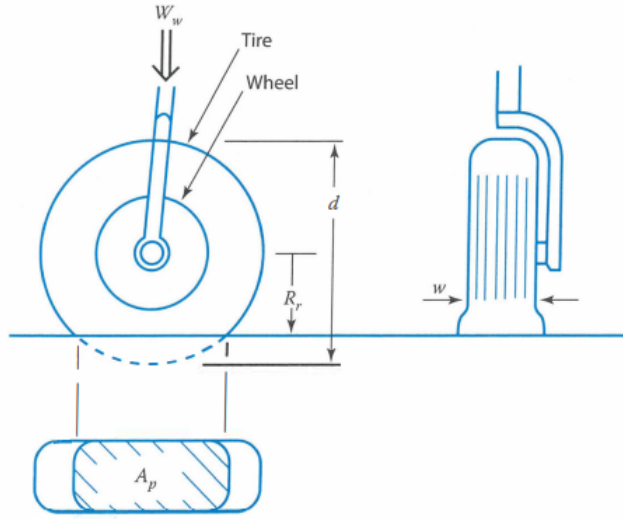


Figure 8.12: Tire Notations [8]

Thus using the above values(taking the weight on the main gear as 90% of the total weight divided equally between the two wheels), we find,

$$A = 317.74 \text{ mm}^2, R_r = 0.068 \text{ m}$$

#### 8.4.4 Shock Absorber

The shock absorbers and tire act together to decelerate the UAVs from landing vertical velocity to zero vertical velocity. Therefore shock absorber and tire must also absorb the sum of the kinetic energy and potential energy of the aircraft.

$$\text{Tire energy} = \Delta t \times \eta_t \times \lambda M$$

$$\text{Struct Energy} = S \times \eta_s \times \lambda M$$

$$\text{Kinetic Energy of aircraft} = \text{Tire energy} + \text{Shock absorber energy}$$

$$\frac{MV^2}{2} = \Delta t \times \eta_t \times \lambda M + S \times \eta_s \times \lambda M$$

where,

- $\Delta t$  = Tire deflection
- $\eta_t$  = tire efficiency
- $\lambda$  = Reaction factor
- $M$  = mass of the UAV
- $S$  = vertical axel travel
- $\eta_s$  = shock absorber efficiency

The above equation is for a oleo-pneumatic shock strut. If the landing gear is decided to be retracted, the hydraulic shock absorber (preferably oleo-pneumatic shock strut) is an

appropriate option. In terms of cost, an oleo shock absorber is much more expensive than a solid spring. Furthermore, the maintenance of an oleo shock absorber is very much more labor-extensive than a solid spring. Since our UAV is 21.98 kg, the use of hydraulic shock absorber will have more demits than merits. The operating costs will be increased to a great extent. Since our UAV is designed to land on any rough surfaces, having a hydraulic shock absorber makes it vulnerable to damage easily. It also increases the weight of the UAV significantly.



(a) Rigid axle shock absorber



(b) Solid Spring Shock absorber

Hence, a solid shock absorber is more suitable for our configuration. But most of the types of solid shock absorber - **Rigid Axle Shock Absorber**, **Solid Spring shock absorber** aren't efficient in performing the damping function against shock-induced vibrations, which results in damaging the components in fuselage. So, a **Levered Bungee Shock Absorber** will be used for our landing gear. This shock absorber model is slightly more sophisticated than the solid spring shock absorber model.



Figure 8.14: Levered Bungee shock absorber

This design uses bungee chords between the fuselage and landing gear to mitigate shock-induced vibrations. Elastic chords, wrapped around the landing gear, transfer impact stresses from the wheels to the aircraft's airframe, reducing impact and preventing damage to critical components within the structure. The aircraft's landing gear flexes outward during initial impact with the ground, causing tires to wear down over time, similar to a solid spring shock absorber system. This type of shock absorber was commonly used in early light aircrafts.

The final shock absorber design for our UAV is **Levered Bungee shock absorber**

The energy equation for a levered bungee shock absorber can be derived based on the principle of conservation of energy. This type of shock absorber system uses a lever mechanism along with a bungee cord to absorb and dissipate energy during impact.

When the vehicle experiences an impact, the lever arm rotates around the pivot point, stretching the bungee cord and absorbing energy in the process.

The energy equation for this system can be written as:

$$E_{\text{initial}} = E_{\text{final}}$$

The final energy ( $E_{\text{final}}$ ) can be broken down into two components:

1. The energy stored in the stretched bungee cord, which can be represented as:

$$E_{\text{bungee}} = \frac{1}{2}kx^2$$

## 2. Tire Energy

The total final energy ( $E_{\text{final}}$ ) is the sum of these two components:

$$E_{\text{final}} = E_{\text{bungee}} + \text{Tire energy}$$

$$\frac{MV^2}{2} = \Delta t \times \eta_t \times \lambda M + \frac{1}{2}kx^2$$

- $k$  is the spring constant of the bungee cord
- $x$  is the distance the bungee cord is stretched

The result is improved energy absorption and damping abilities due to frictional forces between rubber strands. This type of shock absorber was commonly used in early light aircrafts. The compression or elongation in the rubber cords will be in the order of touch down velocity, similar to that of compression in Oleo-Pneumatic Shock absorber. But here the tire energy is much greater than that of energy stored in the rubber chords. The rubber chords in this type of shock absorber provides the vibrations resistance which solid struct absorber lacks.

# Chapter 9

## CG Location and 3 View Diagram

The following points are kept in mind while making the CAD model:

- 6mm thick aluminium is used as the fuselage and the wing/tail material.
- The Length of the tail arm/tail boom might change on stability analysis.
- The payloads are arranged as per figure with small changes which are discussed below.

The altered wing and tail parameters during the 3D Model are as follows(the parameters not mentioned in this table are taken same as the ones in previous chapters): The fuselage di-

Parameter	Value
Wing taper ratio	0.6m
root chord-wing	0.53m
tip chord-wing	0.32m
tail arm	1.17m
Vertical tail - root chord	0.49m
Vertical tail Tip chord	0.29m

mensions and the placement of the payloads are varied due to certain landing gear restrictions as will be discussed further.

1. The length of tail boom is decreased to 900mm and the length of the main body to 600mm.
2. The slot to access items which was initially planned to be on the top of the fuselage, is now at the side as shown in the figure.
3. The Camera is shifted behind to avoid restricted view due to the main landing gear due to which the fuselage main body dimensions had to be varied.
4. The nose type is changed to a little more ellipsoid( for drag reduction) compared to complete spherical as mentioned in chapter 7.

5. Note that such a shape of Landing gear is used to incorporate the Bungee Catapult suspension system in the actual design. The Bungee catapult design is ignored as of now since it is anyways lightweight and complex to make on CAD.
6. The additional platform made in the CAD is of plastic and is not Incorporated in the CG calculations.
7. The winglets, as mentioned before, are not used due to weight limitations and since they did not add much to the aerodynamic benefits.

## 9.1 CG of the fuselage

The origin in all these cases is taken at the start of the cylindrical part of fuselage at the midpoint.

The CG of the fuselage as shown in the fig 9.8, is

$$X_{cg} = 477mm, Y_{cg} = 177mm, Z_{cg} = 0$$

This CG covers the main fuselage body, the propellers, wing and the horizontal/vertical tail.

## 9.2 Payload CG

The payload is distributed as shown in the figure below. The figure also shows a slot to access the payloads as marked in blue.

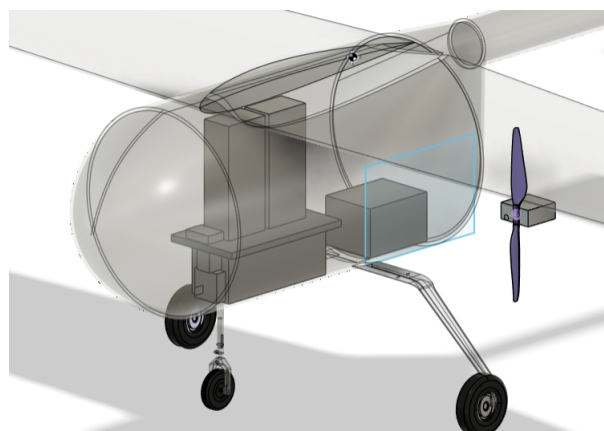


Figure 9.1: Distribution

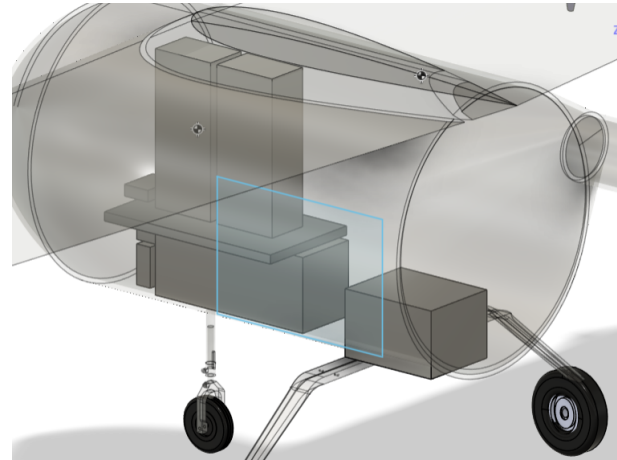


Figure 9.2: Slot to access the Payloads

### 9.2.1 Batteries

The batteries as mentioned are kept as forward as possible.

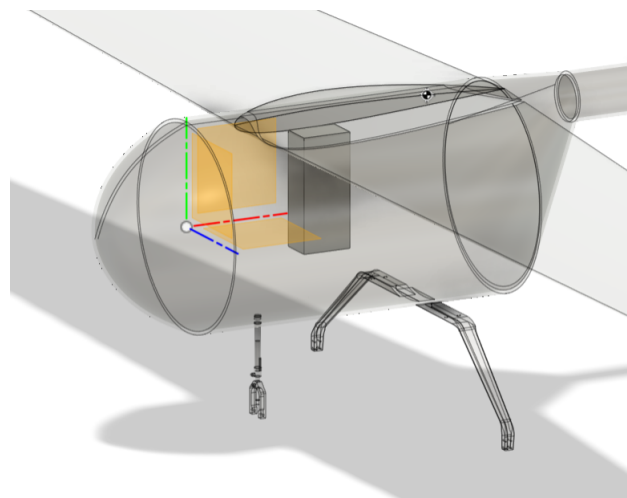


Figure 9.3: Battery Position

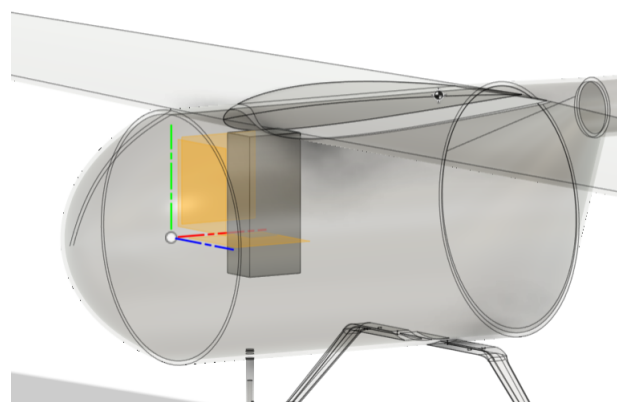


Figure 9.4: Battery Position

For battery 1:

$$X_{cg\text{battery}} = 145\text{mm}, Y_{cg\text{battery}} = 54\text{mm}, Z_{cg\text{battery}} = 0\text{mm}$$

For battery 2:

$$X_{cg\text{battery}} = 235\text{mm}, Y_{cg\text{battery}} = 54\text{mm}, Z_{cg\text{battery}} = 0\text{mm}$$

## 9.2.2 Camera/Gimbal

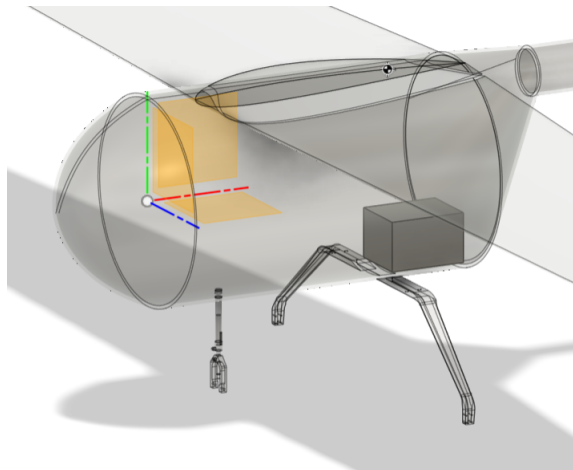


Figure 9.5: Camera/Gimbal Location

As mentioned before the Camera is shifted further from the nose for unrestricted view.

$$X_{\text{Camera}} = 570\text{mm}, Y_{\text{Camera}} = -110\text{mm}, Z_{\text{Camera}} = 0$$

## 9.2.3 Seed dropping system

The seed dropping system has the highest volume.

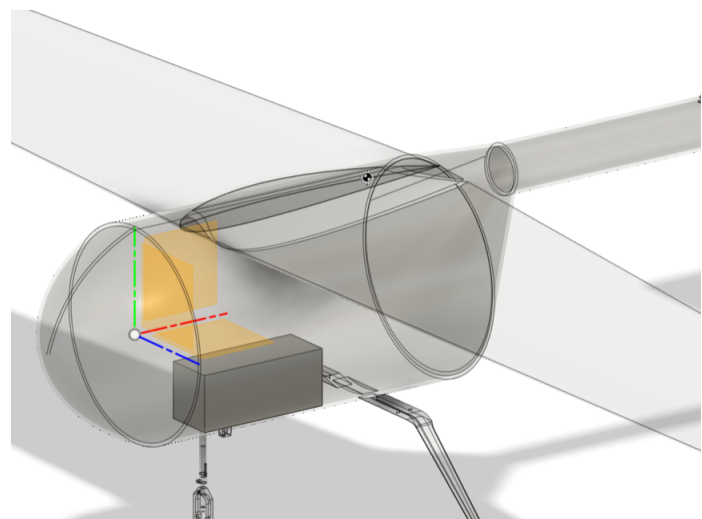


Figure 9.6: Seed Dispersal Mechanism Position

$$X_{\text{Seed}} = 303\text{mm}, Y_{\text{Seed}} = -115.5\text{mm}, Z_{\text{Seed}} = 0$$

#### 9.2.4 Sensors

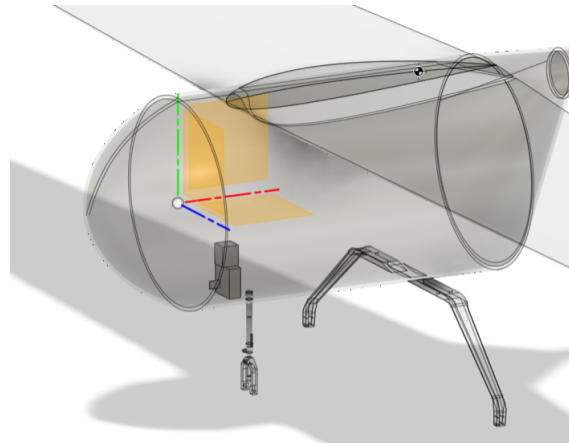


Figure 9.7: Sensors Location

$$X_{\text{Neo}} = 85\text{mm}, Y_{\text{Neo}} = -122\text{mm}, Z_{\text{Neo}} = 0$$

$$X_{\text{NDVI}} = 85\text{mm}, Y_{\text{NDVI}} = -155\text{mm}, Z_{\text{NDVI}} = 0$$

$$X_{\text{Pixhawk}} = 97.5\text{mm}, Y_{\text{Pixhawk}} = -161\text{mm}, Z_{\text{Pixhawk}} = 0$$

#### 9.2.5 Motor

$$X_{\text{Motor}} = 85\text{mm}, Y_{\text{Motor}} = -17.5\text{mm}, Z_{\text{Motor}} = 0$$

## 9.3 Final CG

Table 9.1: Payload exact CG location

Component	X(mm)	Y(mm)	Mass(kg)
Fuselage	477	177	8.35
Battery1	145	54	3.8
Battery2	235	54	3.8
Camera	570	-110	0.665
Flight controller	97.5	-161	0.0024
NDVI sensor	134.5	-155	0.05
Seed dispersal	303	-115.5	3
Neo	85	-122	0.023
Motor	85	-17.5	0.4

Hence, the CG location based on first estimate is

1.  $X_{CG} = 337.93mm$
2.  $Y_{CG} = 70.995mm$
3.  $Z_{CG} = 0$

## 9.4 Verifying the empty weight

Using the formulas given in [9], Chapter 10, and using the design parameters, we find the weight of each of the different segments that constitute the empty weight and thus verify it with the second weight estimate:

### 9.4.1 Wing

$$W_W = S_W \cdot MAC \cdot \left( \frac{t}{C} \right)_{\max} \cdot \rho_{\text{mat}} \cdot K_p \cdot \left( \frac{\text{AR} \cdot n_{\text{ult}}}{\cos(\Lambda_{0.25})} \right)^{0.6} \cdot \lambda^{0.04} \cdot g$$

Taking  $K_p = 0.0013$  as per general values given in [9],

$$W_w = 20.58N$$

## 9.4.2 Horizontal Tail

$$W_{HT} = S_{HT} \cdot MAC_{HT} \cdot \left( \frac{t}{C} \right)_{\max_{HT}} \cdot \rho_{mat} \cdot K_{\rho_{HT}} \cdot \left( \frac{AR_{HT}}{\cos(\Lambda_{0.25HT})} \right)^{0.6} \cdot \lambda_{HT}^{0.04} \cdot \bar{V}_H^{0.3} \cdot \left( \frac{C_e}{C_T} \right)^{0.4} \cdot g$$

Taking  $K_{pht} = 0.023$  as per general values given in [9],

$$W_{HT} = 8.3N$$

## 9.4.3 Vertical Tail

$$W_{VT} = S_{VT} \cdot MAC_{VT} \cdot \left( \frac{t}{C} \right)_{\max_{VT}} \cdot \rho_{mat} \cdot K_{\rho_{VT}} \cdot \left( \frac{AR_{VT}}{\cos(\Lambda_{0.25VT})} \right)^{0.6} \cdot \lambda_{VT}^{0.04} \cdot \bar{V}_V^{0.2} \left( \frac{C_r}{C_V} \right)^{0.4} \cdot g$$

Taking  $K_{pvt} = 0.067$  as per general values given in [9],

$$W_{VT} = 16.53N$$

## 9.4.4 Fuselage

$$W_F = L_f \cdot D_{f_{max}}^2 \cdot \rho_{mat} \cdot K_{\rho_f} \cdot n_{ult}^{0.25} \cdot K_{inlet} \cdot g$$

Here,

$$K_{inlet} = 1, K_{pf} = 0.003$$

we get,

$$W_F = 27.34N$$

## 9.4.5 Landing gear

$$W_{LG} = K_L \cdot K_{ret} \cdot K_{LG} \cdot W_L \cdot \left( \frac{H_{LG}}{b} \right) \cdot n_{ult\ land}^{0.2}$$

$$K_{ret} = 1, K_l = 1, K_{LG} = 0.5, W_L = 219.8N$$

$$W_{LG} = 6.68N$$

Hence the total weight along with the motors and propellers adds upto 8.2kg, a close approximation to what is used in our CG calculations and what was obtained using the second weight estimate.

## 9.5 Revised Landing gear Parameters

On recalculating the CG location, the Landing gear parameters change as mentioned in chapter8. The landing gear parameters are calculated using the CG from the 3D CAD and then added in the CAD model. If the CG changes again due to addition of the landing gear, then we find a new CG and iteratively change the landing gear parameters till we converge to a certain CG value. However for our case, the CG, before and after the landing gear are within a difference of 0.5% and hence we do not need to again calculate the landing gear parameters. The below pictures show the comparision of the CG location for the empty weight of the aircraft( with) and empty weight of the aircraft(without) the landing gear

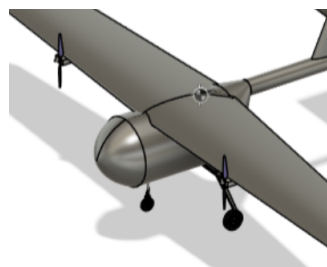


Figure 9.8: With landing gear CG

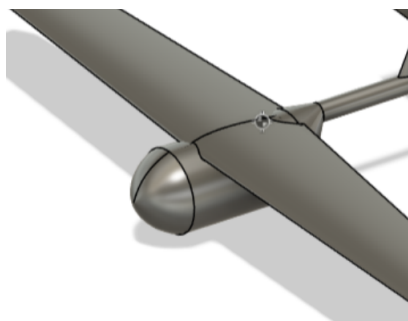


Figure 9.9: Without landing gear CG

Thus the final landing gear parameters are:

Note that we have increased the value of  $\frac{F}{W}$  to 0.3 as compared to 0.15 in previous section as

Parameter	Value
AB	135mm
Base	425mm
Track	735.4mm
Height	166.8mm
Clearance distance	150mm
$B_m$	127mm

we now account for the additional dynamic stress that the nose landing gear will have to face.

### 9.5.1 Detailed View of Landing Gear

As mentioned before, the main landing gear is made in such a way that it can best incorporate the bungee catapult mechanism in the actual design. Note that in figure 9.12, hooks are made on the front and back landing gear which will hold the bungee catapult suspension chords.



Figure 9.10: Landing gear detailed view 1



Figure 9.11: Landing gear detailed view 2

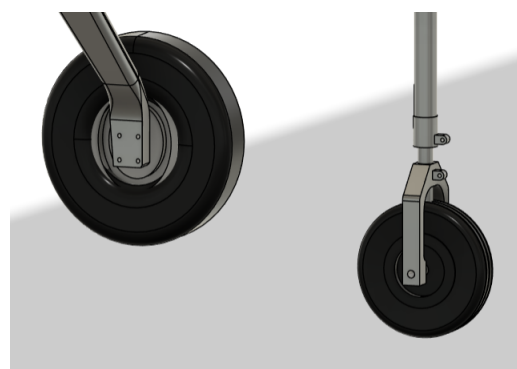


Figure 9.12: Landing gear detailed view 3

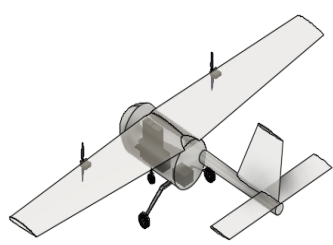
## 9.6 Final CAD Model and 3 view Diagram



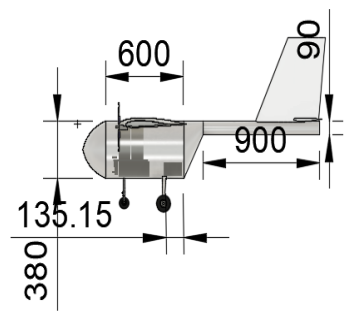
(a) Oblique view



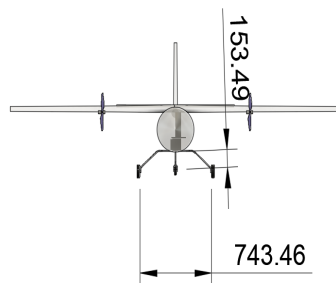
(b) Rendered CAD view



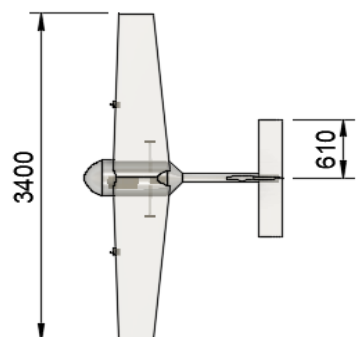
(a) Oblique view



(b) Side view



(a) Front view



(b) Top view

# Chapter 10

## Static Stability Analysis

### 10.1 Longitudinal Stability

Static longitudinal stability of an aircraft ensures that the aircraft is stable about the pitching plane i.e any change in the angle of attack will modify the pitching moment so as to bring the angle of attack back to initial equilibrium condition. Analytically by moment analysis, we can conclude that to have static longitudinal stability the aircraft pitching moment curve must have a negative slope.

$$\frac{\partial C_M}{\partial \alpha} < 0$$

The lift-curve slope is considered positive, therefore the above condition can be represented as,

$$\frac{\partial C_M}{\partial C_L} < 0$$

And for a balanced flight condition, the intercept of the curve,

$$C_{M_0} > 0$$

As we have taken the angle of attack at cruise zero and the corresponding wing setting angle as  $5^\circ$ . The Moment should be zero about the Cg for stable flight which means the moment is zero and zero angle of attack/cruise. Considering a linear-variation of the pitching-moment coefficient with respect to the angle of attack of the aircraft. The pitching moment coefficient  $C_M$  can be expressed as,

$$C_M = C_{M_0} + C_{M_\alpha} \alpha \quad (10.1)$$

Where, -  $C_{M_0}$  is the Pitching moment coefficient of the aircraft at zero angle of attack, -  $C_{M_\alpha}$  is the slope of the Pitching moment curve, and -  $\alpha$  is the angle of attack of the aircraft.

The main contribution to  $C_{M_0}$  and  $C_{M_\alpha}$  are from the wing, fuselage, power-plant and horizontal tail.

### 10.1.1 Contribution by wing

The Wing Aerodynamic Centre is at usually 40% of the fuselage length from the nose of the fuselage. The wing is shifted behind compared to what was in the previous CAD images to achieve this and the components like battery are brought further (towards the nose cone tip) to maintain the CG location same (so that the landing gear parameters do not change). Also, the aerodynamic centre of the wing is supposed to be behind the CG of the airplane to ensure moment stability. Thus,

-  $\frac{x_{cg}}{c}$  is the location of the centre of gravity of the aircraft from the nose of the aircraft, non dimensionalized with respect to the mean aerodynamic chord of the wing.

$$\frac{x_{cg}}{\bar{c}} = 1.2$$

$\frac{x_{ac}}{c}$  is the location of the aerodynamic center of the wing from the nose of the aircraft, non dimensionalized with respect to mean aerodynamic chord of the wing. The location of aerodynamic center of the wing, according to [8], is usually 1-2% of the quarter chord of the wing. Thus,

$$\frac{x_{ac}}{\bar{c}} = 1.4$$

-  $(C_{m_{ac}})_w$  is the pitching moment coefficient about the aerodynamic center of the wing. We find this using the value generated using the XFLR5 analysis of the airfoil. Using the formula from [8], we find the  $(C_{m_{ac}})_w$ .

$$C_{m_w} = C_{m_0 \text{airfoil}} \left( \frac{A \cos^2 \Lambda}{A + 2 \cos \Lambda} \right) \quad (10.2)$$

$$(C_{m_{ac}})_w = -0.04$$

-  $C_{L_{0w}}$  is the lift coefficient at zero angle of attack.

$$C_{L_{0w}} = a \times (0 - \alpha_{L=0}) = 0.26$$

$a$  is the lift-curve slope of the wing in per degrees.  $\alpha_{L=0}$  is the zero-lift angle of attack of the wing.

$C_{L_{\alpha_{wb}}}$  is the lift coefficient for the wing, found from XFLR5 analysis of the wing.

$$C_{L_{\alpha_{wb}}} = 0.20$$

### 10.1.2 Contribution of Fuselage to $C_{m_{\alpha cg}}$

:

The contribution of fuselage to  $C_{M_\alpha}$  is typically small positive or negative. The contribution

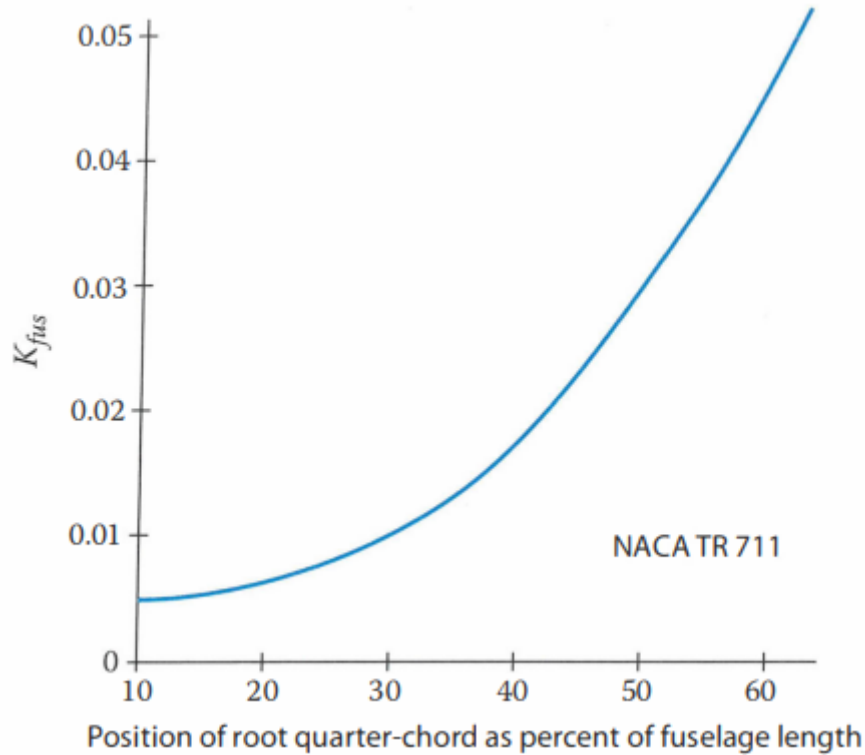


Figure 10.1: Empirical Plot for  $K_f$

of fuselage to  $C_{M_n}$  is expressed as,

$$C_{m_{\alpha}fuselage} = \frac{K_f * W_f^2 L_f}{c S_w} \quad (10.3)$$

where,

- $W_f = 0.350$  m is the maximum diameter of the fuselage
- $c_f = 1.852$  m is the length of the fuselage in the chord-wise direction.
- $S_v = 1.5000$  m<sup>2</sup> is the planform area of the wing.
- $c_w = 0.425$  m is the mean aerodynamic chord of the wing.

The value of K was found from an empirical plot given in [8].

### 10.1.3 Contribution of Tail to $C_{m_{\alpha}}$

As explained in detail in the next section, the volume ratio of horizontal tail is altered,

$$V_H = \frac{S_t l_t}{S \bar{c}} = 0.55$$

Corresponding to this, the non dimensionalized tail arm is given as,

$$X_{ac_h} = 4.04$$

$\eta$  is the tail efficiency factor,

$$\eta = \frac{C_{l_{\alpha_t}}}{2\pi} = 0.9119$$

$\varepsilon_0$  is the downwash angle at zero lift.

$$\varepsilon_0 = \frac{2C_{L_0}}{\pi e A R_w} = 0.0225 \quad (10.4)$$

$C_{L_{\alpha_t}}$  is the lift slope of tail for aspect ratio less than 5 in subsonic flow regime.

$$C_{L_{\alpha_t}} = 0.118 \text{ per}^\circ$$

-  $\frac{\partial \varepsilon}{\partial \alpha}$  is the rate of change of the downwash angle with respect to the angle of attack

$$\frac{\partial \varepsilon}{\partial \alpha} = \frac{2C_{L_\alpha}}{\pi e A R_w} = 0.01194 \quad (10.5)$$

## Calculation of tail setting angle

The tail setting angle is calculated using moment balance during cruise conditions. During cruise conditions, the  $\alpha_f = 0$  as the motion of the aircraft is horizontal.

$$C_{m_{o\_wf}} + C_L (h - h_o) - \eta_h \bar{V}_H C_{L_h} = 0$$

$$\begin{aligned} \alpha_h &= \alpha_f + i_h - \varepsilon \\ C_{L_{\alpha\_h}} &= \frac{C_{L_h}}{\alpha_h} \Rightarrow \alpha_h = \frac{C_{L_h}}{C_{L_{\alpha\_h}}} \end{aligned}$$

Thus we find the value of tail setting angle as  $i_h = 1.6^\circ$

### 10.1.4 Final Values

Using the parameters found above and the formulas from [8],

$$C_{m_\alpha} = C_{L_\alpha}^{wb} (\bar{X}_{cg} - \bar{X}_{acw}) + C_{m_{\alpha_{fus}}} - \eta_h \frac{S_h}{S_w} C_{L_\alpha}^t (\bar{X}_{ach} - \bar{X}_{cg}) \left( 1 - \frac{\partial \epsilon}{\partial \alpha} \right) = -5.27 \text{ rad}^{-1}$$

The value of  $C_{m_0} > 0$  which implies that the flight condition is balanced and the value of  $C_{m_\alpha} < 0$  which implies that the aircraft is statically stable about its longitudinal axis

### 10.1.5 Stick Fixed Neutral Point

In chapter 7, we have calculated the optimum tail arm as  $1.17m$ , using the altered parameters mentioned in chapter 9. However, with a horizontal tail arm of  $1.17m$ , the static margin is slight negative. Hence, without changing the CG, we increase the tail arm(i.e. the distance between the centre of gravity to the Aerodynamic centre of the horizontal tail) to make the

horizontal tail arm  $1.25m^2$ . Hence, the volume ratio of the horizontal tail( $V_H$ ) also changes to 0.55.

Using these values in the equation below,

Note that the vertical tail arm is kept at 1.17m as decided in previous chapter.

$$\bar{X}_{np} = \frac{C_{L_\alpha}^{wb} \bar{X}_{acw} - C_{m_{\alpha_{fus}}} + \eta_h \frac{S_h}{S_w} C_{L_{\alpha_h}} \left(1 - \frac{\partial c}{\partial \alpha}\right) \bar{X}_{ach} + \frac{F_{p\alpha}}{qS_w} \frac{\partial \alpha_p}{\partial \alpha} \bar{X}_p}{C_{L_\alpha}^{wb} + \eta_h \frac{S_h}{S_w} C_{L_{\alpha_h}} \left(1 - \frac{\partial c}{\partial \alpha}\right) + \frac{F_{p\alpha}}{qS_w}}$$

$$X_{np}/C = 1.667$$

$$\text{Static Margin,SM} = \frac{X_{NP} - X_{CG}}{\bar{c}} = 0.433 \quad (10.6)$$

### 10.1.6 Longitudinal Control derivatives

The elevator power,  $C_{m_{\delta_e}}$  is given as:

$$C_{m_{\delta_e}} = -\eta V_H C_{l_{\alpha_t}} \tau = -1.413 \text{rad}^{-1}$$

Here,  $\tau$  is the hinge effectiveness, estimated to be 0.5 based on the plot given in [9].

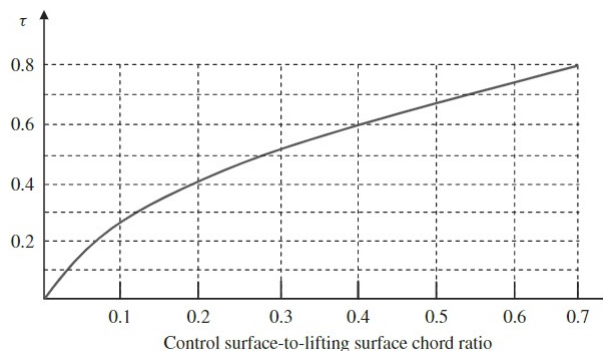


Figure 10.2: Value of Tau

## 10.2 Directional Stability $C_{n_\beta}$

The directional stability formulas used in this section can be found at [4]

Directional static stability is concerned with the ability of the aircraft to yaw or weathercock into wind in order to maintain directional equilibrium. Since all aircraft are required to fly with zero sideslip in the yaw sense, positive directional stability is designed in from the outset.

Yaw (or directional) stability is easy to obtain by incorporating the proper amount of vertical fin or stabilizer area. The fuselage and vertical tail surfaces are the two major contributors. As in the case of pitch, the side force coefficient versus yaw angle must have a negative slope for stability. The vertical fin must be able to create a restoring moment that minimizes the

yaw angle caused by a side force disturbance.

When a laterally directionally dynamically stable aircraft encounters a lateral-directional disturbance (for example, a horizontal wind strikes the vertical tail), it resists the disturbance and eventually returns to the initial trim point. There are static and dynamic requirements for lateral-directional stability. The condition for an aircraft to be directionally stable is thus readily established:

$$\frac{dC_l}{d\beta} < 0 \Rightarrow C_{l_\beta} < 0 \quad (10.7)$$

$$\frac{dC_n}{d\beta} > 0 \Rightarrow C_{n_\beta} > 0 \quad (10.8)$$

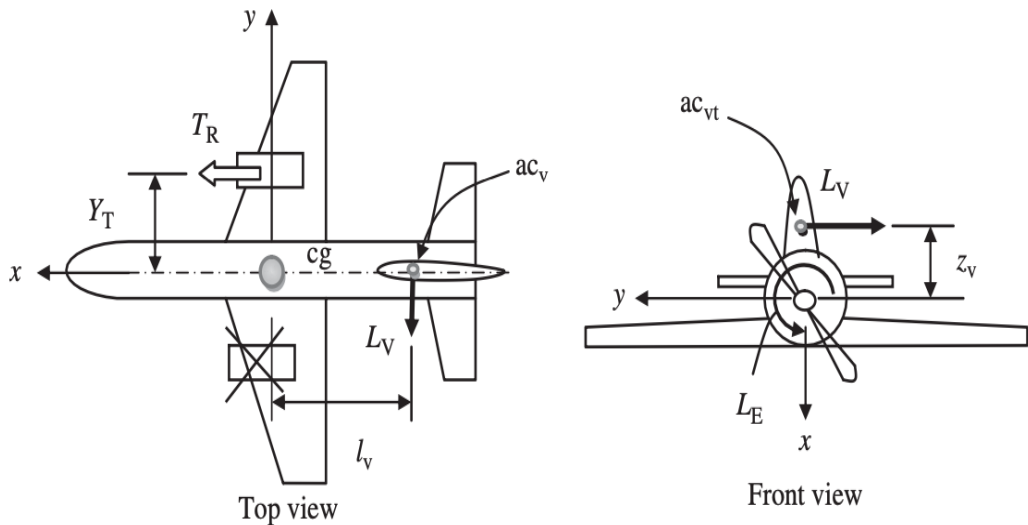


Figure 10.3: Vertical tail role in the aircraft directional trim

The rudder is a primary control surface and is responsible for the aircraft directional control. The rudder is a movable surface located on the trailing edge of the vertical tail. When the rudder is rotated (i.e., deflected,  $\delta_R$ ), a lift force (i.e., side force,  $L_v$ ) is created by the rudder/vertical tail combination. Consequently, a yawing moment (N) about the aircraft center of gravity (about the aircraft z-axis) is generated.

The vertical tail, fuselage, and wing contribute the most to directional stability. Other contributions are generally minimal.

$$C_{n_\beta} = C_{n_{\beta_w}} + C_{n_{\beta_{VT}}} + C_{n_{\beta_{FUS}}} + C_{n_{\beta_{NAC}}} + C_{n_{\beta_{TY}}}$$

where,

- $C_{n_{\beta_w}}$  = Directional derivative due to the wing
- $C_{n_{\beta_{VT}}}$  = Directional derivative due to the vertical tail

- $C_{n_{\beta_{FUS}}} =$  Directional derivative due to the fuselage
- $C_{n_{\beta_{NAC}}} =$  Directional derivative due to the nacelles
- $C_{n_{\beta_{TY}}} =$  Directional derivative due to the propeller side forces

Since our UAV is smaller in size when compared to actual aircraft, we are neglecting  $C_{n_{\beta_{TY}}}$  and  $C_{n_{\beta_{NAC}}}$  as our UAV does have nacelles. We know that contribution due to fuselage is very small negative value, hence we are also neglecting  $C_{n_{\beta_{FUS}}}$

$$\Rightarrow C_{n_{\beta}} = C_{n_{\beta_w}} + C_{n_{\beta_{VT}}} \quad (10.9)$$

### 10.2.1 Contribution due to wing

The wing's contribution to directional stability is often minor. Here, two contributions are integrated into one: **(1) yawing moment owing to wing sweep** and **(2) yawing moment due to the wing's vertical position**. The yawing moment caused by wing sweep is only important for wings that are swept forward or back. The contribution is given by,

$$\begin{aligned} C_{n_{\beta_w}} &= 0.00006k\sqrt{\Lambda_{c/4}} + \Delta_{pos} \text{ per degree} \\ &= 0.00344k\sqrt{\Lambda_{c/4}} + \Delta_{pos} \text{ per radian} \end{aligned}$$

where,

- |   |   |
|---|---|
| • $k = -1$ for a forward swept wing             | • $\Delta_{pos} = 0.0057$ for mid wings |
| • $k = +1$ for an aft swept wing                |   |
| • $\Delta_{pos} = 0$ for low wing configuration | • $\Delta_{pos} = 0.0115$ for high wing |

$C_{n_{\beta_w}}$  is in the order of  $10^{-3}$  which is very negligible when compared to  $C_{n_{VT}}$  so we are neglecting that in our case.

### 10.2.2 Contribution due to Fuselage

The contribution of the fuselage to directional stability is shown in the yawing moment coefficient below.

$$C_{N_{\beta_{FUS}}} = -\frac{\pi(k_2 - k_1)}{2Sb} \int_0^{l_{FUS}} w_f^2 dx \quad \text{per radian}$$

where,

- $k_2 - k_1$  = Correction factor to account for the fuselage slenderness ratio
- $w_f$  = Average width of a fuselage section.
- $k_2 - k_1 = 1 - \frac{1}{f} + \left( \frac{0.24f^3 - 5.6f^2 + 44f - 72}{1000} \right)$
- $f$  = Fuselage fineness ratio =  $\frac{\text{Fuselage length}}{\text{Fuselage depth}}$

The wing fuselage contribution can also be calculated from the following empirical expression:

$$C_{N_{\beta FUS}} = -K_N K_{Rl} \frac{S_{fs} l_f}{S_w b} \quad (10.10)$$

where  $K_N$  is the wing body interference parameter. The value of  $C_{N_{\beta FUS}}$  will be in the order of negative  $10^{-4}$  which is very negligible when compared to the  $C_{n_{VT}}$ , so we are neglecting the value to the total contribution of  $C_{n_{\beta}}$

### 10.2.3 Contribution due to Vertical Tail

The yaw moment coefficient contribution due to tail is given by:

$$\begin{aligned} C_{n_{VT}} &= \eta_v \frac{S_v l_v}{S_b} C_{l_v} \\ \Rightarrow \frac{\partial C_{n_{VT}}}{\partial \beta} &= \eta_v \frac{S_v l_v}{S_b} \frac{\partial C_{l_v}}{\partial \alpha} \end{aligned} \quad (10.11)$$

where,  $C_{l_v}$  is lift coefficient of vertical tail and  $\eta_v$  is the vertical tail efficiency factor. By substituting the values we get,

$$\frac{\partial C_n}{\partial \beta} = 0.9119 \times 0.05 \times 0.118 \times 57.2958 \quad (10.12)$$

$$\frac{\partial C_{n_{VT}}}{\partial \beta} = 0.3082 \text{ per radians}$$

(10.13)

$\frac{\partial C_n}{\partial \beta} > 0$  , we can confirm that UAV has yaw stability.

### 10.2.4 Directional Control

The rudder control effectiveness is the rate of change of yawing moment with rudder deflection angle expressed as,

$$C_{N_{\delta r}} = -\eta_v V_v C_{L_{\alpha_V}} \tau = -0.125 \text{ rad}^{-1}$$

Here we take,  $\eta_v = 0.80$  and  $\tau = 0.5$ .

## 10.3 Lateral Stability

An airplane is considered to possess static lateral stability if it autonomously returns to a wings-level position when perturbed. This stability is characterized by the development of a restoring moment that corrects any deviation from straight and level flight, particularly when the aircraft banks to the right at an angle known as  $\beta$ . When such a bank occurs, a negative rolling moment must be generated to counteract the bank and restore the aircraft to its original wings-level state, thus ensuring lateral stability.

For an aircraft to exhibit static lateral stability, it's essential that the contribution to a stability parameter denoted as  $C'_l$  (indicative of lateral stability) from various aerodynamic components meets specific criteria.

The overall contribution to  $C'_l$  is comprised of three primary components: the wing ( $C'_{l\beta w}$ ), the fuselage ( $C'_{l\beta f}$ ), and the vertical tail ( $C'_{l\beta V_T}$ ).

### Contribution of the Wing to $C'_{l\beta}$

The dihedral angle ( $\gamma$ ) and sweep angle ( $\Lambda$ ) of the wing typically play a significant role in lateral stability. However, in the case of our model, where both dihedral and sweep angles are set to zero. The  $(C_{\ell_\beta})_\Gamma$  is thus zero.

$$\begin{aligned} (C_{\ell_\beta})_\Gamma &= -\frac{C_{L_\alpha}\Gamma}{4} \left[ \frac{2(1+2\lambda)}{3(1+\lambda)} \right] \\ C_{\ell_{\beta wf}} &= -1.2 \frac{\sqrt{A}Z_{wf}(D_f + W_f)}{b^2} \\ C_{\ell_{\beta w}} &= \left( \frac{C_{\ell_{\beta wing}}}{C_L} \right) \\ C_L + (C_{\ell_\beta})_\Gamma + C_{\ell_{\beta wf}} & \end{aligned} \tag{10.14}$$

Here, A = Aspect ratio of the wing=8,

$D_f$  = Depth of the fuselage=0.350m,

$W_f$  = Width of the fuselage=0.350m,

B = span of the wing=3.49m The value of  $\left( \frac{C_{\ell_{\beta wing}}}{C_L} \right)$  is approximated from the empirical plots below from [8]. Thus we get  $C_{l_{\beta wing}} = -0.0027 rad^{-1}$

### Contribution of the Fuselage to $C'_{l\beta}$

The fuselage affects lateral stability primarily due to interference effects. In a high-wing configuration, when the aircraft banks to the right, there's a positive change in angle of attack on the right wing and a negative change on the left wing. This differential change induces a negative rolling moment, effectively aiding in lateral stability. Conversely, in a low-wing configuration,

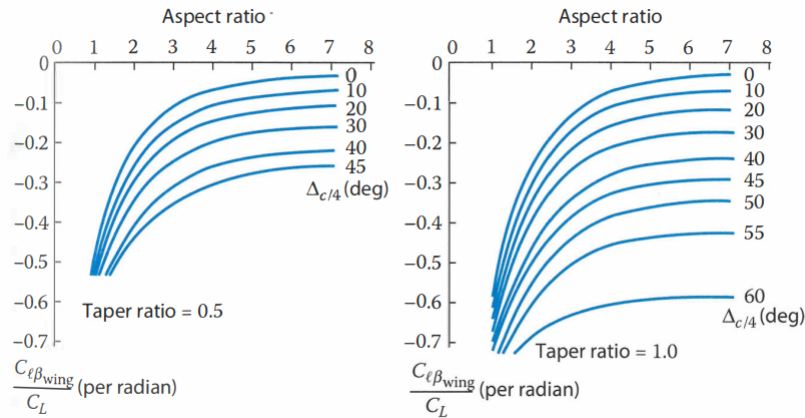


Figure 10.4: Empirical plots [8]

the effect can be destabilizing.

$$\Delta C'_{l\beta_w} = -0.0006 \text{ degree}^{-1} \text{ for high wing configuration.}$$

$$\Delta C'_{l\beta_w} = 0.0000 \text{ degree}^{-1} \text{ for mid wing configuration.}$$

$$\Delta C'_{l\beta_w} = 0.0006 \text{ degree}^{-1} \text{ for low wing configuration.}$$

## Contribution of the Vertical Tail to $\Delta C'_{l\beta}$

The vertical tail generates a side force when the aircraft banks, contributing to lateral stability. This force acts above the aircraft's center of gravity (c.g.) and helps counteract the rolling motion. The contribution of the vertical tail to lateral stability is calculated using parameters like the lift-curve slope ( $C_{L\alpha V}$ ) of the vertical tail, the tail efficiency factor ( $\eta_v$ ), the tail area ( $S_v$ ), the distance from the fuselage centerline to the vertical tail's aerodynamic center ( $Z_v$ ), wing planform area ( $S_w$ ), and wing span ( $b$ ).

$$\Delta C'_{l\beta} = -\eta_v C_{L\alpha V} \frac{S_v Z_v}{Sb} \quad (10.15)$$

Where,

- $C_{L\alpha V} = 0.118 \text{ degree}^{-1}$  is the lift-curve slope of the vertical tail.
- $\eta_v = 0.9119$  is assumed to be the vertical tail efficiency factor.
- $S_v = 0.206 \text{ m}^2$  is the area of the vertical tail.
- $Z_v = 0.1466$  is the distance from the fuselage centerline to the aerodynamic center of the vertical tail.
- $S_w = 1.5 \text{ m}^2$  is the planform area of the wing.
- $b = 3.49 \text{ m}$  is the span of the wing.

The specific contribution of the vertical tail to lateral stability is estimated to be  $\Delta C'_{L_\beta} = -0.03083 \text{ rad}^{-1}$  (a negative value), ensuring that  $C'_{l_\beta} = -0.03953 \text{ rad}^{-1} < 0$ , thereby confirming the aircraft's static lateral stability.

$$C_{\ell_\beta} = C_{\ell_{\beta_w}} + C_{\ell_{\beta_v}}$$

In summary, static lateral stability is a critical characteristic of aircraft design, ensuring that the aircraft naturally corrects any deviations from level flight due to banking maneuvers. The combination of wing configuration, fuselage design, and vertical tail characteristics all contribute to maintaining this essential stability property during flight.

## 10.4 Control Surface Sizing

### 10.4.1 Elevators

As mentioned in chapter 7, we take the conventional sizing for the elevator,

$$S_e = 0.056m^2, b_e = b_h = 1.2m, c_e = 0.066m$$

The maximum elevator deflection is calculated by calculating at what angle of attack is the aircraft stalling and using the derivatives  $C_{m_\alpha}$  and  $C_{m_{\delta_e}}$ , we find the corresponding elevator deflection that causes the aircraft to pitch. This is the maximum deflection as beyond this, if the aircraft pitches, it will stall.

Thus, maximum elevator deflection is  $15^\circ$ .

### 10.4.2 Rudder

As mentioned in chapter 7, since we will be loitering at low speeds, we have selected an **all flying vertical tail/rudder** for our uav.

If a particular engine fails, then the rudder should be capable of producing the required force to counteract the moment caused due to single engine operating. This is important for our case as we are going for a twin motor tractor configuration.

If one of the the motor fails, during take off, cruise or loiter, the maximum moment(yawing motion) that will be generated by the remaining working motor (assuming that it is providing all the thrust required to complete the given segment and land safely) is :

$$M = l_p T$$

Where  $l_p$  is the distance from the fuselage reference line to where the propeller is on the wing. Usually it is taken as 15-20% of the half wing span.

Thus, the Maximum Moment required to be generated by rudder deflection is 3.45Nm. Now,

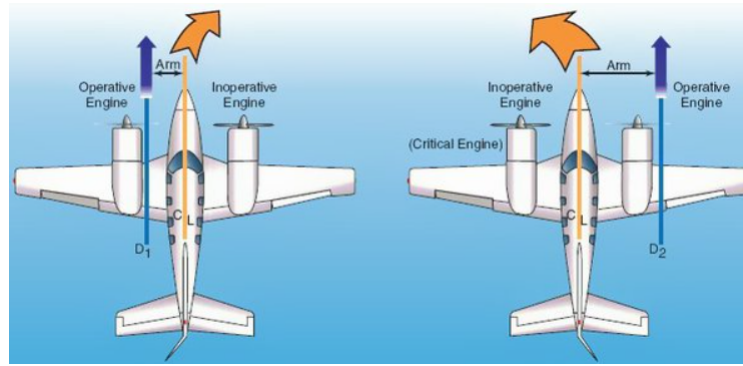


Figure 10.5: One engine/Motor Fail scenario

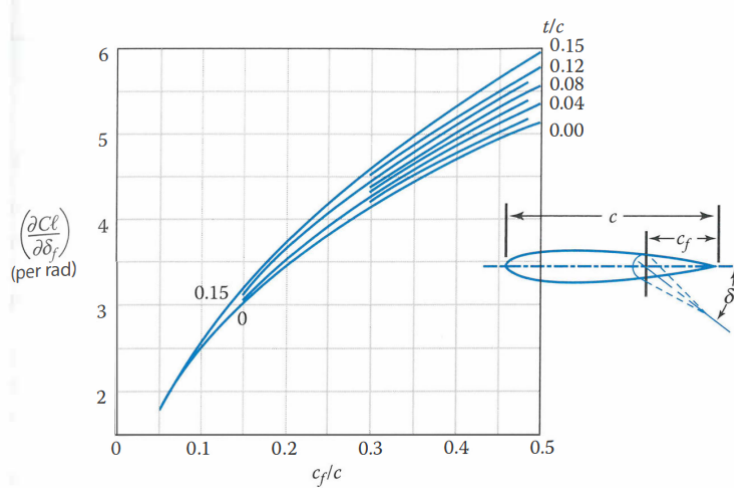


Figure 10.6: Empirical plots [8]

using the value of  $C_{N_{\delta_r}}$  control derivative found, we find the maximum rudder deflection as  $25.7^\circ$ .

This maximum rudder deflection will also be the maximum the rudder will be able to counter balance the crosswinds during takeoff.

### 10.4.3 Aileron

The aileron effectiveness is calculated based on the formulas from [8]. Based on an iterative method and the historical rule of thumb for aileron sizing, we fix the aileron sizing.

$$C_{\ell_{\delta_a}} = \frac{2 \sum K_f \left( \frac{\partial C_L}{\partial \delta_f} \right)' Y_i S_i \cos \Lambda_{H.L.}}{S_w b} = -0.145 \text{ rad}^{-1} \quad (10.16)$$

$$\begin{aligned} \frac{\Delta \alpha_{0L}}{\delta_e} &= \frac{1}{C_{L_\alpha}} \frac{\partial C_L}{\partial \delta_f} \\ &= 1.576 (C_f/C)^3 - 3.458 (C_f/C)^2 + 2.882 (C_f/C) \\ &= 0.7003 \end{aligned}$$

The span and cord of the ailerons are approximated at 15% and 30% of the wing of the UAV.

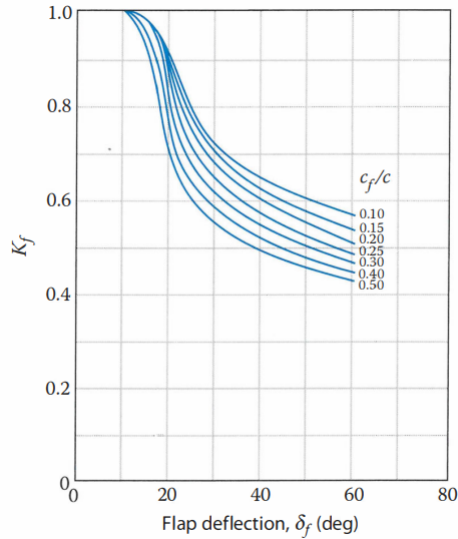


Figure 10.7: Empirical plots [8]

## 10.5 High Lift Devices

As mentioned before, we will be using high lift devices mainly flaps and slats. The maximum deflection of the fowler flap during take off will be  $40^\circ$ as per the required lift calculations in chapter 6.

The maximum deflection of the slats to give the required rotation angle during the transition phase is  $20^\circ$ as per the transition phase calculations done in landing gear calculations in chapter 8.

The sizing of the fowler flaps is does on basis of the wing loading we require at take off for the changed planform area of the wing. In normal conditions(i.e. in cruise), the wing loading required is  $150\text{N/m}^2$ . However, during Take off and landing, to generate a  $C_l$  of greater than 3 for a short take off landing distance, we need a wing loading of  $100\text{N/m}^2$  as per the calculations done in chapter 4.

# Chapter 11

## Performance Analysis

### 11.1 Drag Polar

The drag polar equation can be written as :

$$C_D = C_{D_0} + KC_L^2$$

#### 11.1.1 Calculation of $C_{D_0}$

$$(C_{D_0})_{\text{subsonic}} = \frac{\sum (C_{f_c} FF_c Q_c S_{\text{wet}_c})}{S_{\text{ref}}} + C_{D_{\text{misc}}} + C_{D_{\text{L&P}}} \quad (11.1)$$

#### Calculation of $C_f$

The most important factor affecting skin-friction drag is the extent to which the aircraft has laminar flow over its surfaces. The skin-friction drag can literally be doubled if the flow is turbulent rather than laminar.

The below figure shows general predictions of the location where the flow transitions to turbulence.

$$R_e = \frac{\rho v l}{\mu}$$

where,  $l$  is the characteristic length taken to be the length of the component along the flow.

$R_e$  is the Reynolds number  $\rho = 1.225 \text{ kg/m}^3$

$\mu = 1.872 \times 10^{-5}$  is the dynamic viscosity

For laminar flow:

$$C_f = 1.328/\sqrt{R}$$

For Turbulent Flow:

$$C_f = 0.059/(Re)^{\frac{1}{5}}$$

Once laminar and turbulent flat-plate skin-friction coefficients have been calculated, an aver-

**Table 12.4** Laminar Flow Estimation Guidelines

Attainable Laminar Flow as a Percentage of Wetted Area	Fuselage, %	Wing and Tails, %
<b>Subsonic</b>		
General aviation—classic production metal	0	10
General aviation—smooth metal (no rivets or cracks)	10	35
General aviation—smooth molded composites	25	50
Sailplane—smooth molded composites	35	70
Helicopter—traditional design	0	0
Helicopter—smooth design	20	20
Civil jet—classic production metal	5	10
Civil jet—research goal (passive)	25	50
Civil jet—research goal (with active suction)	50	80
Military aircraft with camouflage	0	0
<b>Supersonic</b>		
Current	0	0
Research goal (with active suction)	20	40

Figure 11.1: Turbulent-Laminar % [8]

aged coefficient is found as the weighted average of the two, based on the attainable percent of laminar flow estimated above.

Table 11.1: Component wise calculated parameters

Component	Characteristic length(m)	Reynolds No.	Skin Friction Coefficient	Swet/Sref
Fuselage	0.952	1295777.77	0.0035346	0.4311
Vertical Tail	0.37	503611.11	0.004030	0.3375
Horizontal Tail	0.22	299444.44	0.004506	0.295
Tail boom	0.9	1225000.0	0.003574	0.085
Wing	0.425	578472.22	0.00391	2.05

## Calculation of form factor

Wing, tail, strut, and pylon:

$$FF = \left[ 1 + \frac{0.6}{(x/c)_m} \left( \frac{t}{c} \right) + 100 \left( \frac{t}{c} \right)^4 \right] [1.34M^{0.18} (\cos \Lambda_m)^{0.28}] \quad (11.2)$$

Fuselage/Tail boom and smooth canopy\*:

$$FF = \left( 0.9 + \frac{5}{f^{1.5}} + \frac{f}{400} \right) \quad (11.3)$$

$(t/c)_{\max}$  is maximum thickness-to-chord ratio of the airfoil,  $(x/c)$  is the position of the maximum thickness with respect to the chord.

$\Lambda$  is the sweep of the component.

$M$  is close to 0.

Here,  $f = \frac{l_f}{d_f}$

$l_f$  and  $d_f$  the lengths and diameters of the fuselage/tailboom respectively.

## Calculation of interference factor

For a nacelle or external store mounted directly on the fuselage or wing, the interference factor Q is about 1.5. If the nacelle or store is mounted less than about one diameter away, the Q factor is about 1.3. If it is mounted much beyond one diameter, the Q factor approaches 1.0. Wing-tip-mounted missiles have a Q factor of about 1.25. For a high-wing, a mid wing, or a well-filletted low wing, the interference will be negligible so that the Q factor will be about 1.0. An undiluted low wing can have a Q factor from about 1.1-1.4. The fuselage has a negligible interference factor (Q = 1.0) in most cases. Also, Q = 1.0 for a boundary-layer diverter. For tail surfaces, interference ranges from about 3% (Q = 1.03) for a clean V-tail to about 8% for an H-tail. For a conventional tail, 4-5% can be assumed.

Table 11.2: Component wise Calculated values

Component	FF	Q	$\frac{(C_{fc} FF_c Q_c S_{wet\_c})}{S_{ref}}$
Fuselage	2.023	1	0.0271
Vertical Tail	1.156	1.08	0.0019
Horizontal Tail	1.156	1.03	0.0015
Tail boom	1.083	1	0.0003
Wing	1.261	1	0.0101

$$C_{D_0} = 0.0166$$

To account for the miscellaneous drag (caused due to the protruding part of the seed chamber), we add a factor to this and thus final value is taken as 0.017.

As we can see, this  $C_{D_0}$  value is very close to what we had initially assumed for the wing loading and power loading calculations from previous aircraft data.

### 11.1.2 Calculation of K

K is given as,

$$K = \frac{1}{\pi A Re}$$

$$e = 1.78 (1 - 0.045 A^{0.68}) - 0.64 = 0.81 \quad (11.4)$$

Hence,  $K = 0.049$

### 11.1.3 Final Diagram

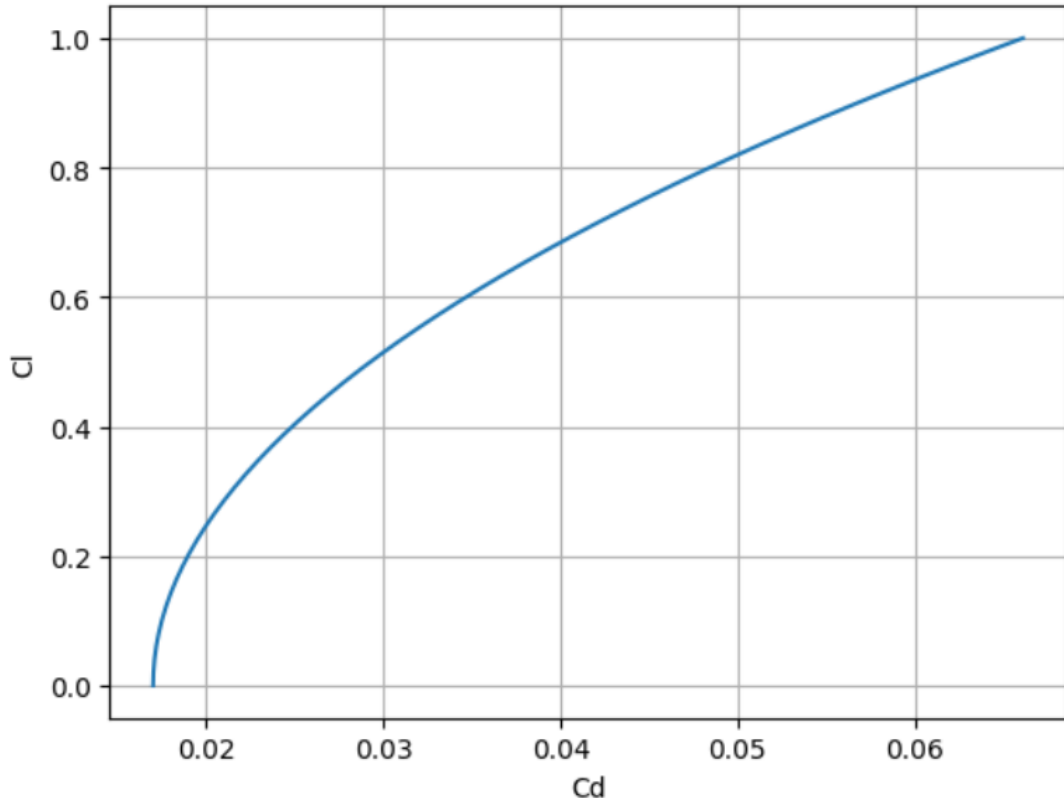


Figure 11.2: Drag Polar

## 11.2 Variation of Power vs Velocity

To determine the range of velocities that correspond to the variation of velocity from minimum to maximum, we can analyze the intersection points of the power required and power available curves when plotted against velocity. These curves represent the power needed to maintain a certain velocity and the power available from the propulsion system at different speeds, respectively. By identifying the velocity values at which the power required equals the power available, we can find the minimum and maximum velocities for the given system.

$$\begin{aligned}
 T &= D = \frac{1}{2} \rho v^2 S C_D \\
 C_D &= C_{D,0} + K C_L^2 \\
 C_L &= \frac{L}{\frac{1}{2} \rho v^2} = \frac{W}{\frac{1}{2} \rho v^2} \\
 P &= T v \\
 P &= \frac{1}{2} \rho v^3 S C_{D,0} + \frac{kW}{\frac{1}{2} \rho v S}
 \end{aligned} \tag{11.5}$$

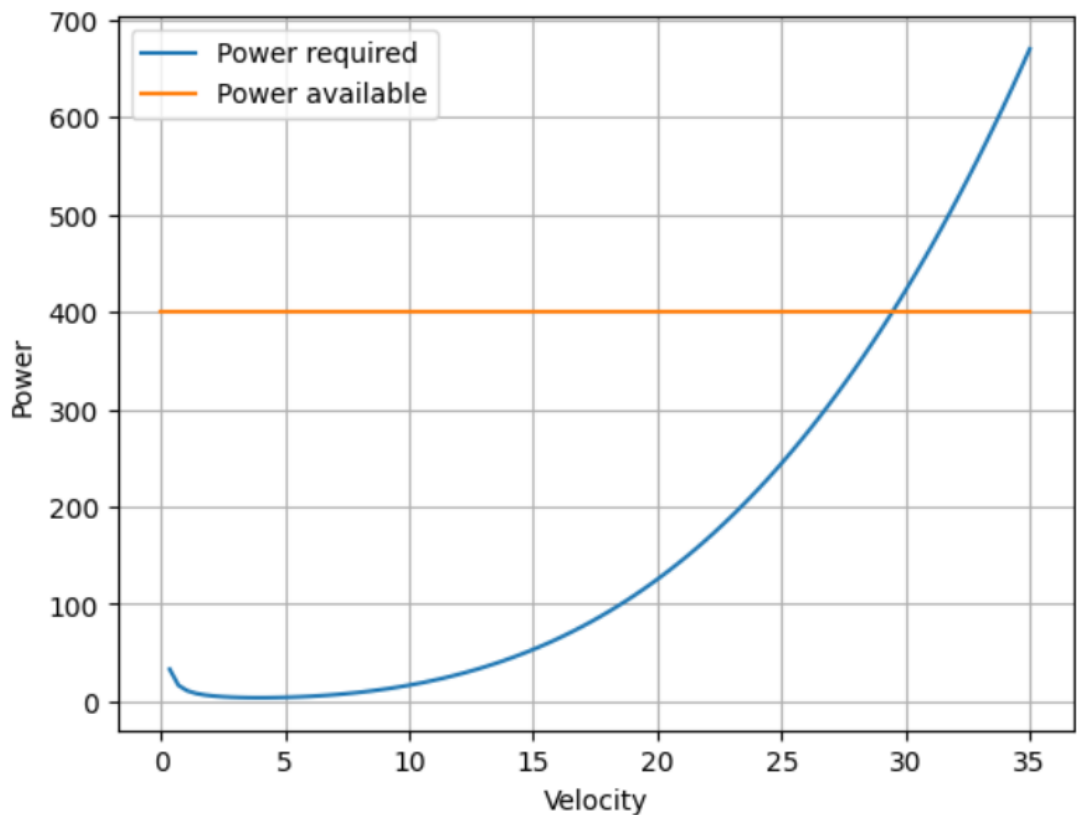


Figure 11.3: Power Velocity Bucket curve

### 11.3 V-n Diagram

V-n diagrams (speed - load factor) define the strength limitations of an aircraft. V-n diagrams are created at the conceptual or preliminary design stages. Aircraft performance is often limited by aerodynamics, structure, and engine capability. A V-n diagram depicts an aircraft's operational envelope. Before presenting the diagram, we shall examine aerodynamic and structural limitations.

Four factors affect a V-n Diagram

- MGTOW
- Altitude
- Configuration of aircraft: cruise or landing, etc.
- Symmetry of loading

As previously stated, stall limits an aircraft's aerodynamic performance. In Sec. 1.5, we constructed an equation for stall airspeed, which is replicated in Eq. (3.70), but in a more generic version with lift substituted by  $nW$ . Previously, we assumed a load factor of 1 ( $L = W$ ).

$$V_{STALL} = \sqrt{\frac{2nW}{\rho_\infty SC_{L,max}}}$$

A V-n diagram demonstrates that pulling gs causes an airplane to stall at a higher airspeed. An airplane can only endure a certain amount of g loading before structural failure. This g loading is commonly indicated as  $n_{max}$ . At the corner velocity, an aircraft is on the verge of stalling and achieving max g (or maximum load factor), as defined:

$$\text{Corner velocity} = V^* = \sqrt{\frac{2n_{max}W}{\rho_\infty C_{L,max}S}} \quad (11.6)$$

Important points about V-n diagram:

- A V-n diagram is suitable for a single weight, altitude, and arrangement.
- The operational envelope refers to the safe operating range for an aircraft based on airspeed and load factor.
- Check the positive and negative stall limits. The higher the load factor, the higher the stall airspeed. At a load factor of 1.0 (lift equals weight), the 1-g stall limit is easily determined.
- The corner velocity V is displayed. It is at the intersection of the aircraft's stall and structural limits.
- The aircraft has a positive and negative limit load factor, over which would cause damage. An airplane is often built to withstand greater positive than negative gs.
- At high speeds, the airplane reaches a 'q limit'. The limit could be either aeroelastic or temperature-related. Exceeding this limit results in unsatisfactory structural and handling attributes.
- Using equivalent velocity ( $V_e$ ) on the horizontal axis of the V-n diagram ensures it remains unaffected by altitude variations.

Gusts are vertical draughts of air, they could be upwards or downwards. They impose additional vertical load factors in an aircraft.

- If the a/c was in level flight than this additional load factor will add to the existing load factor of 1 (level flight)
- The graph of load factor will start from (0,1)
- The airworthiness authorities have specified certain values of gust velocities to be considered in V-N diagram depending on the type of a/c and the altitude of flight.
- For general Aviation-normal aircraft, typical load factors are given by  $n_{positive}$  is from 2.5 to 3.8 and  $n_{negative}$  is from -1 to -1.5
- Typically, N(negative) is almost half of N(positive).
- We have choose N(positive) to be 3 and subsequently N(negative) = -1.5

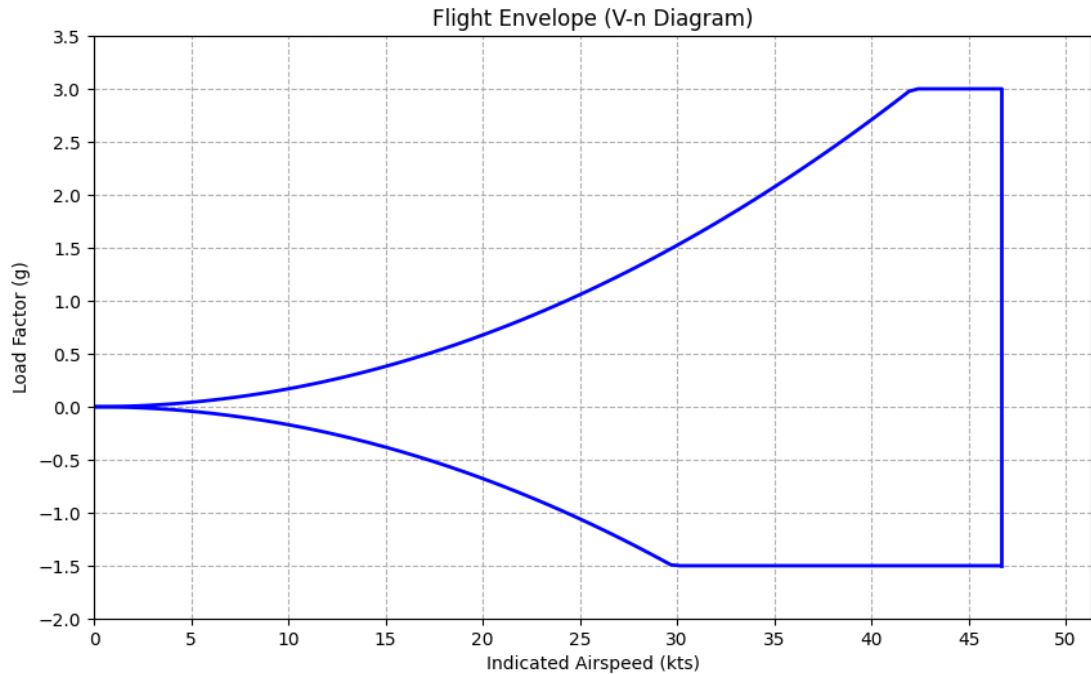


Figure 11.4: V-n diagram at Sea Level

The python code for obtaining the V-n diagram is given in the **Appendix E**

## 11.4 Range and Endurance

Endurance, the maximum length of time that an aircraft can spend in cruise flight Or until 70% of the battery is drained.

$$\frac{P}{V} = D = 0.5\rho SV^2 (C_{D0} + KC_L^2), P = 0.5\rho SV^3 C_{D0} + \frac{2KW^2}{\rho VS} = 169.2W \quad (11.7)$$

$$\text{Endurance} = \frac{0.7 \times \eta_{\text{total}} V_b C}{P} \quad (11.8)$$

Where,

- $\eta_{\text{total}} = \eta_{\text{prop}} \times \eta_{\text{motor}} \times \eta_{\text{dis}} \times PIF = 0.549$

- $V_b = 22.2 \text{ V}$

- $C = 66 \text{ Ah}$

- $\rho = 1.225 \text{ kg/m}^3$

- $V = 20 \text{ m/s}$

- $AR = \text{Aspect ratio}$

- $S = \text{Wetted Area}$

- $C_{D0} = \text{Zero lift Drag coefficient}$

Therefore endurance is: Endurance = 3.328 hours. Therefore we get the range as follows:

$$\text{Range} = V_{\text{cruise}} \times \text{Endurance}$$

$$\text{Range} = 239.60 \text{ kms}$$

The provided estimates for range and endurance represent the maximum potential because they don't consider the increased power and energy demands during phases other than cruising. These estimates are based on the assumption that the aircraft remains in cruise mode for the entire duration of the flight.

## 11.5 Take off Distance

The following pictures show the regions that we will be targetting for the mission of the uav. As we can see the land will be slightly undulated and will have rocks etc to encounter. Thus



Figure 11.5: Coastal region

we have to ensure as less runway as possible. However, as per survey of these regions, there is enough place to have a runway ground distance of 12m (which is lesser than what is needed for a conventional uav (without high lift devices) take off runway distance) for take off and landing which can be achieved using flap and slat deflection and the hard runway can be dealt with using the bungee suspension and the pressure of tired as mentioned in chapter 8.

However the flap deflection is reduced to 30 deg from 45 deg as the 10m runway can be achieved with 30 deg. Note that the slat deflection is kept the same due to the required take off angle we need as explained in chapter 8, landing gear height section.

The updated flap parameters and calculations that prove the same areas follows:

From chapter 4,section 4.1.1, the new  $V_{\text{stall}} = 7.2 \text{ m/s}$  and  $C_{L_{\text{takeoff}}} = 2.8$ .

From XFLR analysis, the wing, without any flaps deployed, can provide  $C_L$  of 1.2 and considering the effects of slats from Chapter 8, the  $\Delta C_L$  needed from flaps is 1.4.

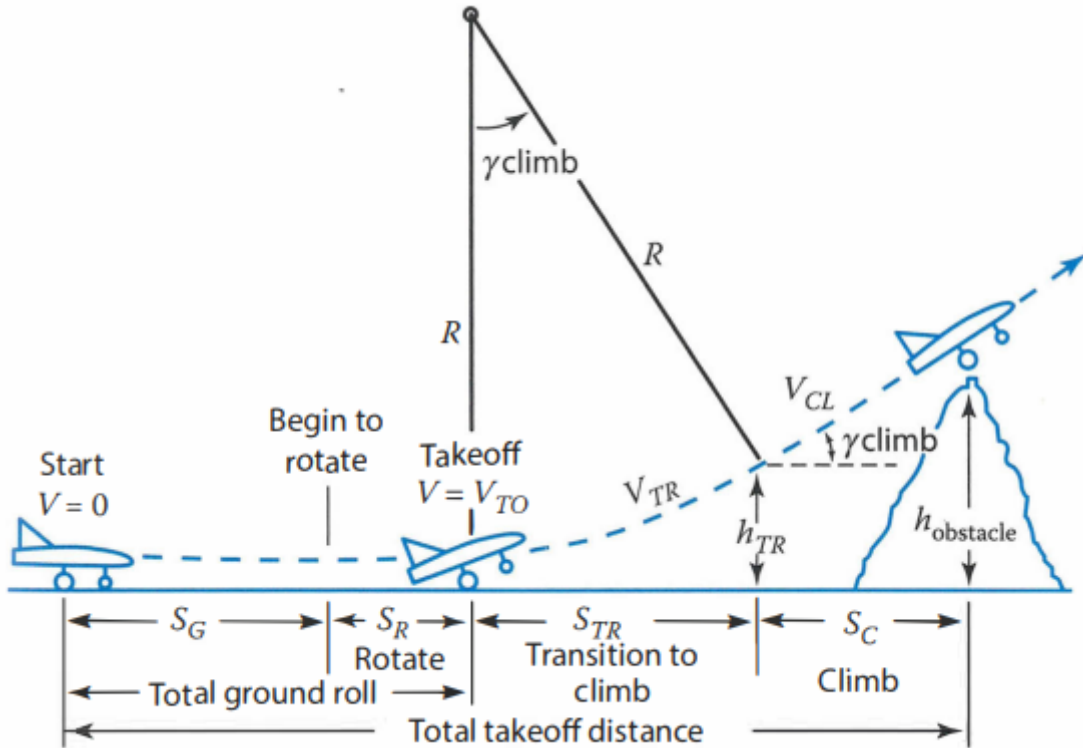


Figure 11.6: Take off distance

Thus, from chapter 6:

Since we are using fowler slaps to change the wetted area of the wing to reduce the wing loading to desired value during take off:

$$\frac{W}{S_{takeoff}} = 105 \text{ N/m}^2$$

$$\left( \frac{S_{flapped}}{S_{ref}} \right) = 0.8$$

$$\Delta C_{L_{max}} = 1.4$$

$$\Delta C_{\ell_{max}} = 1.944$$

Now, using these new parameters, we calculate the final take off and landing distance with rotation.

We have stall speed, as calculated in chapter 4, based on the take off distance constraints. Note that the take off distance that we calculated in chapter 4 was the maximum distance we need without any rotation or pitch up maneuver at  $12^\circ$  as explained in chapter 8, section 8.3. Here, we will see what is the take off distance with the finalized wing parameters take off

rotation included.

$$\begin{aligned} V_{\text{stall}} &= 7.20 \text{ m/s} \\ V_{\text{liftoff}} &= 1.1 \times V_{\text{stall}} \\ V_{\text{clearance}} &= 1.2 \times V_{\text{stall}} \\ V_{\text{liftoff}} &= 7.9 \text{ m/s} \end{aligned}$$

$$V_{\text{clearance}} = 8.6 \text{ m/s}$$

According to [8], during the transition from the moment of takeoff to a stabilized climb angle, the aircraft follows a path that approximates a circular arc. During this time, it also accelerates from takeoff speed  $1.1V_{\text{stall}}$  to climb speed  $1.2V_{\text{stall}}$ .

The time to rotate to liftoff attitude depends mostly on the pilot. Maximum elevator deflection is rarely employed. A typical assumption for large aircraft is that rotation takes 3 s. The acceleration is assumed to be negligible over that short time interval, so the rotation ground-roll distance  $S_R$  is approximated by three times  $V_{TO}$ . For small aircraft the rotational time is on the order of 1 s, and  $S_R = V_{TO}$

#### Ground Roll distance:

$$S_G = \frac{1}{2g} \int_{V_i}^{V_f} \frac{d(V^2)}{K_T + K_A V^2} = \left( \frac{1}{2gK_A} \right) \ln \left( \frac{K_T + K_A V_f^2}{K_T + K_A V_i^2} \right) \quad (11.9)$$

$$K_T = \left( \frac{T}{W} \right) - \mu = 0.0055 \quad (11.10)$$

$$K_A = \frac{\rho}{2(W/S)} (\mu C_L - C_{D_0} - KC_L^2) = -0.002 \quad (11.11)$$

Thus  $S_g = 5.6m$

#### Transition distance:

$$\begin{aligned} n &= \frac{L}{W} = \frac{\frac{1}{2}\rho S (0.9C_{L_{\max}}) (1.15V_{\text{stall}})^2}{\frac{1}{2}\rho S C_{L_{\max}} V_{\text{stall}}^2} = 1.2 \\ n &= 1.0 + \frac{V_{\text{TR}}^2}{Rg} = 1.2 \\ R &= \frac{V_{\text{TR}}^2}{g(n-1)} = \frac{V_{\text{TR}}^2}{0.2g} \end{aligned} \quad (11.12)$$

$$S_{\text{TR}} = \sqrt{R^2 - (R - h_{\text{obstacle}})^2} = 18.36m$$

Based on the dimensions of the runway and literature survey, we take our  $h_{\text{obstacle}} = 10m$ .

#### Total distance required:

$$\begin{aligned} S_{\text{total}} &= S_g + S_{\text{clearance}} \\ &\implies S_{\text{total}} = 24.5 \text{ m} \end{aligned}$$

This take off distance with rotation is almost half the distance that we took for calculating  $V_{\text{stall}}$  with the runway distance without an rotation maneuver. Thus satisfies our runway

constraint - short take off landing.

## 11.6 Landing Distance

Assuming that for safe landing, no human has to be affected, the airplane can be considered to be approaching for landing below a height of 4 m.

$$S_{\text{landing}} = S_{\text{groundroll}} + S_{\text{flare}} + S_{\text{approach}} \quad (11.13)$$

Stall speed is calculated as

$$V_{\text{stall}} = 7.20 \text{ m/s}$$

$$V_{\text{flare}} = 1.23V_{\text{stall}} \quad (11.14)$$

$$V_{\text{Flare}} = 8.86 \text{ m/s}$$

Flight path radius is given by

$$R = \frac{V_{\text{flare}}^2}{0.2 * 9.81} \quad (11.15)$$

$$R = 39.58 \text{ m}$$

Approach angle is given by

$$\sin \theta_{\text{approach}} = \frac{T - D}{W} \quad (11.16)$$

From the approach angle of degrees, the flare height is given by,

$$h_f = R(1 - \cos \theta) \quad (11.17)$$

$$h_f = 1.33 \text{ m}$$

To clear a 4 m obstacle, the approach distance is given by

$$S_a = \frac{4 - h_f}{\tan \theta} \quad (11.18)$$

$$S_a = 12 \text{ m}$$

The flare distance along the ground is,

$$S_f = R \sin \theta \quad (11.19)$$

$$S_f = 9.5 \text{ m}$$

$V_{td}$  is the touchdown velocity and is given by

$$V_{td} = 1.15V_{\text{stall}} \quad (11.20)$$

$$V_{td} = 7.59 \text{ m/s}$$

We can find the Thrust with the value of Power we calculated and the Average Velocity we have:

$$T = \frac{P_{\text{available}}}{V_{\text{avg}}} = 45 \text{ N} \quad (11.21)$$

Ground roll distance by power Calculations,

$$S_{g_{\text{power}}} = \frac{WV_{td}^2}{2gT} \quad (11.22)$$

$$S_{g_{\text{power}}} = 12m$$

The maximum ground roll distance for an aircraft is typically calculated assuming a minimum ground diameter of 150 meters. However, in practice, it is often sufficient to consider only a portion of this diameter, such as 30%, depending on the available runway length and other factors.

$$S_{g_{\text{max}}} = (0.4 * 150) - S_a - S_f$$

$$S_{g_{\text{max}}} = 22 \text{ m}$$

The comparison between the calculated landing distance based on power considerations ( $S_{g_{\text{power}}}$ ) and the maximum possible landing distance ( $S_{g_{\text{max}}}$ ) indicates that the UAV will be able to safely land within a distance shorter than the maximum allowable limit.

Thus the landing and take off distance is within the range that the targeted region provides!

## 11.7 Final Three view diagram

As seen in stability analysis, the tail arm for the horizontal tail is modified for a better static stability value. Also, the batteries are brought forward, towards the cone to account for the CG change caused due to increased tail arm. However the outer structure of the fuselage, diameter, cone etc remain the same.

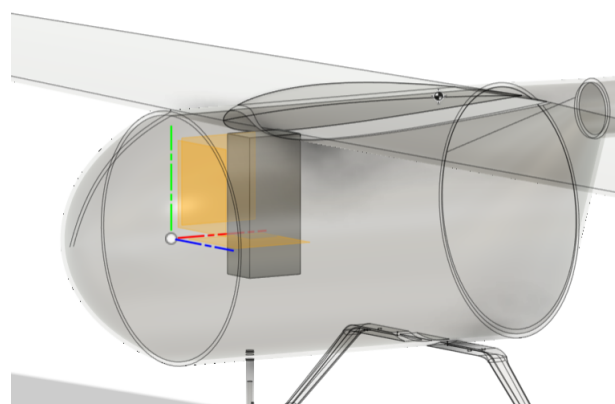
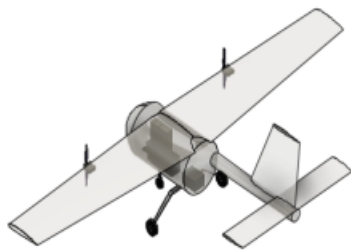
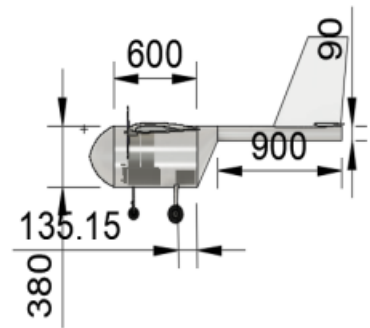


Figure 11.7: New battery location - brought ahead (towards nose) by 7cm in CAD to compensate for changed tail arm so that CG remains same in X axis

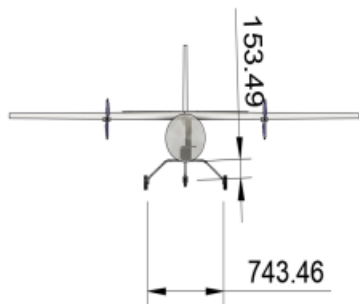
The final three view diagram with slight modifications in the geometry is given below:



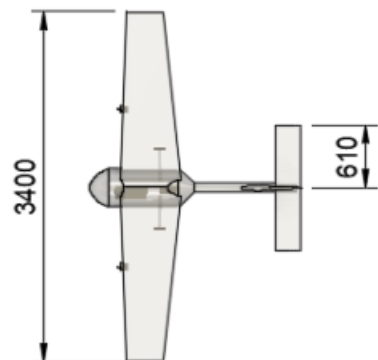
(a) Oblique view



(b) Side view



(a) Front view



(b) Top view

Figure 11.8: Different Views of Final Airplane

# Bibliography

- [1] John D. Anderson. *Fundamentals of aerodynamics*. 5th. McGraw-Hill, Feb. 2011. ISBN: 9780073398105. URL: <http://www.worldcat.org/isbn/9780073398105>.
- [2] Zenith Aircraft Company. *STOL CH 801 Tail Design (empennage: rudder, elevator, stabilizer)*. URL: <http://www.zenithair.com/stolch801/design-tail.html>.
- [3] Arravind Dr.R., Manjunath J., and Midhunesh E. “Seed Dropping UAV: Design of Seed Dropping UAV in Afforestation”. In: *IARJSET* 8 (June 2021), pp. 490–494. DOI: [10.17148/IARJSET.2021.8687](https://doi.org/10.17148/IARJSET.2021.8687).
- [4] Snorri Gudmundsson. “Chapter 25 - LAT-DIR Stability and Control”. In: *General Aviation Aircraft Design (Second Edition)*. Ed. by Snorri Gudmundsson. Second Edition. Butterworth-Heinemann, 2022, pp. 975–1005. ISBN: 978-0-12-818465-3. DOI: <https://doi.org/10.1016/B978-0-12-818465-3.00025-2>. URL: <https://www.sciencedirect.com/science/article/pii/B9780128184653000252>.
- [5] Chris Heintz. “Anatomy of a STOL Aircraft: Designing a Modern Short Take-Off and Landing Aircraft”. In: () .
- [6] Spyridon Kontogiannis and John Ekaterinidis. “Design, performance evaluation and optimization of a UAV”. In: *Aerospace Science and Technology* 29 (Aug. 2013), pp. 339–350. DOI: [10.1016/j.ast.2013.04.005](https://doi.org/10.1016/j.ast.2013.04.005).
- [7] Pakorn Poksawat, Liuping Wang, and Abdulghani Mohamed. “Automatic Tuning of Attitude Control System for Fixed-Wing Unmanned Aerial Vehicles”. In: *IET Control Theory and Applications* 10 (July 2016). DOI: [10.1049/iet-cta.2016.0236](https://doi.org/10.1049/iet-cta.2016.0236).
- [8] Daniel P Raymer. *Aircraft design: A conceptual approach*. 4. ed. AIAA education series. Reston, Va.: American Institute of Aeronautics and Astronautics, 2006. ISBN: 1563478293. URL: <http://www.loc.gov/catdir/toc/ecip068/2006004706.html>.
- [9] Mohammad H. Sadraey. *Aircraft design: A systems engineering approach*. Aerospace Series. Chichester: John Wiley and Sons, 2013. ISBN: 9781118352700. DOI: [10.1002/9781118352700](https://doi.org/10.1002/9781118352700). URL: <http://dx.doi.org/10.1002/9781118352700>.
- [10] Mustafa Şahin and M. Yıldırım. “APPLICATION OF A FIXED-WING UNMANNED AERIAL VEHICLE (UAV) IN REFORESTATION OF LEBANON CEDAR”. In: Sept. 2011.

# Appendix A

## Codes for weight estimation

### A.1 Linear model for weight estimation(empty weight ratio vs total weight)

```
import numpy as np
from scipy.optimize import curve_fit
from matplotlib import pyplot as plt

# Define the function based on the given relationship
def func(wo, A, L):
    return A * wo**L

# All planes data
Wo = np.array([ 9, 10, 15, 17.5, 9.75, 3.55, 5.7, 7])
We = np.array([ 3.3, 3, 6.5, 9.5, 5.5, 2.4, 4, 5.9])

We_Wo = We / Wo
p0 = [4, 0.7]

# Perform curve fitting using least squares method
popt, pcov = curve_fit(func, Wo, We_Wo, p0=p0)
A = popt[0]
L = popt[1]

sorted_indices = np.argsort(Wo)
Wo_sorted = Wo[sorted_indices]
We_Wo_sorted = A * Wo_sorted**L

print("A:", A)
print("L:", L)

plt.figure(figsize=(8, 6))
plt.scatter(Wo, We_Wo, label='Data Points')
plt.plot(Wo_sorted, We_Wo_sorted, color='red', label='Regression Line')
```

```

plt.ylabel('W_e/W_0')
plt.xlabel('W_0')
plt.title('Total Empty weight empirical Equation')
plt.legend()
plt.grid(True, linestyle='dashed')
plt.show()

```

## A.2 Logarithmic Model for weight estimation(empty weight ratio vs total weight)

```

import numpy as np
import matplotlib.pyplot as plt
from sklearn.linear_model import LinearRegression

# Data of empty weight and total weight (Wo) of different planes
Wo_data = np.array([ 9, 10, 15, 17.5, 9.75, 3.55, 5.7, 7]).reshape(-1, 1)
We_data = np.array([ 3.3, 3, 6.5, 9.5, 5.5, 2.4, 4, 5.9])

# Calculation of the empty-to-weight ratio (we/wo)
we_wo_data = We_data / Wo_data.ravel()

# Natural logarithm of both sides of the equation
ln_We_Wo = np.log(we_wo_data)
ln_Wo = np.log(Wo_data)

regression_model = LinearRegression().fit(ln_Wo, ln_We_Wo)
R_squared = regression_model.score(ln_Wo, ln_We_Wo)

L = regression_model.coef_[0]
ln_A = regression_model.intercept_

A = np.exp(ln_A)

# Plotting the data points and the regression line
plt.figure(figsize=(8, 6))
plt.scatter(ln_Wo, ln_We_Wo, label='Data Points')
plt.plot(ln_Wo, regression_model.predict(ln_Wo), color='red', label='Regression Line')
plt.xlabel('ln(W_0)')
plt.ylabel('ln(W_e/W_0)')
plt.title('Linear Regression of Logarithmic Equation')
plt.legend()
plt.grid(True, linestyle='dashed')
plt.show()

```

```

print("A:", A)
print("L:", L)

```

## A.3 Weight estimation Iteration

```

%% Terminology
%{
w_0=total weight
we_w0=empty weight fraction
wb_w0=battery weight fraction
w_b=weight of the battery
%}

w_0=15; %initial assumption

%w_0=w_payload/(1-we_w0-wb_w0);
A=1.08;% values from previous code
L=-0.333;
w_payload=6;% from payload estimate
iter=0;%count for number of iterations
diff=[];%matrix to store the values of iterations
while(1)
    iter=iter+1;
    wb_w0=0.33;
    we_w0=A*(w_0^L);
    w_0_new=w_payload/(1-we_w0-wb_w0);
    %disp(w_b)
    disp(we_w0)
    disp(w_0_new)
    diff(iter)=abs(w_0_new-w_0);
    if(abs(w_0_new-w_0)<0.0001)%adding tolerence level
        w0_final=w_0;
        break;
    else
        w_0=w_0_new;
    end
end
x=linspace(1,iter,iter);
disp("final weight")
disp(w0_final)
disp("no. of iterations needed")
disp(iter)
plot(x,diff)
xlabel('iterations')
ylabel('Difference in consecutive iterations')
ylim([4e-08,10])

```

```
grid("on")
```

## A.4 Second wt estimation

```
main=0;
w_initial=21.98;
s_initial=2.20;
w_0=21.89;
s=s_initial;
acc=[];
while(1)

main=main+1;
w_initial=w_0;
acc(main)=s;

AR=8;
e=0.81;
S_Swet=3;
L_D_cruise=17.32;
L_D_loiter= 15.1144;
Cl_max=3.7;
rho=1.225;
CD0_avg=0.0130;
K=1/(3.14*e*AR);
span=sqrt(AR*s);
v_stall=sqrt(w_initial*10/(0.5*rho*s*Cl_max));
W_S_stall = 0.5*rho*Cl_max*(v_stall)^2;
s_new=w_initial*10/W_S_stall;
if(abs(s_new-s)<0.001)
    s=s_new;
    disp('area final')
    disp(s)
    break;
else
    s=s_new;
    disp('area')
    disp(s)
end
end

P_W_To=((0.5*1.225*((1.1*v_stall)^2)*0.04*1.125 + 0.045*w_initial*10)*(1.2*
v_stall))/(w_initial*10);
P_cruise=0.91;
P_loiter=0.53;
```

```

v_rc=sqrt((2*w_initial*10*cos(7*3.14/180))/(rho*s*(sqrt(3*CD0_avg/K))) ;
r_c=v_rc*sin(7*3.14/180);

K=1/(3.14*e*AR);
P_W_climb=(r_c + v_rc*(sqrt((K*CD0_avg)/3)+ sqrt(3*K*CD0_avg)))*(0.8)^-1;

t_climb=6/60;
t_cruise= 1.2;
t_loiter= 0.8;
t_to=2/60;
E=1.5*(P_W_climb*t_climb + P_loiter*t_loiter + P_cruise*t_cruise +P_W_To*
t_to);
SED=200;
n=0.85*0.9*0.8;

```

# Appendix B

## Code for Power Plant Estimation

```
%% for previous aircraft
l_d=[8.35,4.463,5.431,7.88,6.68,8.89,11.61,6.21,8.244,15.04,8.73,9.36];%
length to diamater ratio
FF=[];
l=[1.52,0.982,1.939,2.27,1.05,1.673,1.15,2.05,1.921,2.093,1.1,1.657];%
length of fuselage
S_ref=[0.815,0.328,1.314,2.27,1.05,1.673,1.15,2.05,1.921,2.093,1.1,1.657];%
reference area or span
rho=1.225;
v=20;
u=1.8*(10^(-05));
c=[0.2615,0.22,0.274,0.2265,0.217,0.274,0.208,0.274,0.3385,0.237,0.345,0.177
,0.2985];
re_wing=[];
re_fuse=[];
cf_wing=[];
cf_fuse=[];
b=[3,1.5,5.16,3.3,3.16,3,2.1,2.6,3.22,3.22,1.6,2.8];
e=0.81;
%finding form factor
for i =1:length(l_d)
    f=l_d(i);
    if f > 6
        FF(i)=(0.9 + 5/(f^(1.5))+ f/400);
    else
        FF(i)= (1+ 60/(f^3) + f/400);
    end
end
% finding reynolds number for fuselage and the wing separately
for i = 1:length(l_d)
    re_wing(i)= rho*c(i)*20/(u);
    cf_wing(i)=0.074/(re_wing(i)^(1/5));
end
```

```

for i = 1:length(l_d)
    re_fuse(i)= rho*l(i)*20/(u);
    cf_fuse(i)=0.074/(re_fuse(i)^(1/5));

end
s_wet_fuse=[0.45,0.151,1.407,0.637,0.294,0.683,0.393,0.167,0.488,0.268,0.295
            ,0.535];
Cd0=[];
% find the coefficient of drag using the formula
for i=1:length(S_ref)
    Cd0(i)= cf_wing(i)*(2.01) + cf_fuse(i)*FF(i)*(s_wet_fuse/S_ref);

end

L_D_max=[];
AR_normal [];

for i=1:length(b)
    AR_normal(i)=(b(i)^2)/S_ref(i);
end

sq=[];
for i =1:length(S_ref)
    L_D_max(i)= sqrt((3*3.14*e*AR_normal(i))/(16*Cd0(i)));
    %AR_wet(i)=AR_normal(i)/(s_wet_fuse(i)/S_ref(i));
    AR_wet(i)=AR_normal(i)/(2.01);
    sq(i)=sqrt(AR_wet(i));

end
%finding averaged quantities
avg=mean(L_D_max);
CD0_avg=0.013;
AR_avg=8;
span_avg=3;
%plotting
figure
scatter(sq,L_D_max)
xlabel("sqrt(Wetted Aspect Ratio)")
ylabel("(L/D)@ minimum power")
hold on
%linear regression for best fit curve
val= polyfit(sq,L_D_max,1);
m=val(1);
inter=val(2);
y_est = polyval(val,sq);
plot(sq,y_est,'r--','LineWidth',2)
hold off
figure

```

```

scatter(AR_wet,L_D_max)
xlabel("(Wetted Aspect Ratio)")
ylabel("(L/D)@ minimum power")
ratio=[];
for i = 1:length(S_ref)
    ratio(i)=s_wet_fuse(i)/S_ref(i)+2.003;
end

%% for cruise
eff=0.85;
P_w_cruise = (avg^-1)*v*eff;

%% for climb
r_c=2;
v_rc=17;
K=1/(3.14*e*AR_avg);
P_W_climb= (r_c + v_rc*(sqrt((K*CDO_avg)/3)+ sqrt(3*K*CDO_avg)))*(0.85)^-1;

%% take off
Cl_max=1.3;
w=21*10;
v_stall=sqrt(w/(0.5*rho*span_avg*Cl_max));
P_W_To=((0.5*1.225*((1.2*v_stall)^2)*0.04*1.125 + 0.03*w)*(1.2*v_stall))/w;

```

## B.1 Motor/Propeller efficiency

```

import numpy as np
import matplotlib.pyplot as plt

# Motor Data
motor_kv_data = 320
motor_v_data = np.array([24.30, 24.29, 24.27, 24.26, 24.25, 24.23, 24.22, 24
.20, 24.19, 24.17, 24.16, 24.14, 24.12
, 24.11, 24.09, 24.07, 23.97, 23.86,
23.70])
motor_torque = np.array([0.37, 0.39, 0.42, 0.44, 0.48, 0.51, 0.54, 0.57, 0.
60, 0.63, 0.66, 0.69, 0.72, 0.75, 0.78
, 0.80, 0.96, 1.11, 1.30])
motor_thrust = np.array([1573, 1677, 1795, 1895, 2048, 2156, 2264, 2409,
2543, 2666, 2788, 2927, 3061, 3194,
3300, 3421, 4112, 4694, 5547])*0.00981
current_data = np.array([5.65, 6.16, 6.81, 7.42, 8.12, 8.83, 9.61, 10.48, 11
.17, 12.04, 12.96, 13.85, 14.81, 15.67
, 16.66, 17.57, 23.37, 29.44, 38.31])

```

```

RPM_data = np.array([2681, 2765, 2858, 2953, 3036, 3120, 3205, 3288, 3369,
                     3454, 3536, 3608, 3684, 3760, 3830,
                     3903, 4256, 4569, 4935]) * 0.1047
power_data = np.array([137, 150, 165, 180, 197, 214, 233, 254, 270, 291, 313
                       , 334, 357, 378, 401, 423, 560, 703,
                       908])
overall_efficiency = np.array([11.47, 11.20, 10.86, 10.52, 10.40, 10.08, 9.
                               73, 9.50, 9.41, 9.16, 8.90, 8.76, 8.57
                               , 8.45, 8.22, 8.09, 7.34, 6.68, 6.11])
                           # in g/Watt

# Motor Efficiency
mecahnical_poweroutput = motor_torque * RPM_data
motor_efficiency = mecahnical_poweroutput / power_data

# Propeller Efficiency
propeller_Efficiency = overall_efficiency / (motor_efficiency*1000)

plt.figure(figsize=(8, 6))
plt.plot( RPM_data , motor_efficiency , color='red' , label='Motor Efficiency'
          )
plt.xlabel('RPM')
plt.ylabel('Efficiency ($\eta$) ')
plt.title('Efficiency of Motor')
plt.legend()
plt.grid(True, linestyle='dashed')
plt.show()

plt.figure(figsize=(8, 6))
plt.plot( RPM_data , propeller_Efficiency , color='blue' , label='Propeller
          Efficiency')
plt.xlabel('RPM')
plt.ylabel('Efficiency ($\eta$) (in Kg/Watt) ')
plt.title('Efficiency of Propeller')
plt.legend()
plt.grid(True, linestyle='dashed')
plt.show()

print("Motor Efficiency:", motor_efficiency)
print("Propeller Efficiency:", propeller_Efficiency)

```

# Appendix C

## Calculation of Wing Loading

```
%% for finding vstall for appropriate take off disatnce

w=210;
g=10;
C_d=0.05;
C_l=1;
rho=1.225;
A=1.9;
mew=0.04;
P=110;

syms r;
v=7.2;
k = (0.5*rho*A*C_d*(0.7*v)^2 + mew*(w - 0.5*rho*A*C_l*(v*0.7)^2));

r = (4*k^3 - 21*(k^2)*v^2 - 4200*k*v - 420000*log(abs(k*v-100)) + 840000*log(10))/(2*k^3);

%% cruise
v_cruise=20;
CD_0=0.014;
prop_eff=0.8;
e=0.81;
AR=8;
K=1/(3.14*e*AR);
%W_S_cruise=[];
W_P_cruise=1/0.97;
syms W_S_cruise;
eqn= W_P_cruise == 0.9*prop_eff/((0.5*rho*CD_0*v_cruise/(W_S_cruise)) + (2*K/(rho*v_cruise))*(W_S_cruise));
cruise=solve(eqn,W_S_cruise);

%% climb
roc=2;
prop_eff= 0.8 ;
```

```

P_W_climb= 3.52;
syms W_S_climb;
K=1/(3.14*e*AR);

eqn2= P_W_climb == 1/(roc/prop_eff + (1.155*prop_eff/13.2)*sqrt((2*W_S_climb
/rho)*sqrt(3*CD_0/K)));

climb2= solve(eqn2,W_S_climb);
%% loiter
n=2.5;
q=0.5*rho*10^2;

T_W_loiter=(0.534);
check=(T_W_loiter)^2 - (4*(n^2)*(CD_0)/(3.14*8*e));
W_S_loiter= (T_W_loiter + sqrt((T_W_loiter)^2 - (4*(n^2)*(CD_0)/(3.14*8*e)))
)/(2*n^2/(q*3.14*8*e));

%% take off
CL_T0=3.3;
P_W_T0=0.411;
TOP=100;
W_S_TO = TOP*CL_T0*P_W_T0;
%% stall
W_S_stall = 0.5*rho*3.5*(v/1.1)^2;
%% max speed
v_max=25;
CD_0=0.014;
prop_eff=0.8;
e=0.81;
AR=8;
K=1/(3.14*e*AR);
%W_S_cruise=[];
W_P_cruise_max=1/1.54;
syms W_S_cruise_max;
eqn_max= W_P_cruise_max == 0.9*prop_eff/((0.5*rho*CD_0*v_max/(W_S_cruise_max
)) + (2*K/(rho*v_max))*(W_S_cruise_max
));
cruise_max=solve(eqn_max,W_S_cruise_max);

```

# Appendix D

## Codes for fuselage length Estimation

```
import numpy as np
import matplotlib.pyplot as plt
from sklearn.linear_model import LinearRegression

# Atlas II, Shahbal, Arya UAV, Lancaster-5, Warmate, Avian Puma AE UAV,
# Blackswift S2, Skyrobot FX-20
Wo_data = np.array([ 10, 17.5, 9.75, 3.55, 5.7, 7, 9.5, 12]).reshape(-1, 1)
fuselage_length = np.array([ 1.15, 1.921, 2.093, 0.982, 1.1, 1.657, 1.673, 1
    .05])

# Natural logarithm of both sides of the equation
ln_fuselage_length = np.log(fuselage_length)
ln_Wo = np.log(Wo_data)

regression_model = LinearRegression().fit(ln_Wo, ln_fuselage_length)
R_squared = regression_model.score(ln_Wo, ln_fuselage_length)

c = regression_model.coef_[0]
ln_a = regression_model.intercept_

a = np.exp(ln_a)

print(ln_fuselage_length)
print("a:", a)
print("c:", c)

# Plotting the data points and the regression line
plt.figure(figsize=(8, 6))
plt.scatter(ln_Wo, ln_fuselage_length, label='Data Points')
plt.plot(ln_Wo, regression_model.predict(ln_Wo), color='red', label='
    Regression Line')
plt.xlabel('ln($W_{0}$)')
plt.ylabel('ln(Fuselage Length)')
```

```

plt.title('Linear Regression of Logarithmic Equation')
plt.legend()
plt.grid(True, linestyle='dashed')
plt.show()

```

```

import numpy as np
import matplotlib.pyplot as plt
from sklearn.linear_model import LinearRegression

# Atlas II, Shahbal, Arya UAV, Lancaster-5, Warmate, Avian Puma AE UAV,
# Blackswift S2

# Skyrobot FX-20 data is removed as it is an outlier
span_data = np.array([ 2.1, 3.22, 3.22, 1.5, 1.6, 2.8, 3]).reshape(-1, 1)
fuselage_length = np.array([ 1.15, 1.921, 2.093, 0.982, 1.1, 1.657, 1.673])

# Natural logarithm of both sides of the equation
ln_fuselage_length = np.log(fuselage_length)
ln_Wo = np.log(span_data)

regression_model = LinearRegression().fit(ln_Wo, ln_fuselage_length)
R_squared = regression_model.score(ln_Wo, ln_fuselage_length)

c = regression_model.coef_[0]
ln_a = regression_model.intercept_

a = np.exp(ln_a)

print(ln_fuselage_length)
print("a:", a)
print("c:", c)

# Plotting the data points and the regression line
plt.figure(figsize=(8, 6))
plt.scatter(ln_Wo, ln_fuselage_length, label='Data Points')
plt.plot(ln_Wo, regression_model.predict(ln_Wo), color='red', label='Regression Line')
plt.xlabel('ln(Wingspan)')
plt.ylabel('ln(Fuselage Length)')
plt.title('Linear Regression of Logarithmic Equation')
plt.legend()
plt.grid(True, linestyle='dashed')
plt.show()

```

# Appendix E

## Python code for V-n Code

```
import numpy as np
import matplotlib.pyplot as plt

def VN(aircraft):
    # Conversions
    fps_per_knot = 1.6878
    g = 32.2

    # Data Setup
    h = aircraft['h']
    W = aircraft['W']
    CLmax = aircraft['CLmax']
    Sref = aircraft['Sref']
    DesignLoadFactor = aircraft['DesignLoadFactor']
    Vne = aircraft['Vne']
    Cla = aircraft['Cla']
    mean_geom_chord = aircraft['mean_geom_chord']

    Vpoints = 100
    Vbuffer = 0.1 * Vne # kts
    Nbuffer = 0.5 # g

    if min(DesignLoadFactor) > 0:
        # warning('Minimum Design Load Factor should be 0 or lower')
        pass

    speed_kts = np.linspace(0, Vne, num=Vpoints) # kts
    Vne_fps = Vne * fps_per_knot # ft/s
    speed_fps = np.linspace(0, Vne_fps, num=Vpoints) # ft/s

    # Gust Line Setup
    Vg = np.array([66, 50, 25]) # ft/s [VB VC VD] gust magnitude

    # Plot Setup
```

```

plt.figure(figsize=(10, 6))
plt.xlim(0, Vne + Vbuffer)
plt.ylim(min(min(DesignLoadFactor) - Nbuffer, -1), max(DesignLoadFactor)
         + Nbuffer)
plt.grid(True)
plt.xlabel('Indicated Airspeed (kts)')
plt.ylabel('Load Factor (g)')
plt.title('Flight Envelope (V-n Diagram)')

# Output Parameter Setup
Vstall_pos = []
Va_pos = []
Vstall_neg = []
Va_neg = []

n_gust_pos = np.zeros((len(Vg), Vpoints))
n_gust_neg = np.zeros((len(Vg), Vpoints))

# Stall line calculations
for alt in h:
    # plot one line for each altitude requested
    rho = stdatm(alt, "R", 1) # density slug/ft^3
    density_ratio = stdatm(alt, "RR", 1)

    # convert IAS to TAS
    speed_fps_true = np.sqrt(speed_fps ** 2 / density_ratio)

    for weight in W:
        # plot one line for each Weight configuration

        # calculate positive stall line
        n_pos = np.maximum.reduce(CLmax) * Sref * rho * speed_fps_true
                ** 2 / (2 * weight)

        # calculate negative stall line
        if len(CLmax) > 1:
            n_neg = np.minimum.reduce(CLmax) * Sref * rho *
                    speed_fps_true ** 2 /
                    (2 * weight)

        else:
            n_neg = np.zeros_like(speed_fps)

        # calculate gust lines
        for j in range(len(Vg)):
            mu = 2 * weight / (Sref * rho * mean_geom_chord * Cla * g)
            Kg = 0.88 * mu / (5.3 + mu)

```

```

        n_gust_pos[j, :] = 1 + (Kg * Cla * Vg[j] * speed_kts) / (498
                                         * weight / Sref)
        n_gust_neg[j, :] = 1 - (Kg * Cla * Vg[j] * speed_kts) / (498
                                         * weight / Sref)

    # Find Stall Speed
    Vstall_pos.append(np.interp(1, n_pos, speed_kts))
    Vstall_neg.append(np.interp(-1, n_neg, speed_kts))

    # truncate stall lines to limit loads
    n_pos[n_pos > max(DesignLoadFactor)] = max(DesignLoadFactor)
    n_neg[n_neg < min(DesignLoadFactor)] = min(DesignLoadFactor)

    # Find Maneuver Speed
    Va_pos.append(np.max(speed_kts[n_pos < max(DesignLoadFactor)]))
    Va_neg.append(np.max(speed_kts[n_neg > min(DesignLoadFactor)]))

    # plot the envelope lines
    plt.plot(speed_kts, n_pos, color='blue', linewidth=2)
    plt.plot(speed_kts, n_neg, color='blue', linewidth=2)

    # plot Vne line
    plt.plot([Vne, Vne], [max(n_pos), min(n_neg)], color='blue',
             linewidth=2)

    # plot Gust lines
    for j in range(len(Vg)):
        if j == 0:
            plt.plot(speed_kts, n_gust_pos[j, :], color='green',
                      linestyle='-.',
                      linewidth=2, label
                      ='Gust Lines')
        else:
            plt.plot(speed_kts, n_gust_pos[j, :], color='green',
                      linestyle='-.',
                      linewidth=2)
            plt.plot(speed_kts, n_gust_neg[j, :], color='green',
                      linestyle='-.',
                      linewidth=2)
    plt.legend()

# Clean up output parameters because we had a leading placeholder value
Vstall_pos = Vstall_pos[1:]
Va_pos = Va_pos[1:]
Vstall_neg = Vstall_neg[1:]
Va_neg = Va_neg[1:]

# plot Vs lines

```

```

for i in range(len(Vstall_pos)):
    plt.plot([Vstall_pos[i], Vstall_pos[i]], [0, 1], color='red',
              linewidth=1)
    plt.plot([Vstall_neg[i], Vstall_neg[i]], [0, -1], color='red',
              linewidth=1)

# plot Va lines
for i in range(len(Va_pos)):
    if Va_pos[i] < Vne:
        plt.plot([Va_pos[i], Va_pos[i]], [0, max(DesignLoadFactor)],
                  color='blue', linewidth=1)
    if Va_neg[i] < Vne:
        plt.plot([Va_neg[i], Va_neg[i]], [0, min(DesignLoadFactor)],
                  color='blue', linewidth=1)

plt.xticks(range(0, 51, 5))
plt.yticks(np.arange(-2, 4, 0.5))
plt.grid(True, linestyle='dashed')
plt.show()

def stdatm(Z, param="all", k=1):
    # Based on stdatm.m from: http://www.dept.aoe.vt.edu/~mason/Mason_f/
    # MRsoft.html

    # k=0 for metric, 1 for std
    #      Z - input altitude, in feet or meters (depending on k)
    #
    #      output:
    #                      units: metric          English
    #      T - temp.                 deg K            deg R
    #      P - pressure              N/m^2           lb/ft^2
    #      R - density (rho)         Kg/m^3          slug/ft^3
    #      A - speed of sound       m/sec           ft/sec
    #      MU - viscosity           Kg/(m sec)     slug/(ft sec)
    #      TS - t/t at sea level
    #      RR - rho/rho at sea level
    #      PP - p/p at sea level
    #      RM - Reynolds number per Mach per unit of length
    #      QM - dynamic pressure/Mach^2

    KK = 0
    K = 34.163195
    C1 = 3.048e-4
    T = 1
    PP = 0

    if k == 0:
        TL = 288.15

```

```

PL = 101325
RL = 1.225
C1 = 0.001
AL = 340.294
ML = 1.7894e-5
BT = 1.458e-6
else:
    TL = 518.67
    PL = 2116.22
    RL = 0.0023769
    AL = 1116.45
    ML = 3.7373e-7
    BT = 3.0450963e-8

H = C1 * Z / (1 + C1 * Z / 6356.766)

if H < 11:
    T = 288.15 - 6.5 * H
    PP = (288.15 / T) ** (-K / 6.5)
elif H < 20:
    T = 216.65
    PP = 0.22336 * np.exp(-K * (H - 11) / 216.65)
elif H < 32:
    T = 216.65 + (H - 20)
    PP = 0.054032 * (216.65 / T) ** K
elif H < 47:
    T = 228.65 + 2.8 * (H - 32)
    PP = 0.0085666 * (228.65 / T) ** (K / 2.8)
elif H < 51:
    T = 270.65
    PP = 0.0010945 * np.exp(-K * (H - 47) / 270.65)
elif H < 71:
    T = 270.65 - 2.8 * (H - 51)
    PP = 0.00066063 * (270.65 / T) ** (-K / 2.8)
elif H < 84.852:
    T = 214.65 - 2 * (H - 71)
    PP = 3.9046e-5 * (214.65 / T) ** (-K / 2)

M1 = np.sqrt(1.4 * 287 * T)
RR = PP / (T / 288.15)
MU = BT * T ** 1.5 / (T + 110.4)
TS = T / 288.15
A = AL * np.sqrt(TS)
T = TL * TS
R = RL * RR
P = PL * PP
RM = R * A / MU
QM = 0.7 * P

```

```

if param == "all":
    return {'T': T, 'P': P, 'R': R, 'A': A, 'MU': MU, 'TS': TS, 'RR': RR,
            , 'PP': PP, 'RM': RM, 'QM': QM
        }
elif param in ['T', 'P', 'R', 'A', 'MU', 'TS', 'RR', 'PP', 'RM', 'QM']:
    return locals()[param]

# Data Setup

# Vmax = 24 m/s
# platform_area = 1.5 m^2
# Cl_max = 1.5
# Total_weight = 21.98kg
# mean_chord = 0.48m

uav = {

'h': [0],
'W': [21.98*2.20462],
'CLmax': [-1.5,1.5],
'Sref': 1.5*10.7639 ,
'DesignLoadFactor': [-1.5,3],
'Vne': 24*1.94384,
'Cla': 0.2 * 180 / np.pi,
'mean_geom_chord': 0.425* 3.28084

}

VN(uav)

```

Type	Propeller	Throttle	Voltage (V)	Thrust (g)	Torque (N*m)	Current (A)	RPM	Power (W)	Efficiency (g/W)	Operating Temperature (°C)
MN6007 KV320	T-MOTOR P21*6.3" CF	40%	24.31	1342	0.30	4.76	2761	116	11.59	51 (Ambient Temperature: 22°C)
		42%	24.31	1433	0.32	5.18	2859	126	11.38	
		44%	24.29	1554	0.34	5.73	2952	139	11.16	
		46%	24.28	1657	0.37	6.27	3050	152	10.89	
		48%	24.27	1748	0.39	6.78	3150	165	10.63	
		50%	24.26	1845	0.41	7.39	3245	179	10.29	
		52%	24.25	1961	0.43	8.04	3333	195	10.06	
		54%	24.24	2073	0.46	8.64	3427	209	9.89	
		56%	24.22	2179	0.48	9.37	3518	227	9.60	
		58%	24.21	2307	0.51	10.10	3605	245	9.43	
		60%	24.20	2412	0.53	10.87	3689	263	9.17	
		62%	24.19	2536	0.56	11.54	3773	279	9.09	
		64%	24.17	2657	0.59	12.38	3854	299	8.88	
		66%	24.15	2803	0.62	13.29	3928	321	8.73	
		68%	24.13	2952	0.65	14.45	4039	349	8.47	
		70%	24.11	3065	0.67	15.19	4111	366	8.37	
		80%	24.03	3638	0.80	19.85	4471	477	7.63	
		90%	23.94	4263	0.94	25.23	4809	604	7.06	
		100%	23.80	5009	1.10	32.77	5231	780	6.42	
MN6007 KV320	T-MOTOR P22*6.6" CF	40%	24.30	1573	0.37	5.65	2681	137	11.47	62 (Ambient Temperature: 22°C)
		42%	24.29	1677	0.39	6.16	2765	150	11.20	
		44%	24.27	1795	0.42	6.81	2858	165	10.86	
		46%	24.26	1895	0.44	7.42	2953	180	10.52	
		48%	24.25	2048	0.48	8.12	3036	197	10.40	
		50%	24.23	2156	0.51	8.83	3120	214	10.08	
		52%	24.22	2264	0.54	9.61	3205	233	9.73	
		54%	24.20	2409	0.57	10.48	3288	254	9.50	
		56%	24.19	2543	0.60	11.17	3369	270	9.41	
		58%	24.17	2666	0.63	12.04	3454	291	9.16	
		60%	24.16	2788	0.66	12.96	3536	313	8.90	
		62%	24.14	2927	0.69	13.85	3608	334	8.76	
		64%	24.12	3061	0.72	14.81	3684	357	8.57	
		66%	24.11	3194	0.75	15.67	3760	378	8.45	
		68%	24.09	3300	0.78	16.66	3830	401	8.22	
		70%	24.07	3421	0.80	17.57	3903	423	8.09	
		80%	23.97	4112	0.96	23.37	4256	560	7.34	
		90%	23.86	4694	1.11	29.44	4569	703	6.68	
		100%	23.70	5547	1.30	38.31	4935	908	6.11	

Note: Motor temperature is motor surface temperature @100% throttle running 10mins.

(Data above based on benchtest are for reference only, comparison with that of other motor types is not recommended.)